ALMA MATER STUDIORUM – UNIVERSITA' DI BOLOGNA

DOTTORATO DI RICERCA IN BIOINGEGNERIA
CICLO XX

Settore scientifico disciplinare di afferenza: ING-INF/06

MODELS FOR THE STUDY OF NEURONAL ACTIVITY DURING COGNITIVE TASKS

(MODELLI PER LO STUDIO DELL'ATTIVITA' NEURONALE DURANTE TASK COGNITIVI)

Presentata da: Melissa Zavaglia

Supervisore

Prof. Mauro Ursino

Controrelatore

Prof. Carlo Marchesi

Coordinatore Dottorato

Prof. Angelo Cappello

Esame finale anno 2008

ACKNOWLEDGEMENTS

There are lots of people I would like to thank for a variety of reasons.

First of all my Prof. Mauro Ursino, for giving me the opportunity to live this beautiful experience, with his knowledge and kindness he helped me during this "path" and he always showed me the right way to follow; and Elisa Magosso, for the constant and precious help she gave me during these years and for being not only a great teacher but also a good friend; without their guide I would never have finished my work.

I would like to thank Laura Astolfi, Prof. Fabio Babiloni, Prof. Giuseppe di Pellegrino, Prof. Elisabetta Ladavas and Andrea Serino for their collaboration, helpfulness and kindness; thank you also to my examiner Prof. Carlo Marchesi.

I would like to thank the PhD coordinator Prof. Angelo Cappello and all the rest of the academic staff of the Department of Electronics, Computer Science and Systems at the University of Bologna (Cesena), who made me live in a nice and stimulating working environment.

A special thanks to Eli, Luci, Vale, Cla, Eugy, Mara and all my friends for being a constant presence in my life and for always giving me the love I need.

I would like to thank my colleagues for the daily fun moments lived together, in particular my friend Cesare, for helping me with my "pc problems", Matthew for his English suggestions, Aldo, Mari, Cri for the special moments shared. Thanks also to the other PhD students, for the fantastic days spent together during the Bioengineering Annual School. A special thank to my friend Marti, for constantly believing in my capacities, for supporting me all the moments, both working and daily life, and for being so special with me, I can't imagine going to work without her; and Massi, because he has been my reference point during my thesis period, near me all the time and for being so sweet and nice with me.

I would like to thank my family, because they always supported me and because they represent the refuge where I feel protected and safe when I go home and, above all, because they mean all to me.

…finally I want to say that I dedicate this thesis to the most important person in my life, without whom I would not be myself today.

CONTENTS

INTRODUCTION

Every simple motor or cognitive task is the result of the integration among different cortical regions, which are mutually linked and send one another reciprocal connections. Information from different sensory modalities, coming from the external world, are processed by different parts in the brain and are finally integrated to create a single behaviour: this is how the brain works. Mathematical models can be very useful to understand the nature of interaction among cortical regions and examine the integration of all information which merges into the brain.

This thesis work is focused on the study and use of mathematical models to reproduce the activity of cortical regions reciprocally connected. In particular, we deepen the problem of integration in the brain at two different levels: one is about functional connectivity and the other about multisensory integration. These two sides of the same coin have been studied in collaboration with two different research groups respectively: the one of Professor Fabio Babiloni (''La Sapienza'' University and Fondazione Santa Lucia, in Rome) and the one of Professor Elisabetta Ladavas (Psychology Department, University of Bologna, and Cognitive Neurosciences Study and Research Centre, in Cesena). It is important to clarify that these two research studies have been achieved separately during my PhD period; for this reason my thesis has been subdivided in two well distinct parts: Part 1 (connectivity) and Part 2 (multisensory integration). In particular Part 1 includes Chapter 1, 2, 3 and 4, while Part 2 Chapter 5 and 6.

Part 1. The problem of deriving connectivity is assuming increasing importance in recent neurophysiological and neurocognitive research. However, the concept of connectivity is still elusive. In several recent studies, connectivity has been evaluated both starting from neuroimaging data (such as PET or fMRI) and from high-resolution scalp electroencephalograms (EEG) or magnetoencephalograms (MEG). A large number of methods has been proposed for the estimation of functional connectivity on EEG signals, such as the directed coherence (DC), the partial directed coherence (PDC), the directed transfer function (DTF) and the direct DTF (dDTF). Recently, the use of neurophysiological models (i.e., models based on biology) to derive effective connectivity from real data has

been assuming increasing importance. They include Wilson-Cowan oscillators and neural mass-models of cortical columns, developed by Lopes da Silva and Freeman in the late seventies, and subsequently improved and extended by Jansen and Rit and Wendling. These models have been successfully used to simulate specific aspects of electrical brain activity (alpha rhythms, oscillations in the γ-band, epileptic patterns) but they have not been used to study and analyze the overall frequency content of EEG in a cortical region of interest.

In this context, mathematical models and computer simulation techniques may be very useful. Part 1 is focused on estimation of functional connectivity by means of neural mass models; we used a neural mass model to investigate the effect of connectivity, to simulate relationships among brain regions during cognitive/motor tasks and to gain a deeper insight into the origin of different EEG/MEG rhythms. The main objectives of the present study are to create a neural mass model able to simulate realistic EEG rhythms, investigate the effect of different patterns of connectivity among regions of interest (ROIs), each described by the model, and, the most ambitious one, to derive connectivity from real data.

In detail, in the study described in Chapter 1, we used the parallel arrangement of three neural populations, with different synaptic kinetics, to simulate the simultaneous presence of alpha, beta and gamma rhythms in a region of interest (ROI). We showed that real cortical EEGs, measured during cognitive or motor tasks, can be reproduced quite well with that model, by modifying the exogenous input noise and synaptic parameters.

In Chapter 2, a subsequent extension of the same model was used to simulate real EEG power spectral densities by replacing the external noise with excitation coming from other interconnected regions of interest, thus providing some preliminary indications on how connectivity could be estimated from EEG data.

In Chapter 3 we investigated the meaning of information extracted from cortical EEGs, using a different neural mass model of a single ROI; we introduced a substantial novelty compared to Chapter 1 and 2: although a single population can produce just a single peak due to its intrinsic resonance frequency, the same population can also exhibit additional rhythms (i.e., other peaks in the spectrum) if they are furnished by an external source. In this case, one (intrinsic) rhythm is produced inside the population, while the

others are derived from external forcing inputs represented by other populations, oscillating at different frequencies, which cause partial synchronization. Therefore, in this model a single neural population becomes representative of a ROI, while, by contrast, in the previous model (see Chapter 1 and 2), we used the parallel arrangement of three neural populations. The new model of a ROI has been validated with reference to cortical EEG power spectral densities evaluated in the controlateral cingulated cortex of human volunteers.

Finally, in Chapter 4, we used an extension of the model described in Chapter 3 to simulate the EEG power spectral densities of a network of interconnected ROIs, and propose it for the estimation of connectivity among regions from high-resolution EEG data taken on the scalp.

The results described in Part 1 may be of value for a deeper comprehension of mechanism causing EEG rhythms and of neurophysiological information contained in the signal; furthermore with the model we can deepen the problem of estimation of brain connectivity, by testing different neurophysiological hypotheses. Finally, the results obtained in this work con be used in the perspective of an integration with different neuroimaging techniques containing different connectivity information (such as PET or fMRI) into a definite theoretical framework.

Part 2. Part 2 is focused on the problem of multisensory integration in peripersonal space. In order to guide body movement through the space and allow interaction with the immediate surroundings, the brain must continuously monitor the location of the body parts across different postures and analyze the spatial relations between body parts and nearby objects. This process requires the integration of proprioceptive, tactile, visual and even auditory information regarding limb position. Much research has focused on how these various sensory cues may be combined and integrated to achieve perception of limb location and representation of the 'peripersonal' space immediately around the body. Many studies on this topic have been achieved, involving different methodologies: single-cell recordings in animals (Hyvarinen, Rizzolatti, Graziano & Gross, Fogassi); neuropsychological studies in brain-damaged patients (Ladavas, Mattingley), psychophysical and neuroimaging investigation in both healthy and pathological subjects (Holmes & Spence, Ladavas, Macaluso, Taylor-Clarke).

Despite the large collection of data on the subject, a clear comprehension of the mechanisms underlying peripersonal space representation is still lacking.

The work presented in Part 2 describes an original neural network to simulate representation of the peripersonal space around the hands. Three are the main objectives of the present study. The first objective is to develop an original mathematical model of multisensory visual-tactile integration able to summarize the data coming from neurophysiological and clinical experiments into a theoretical scenario and to simulate neuron behaviour in a realistic way. The second objective is to provide a preliminary instrument for analysis and planning of clinical studies. The perception of the peripersonal space, and the link between visual and tactile body information, in fact, may be altered in pathological conditions (as in brain-damaged patients or in patients with arm-amputation). The third objective is to simulate the dynamic and plastic proprieties of peripersonal space representation. Recent data demonstrated that our perception of the peripersonal space is not a static one, but can be modified by experience and training (Farnè, Berti, Maravita). These modifications may reflect changes in the connections among the neurons (Hihara), hence their full understanding requires a network able to summarize the main processing steps from the unimodal sensory areas to the bimodal specialized cortex, and their adapting changes.

In detail, in the study presented in Chapter 5, we described an original model which simulates the two portions of brain hemispheres involved in the peripersonal space representation, each composed of three areas of neurons. The two upstream areas are unimodal and respond to visual and tactile stimuli, respectively. The third downstream area is multimodal and is devoted to multisensory integration. The connections between unimodal and multimodal neurons within the same hemisphere include both feedback and feedforward synapses. The two hemispheres are interconnected via inhibitory synapses. With the model we simulated the multisensory coding of the space around a hand and the competitive interaction between the right and left hand representations in normal subjects. Moreover, the network has been used to simulate the responses characterizing RBD (Right Brain Damage) patients by assuming plausible modifications in some model parameters.

Finally, in Chapter 6, the previous model was used to simulate the expansion of the peripersonal space after the training with a tool used to reach the far space, both in normal and in RBD subjects. The model assumes that synapses linking unimodal to bimodal neurons can be reinforced by a Hebbian rule during training. Results show that the peripersonal space, which includes just a small visual space around the hand in normal conditions, becomes elongated in the direction of the tool after training. This expansion of the peripersonal space depends on an expansion of the visual receptive field of bimodal neurons, due to a reinforcement of visual synapses, which were just latent before training.

The original network model presented in Part 2 may be of value to analyze the neural mechanisms responsible for representing and plastically shaping peripersonal space, and in perspective, for interpretation of psychophysical data on patients with brain damage.

The contents of Chapter 1 have been published in Journal of Neuroscience Methods (Zavaglia et al. 2006).

The contents of Chapter 2 have been published in Biological Cybernetics (Ursino et al. 2007).

The contents of Chapter 3 have been published in Journal of Integrative Neuroscience and IEEE Transactions on Biomedical Engineering (Ursino and Zavaglia 2007;Zavaglia et al. 2008b).

The contents of Chapter 4 have been published in Journal of Bioelectromagnetism (Zavaglia et al. 2008a).

The contents of Chapter 5 have been submitted to Neural Computation (Magosso et al. 2008).

PART 1

CHAPTER 1

A NEURAL MASS MODEL FOR THE SIMULATION OF CORTICAL ACTIVITY ESTIMATED FROM HIGH RESOLUTION EEG DURING COGNITIVE OR MOTOR TASKS

1.1 Introduction

Electrical activity in the cerebral cortex contains important information to characterize brain function and to study the role of individual regions during cognitive or motor tasks. Electroencephalography (EEG) or magnetoencephalography (MEG) are the usual methods adopted in clinics and physiology to extract this information and, in combination with functional magnetic resonance (fMRI), positron emission tomography (PET), and intraneural recording in animals, are universally used today to reach a deeper understanding of large scale brain organisation (David et al. 2005;Rowe et al. 2005;Erickson et al. 2005). EEG/MEG signals are a measure of the collective activity in restricted regions of the cortex. This electrical activity ensues from the interaction of excitatory and inhibitory sub-populations, whose kinetics may vary depending on the particular task, on the particular region involved in the task, and on the instant during the task. Indeed, the EEG/MEG signals are intrinsically very complex, including different rhythms and a large frequency spectrum, which may vary rapidly in time, reflecting the non-stationarity of the underlying phenomena and the changes in the kinetics of the neural mechanisms.

In order to improve our understanding of EEG/MEG signals, and to gain a deeper comprehension of the neurophysiological information contained, various mathematical models have been proposed in past years. These models can be subdivided into two major classes: “detailed models” and “neural mass models”. In the first group, the description of network dynamics is performed at the level of the individual cells, in general using spiking neurons and including the kinetics of the synaptic channels (Makarov et al. 2005). By contrast, in the second group the dynamics of entire neural populations is summarized at a macroscopic level. This

dynamics is generally represented with a few state variables, which mimic the interaction among excitatory and inhibitory sub-populations, arranged in a feedback loop. These models include Wilson-Cowan oscillators (Schillen and Konig 1994) or relaxation oscillators (Wang and Terman 1997) which have been frequently employed to analyze synchronization among neural groups. More sophisticate neural mass-models of cortical columns, particularly useful to simulate some aspects of EEG signals, were developed by Lopes da Silva et al. (Lopes da Silva et al. 1976) and by Freeman (Freeman 1978) in the late seventies, and subsequently improved and extended by Jansen and Rit (Jansen and Rit 1995) and Wendling et al. (Wendling et al. 2002). Although neural mass models have been successfully used to simulate specific aspects of electrical brain activity, such as alpha rhythms (Jansen and Rit 1995), oscillations and synchronisation in the γ-band (Schillen and Konig 1994), dynamics in the olfactory cortex (Freeman 1987), or epileptic patterns (Wendling et al. 2000;Wendling et al. 2002), they have not been exploited to analyze the overall frequency content of EEG in a cortical region of interest.

As pointed out by David et al. (David and Friston 2003), a neural mass model consisting of a single population (such as the model by Jansen et al. (Jansen and Rit 1995), or the extended model by Wendling et al. (Wendling et al. 2002)) produces just a unimodal spectrum, which may represent individual rhythms in the EEG quite well, but it is unable to characterize the entire complexity of the EEG, and to capture the diversity of neural dynamics within a cortical area. For this reason, David et al. (David and Friston 2003) proposed a model composed of N populations deployed in parallel, each characterized by a different kinetics. In their work, the authors simulated a two-population model (dual-kinetics model).

We guess that an N–population model, with N large enough, should be able to mimic an entire cortical area in terms of cortical EEG activity, with its various rhythms and diversity of mechanisms. Nevertheless, we are not aware of any attempt to use this model to mimic real cortical EEG during cognitive/motor tasks.

In the work presented in this chapter we wish to progress on the same route as in the paper by David et al. (David and Friston 2003). Our intention is to analyze whether a neural mass model, consisting of several populations with different kinetics, is able to mimic the complexity of electrical activity

in some cortical region of interests (ROIs). In order to be of practical value, this model should be able to reproduce the power spectral density (PSD) of cortical EEG in real ROIs, by accounting for both spatial and temporal variations (i.e., variations in EEG from one region to another, and temporal variations within the same region) by acting on a few parameters only, with a clear neurophysiological meaning. Here, we assume that these EEG variations can be ascribed to changes in the noise input (mean value and variance) to each region and/or to synaptic alteration in the excitatory/inhibitory balance within the region, since we presumed these are main aspects which can vary considerably during a cognitive/motor task. Changes in input may reflect changes in stimuli from the external world and/or in the connectivity inputs from other regions. Changes in excitatory/inhibitory synapses may reflect short-time adjustments within the cortical regions themselves.

To reach the objective delineated above, two fundamental steps have been followed in this work:

i) cortical EEG in some ROIs has been obtained starting from non-invasive scalp EEG measurement during a motor or cognitive task. This aspect required the use of high-resolution EEG measurement on the scalp, and a model for propagating electrical activity from the scalp to the cortex (Babiloni et al. 2005);

ii) once a reliable cortical EEG has been obtained following step i, we looked for a simple population model able to account for changes in cortical EEG, both in different ROIs and in different instants in the same ROI during the task. With this model, we also investigated how the input and internal parameters of the ROI should vary to report for the observed changes in cortical electrical activity.

The present results may constitute a further step in the use of neural mass models for the interpretation and analysis of EEG data and, in perspective, may contribute to the use of neurophysiological models for the study of effective connectivity in the brain (see Chapter 2). In fact, although the problem of brain connectivity is not explicitly addressed in this work, the present results may open new possibilities for its quantitative analysis. Interpretation of brain connectivity using neurophysiological models has been advocated by various authors recently (Tagamets and Horwitz 1998;Horwitz et al. 1999;Tagamets and Horwitz 2000;David and Friston

2003;David et al. 2004), but this issue benefits from the preliminary formulation of a model able to fit the overall complexity of neural dynamics in real ROIs, and to follow their temporal changes by acting on input and synaptic parameters only.

1.2 Method

1.2.1 Mathematical model

Model of a single population

The model of a single population was obtained by modifying equations proposed by Wendling et al. (Wendling et al. 2002). The model consists of a population of neurons which are lumped together and which are assumed to share the same membrane potential. There are no dendrites and no intrinsic conductances. Rather, one lumped circuit communicates with another through the average firing rate corresponding to what that given population of cells is doing, on average. In this model, four lumped neural groups communicate: pyramidal cells, excitatory interneurons, inhibitory interneurons with slow synaptic kinetics, and inhibitory interneurons with faster synaptic kinetics (see Fig. 1.1a).

a)

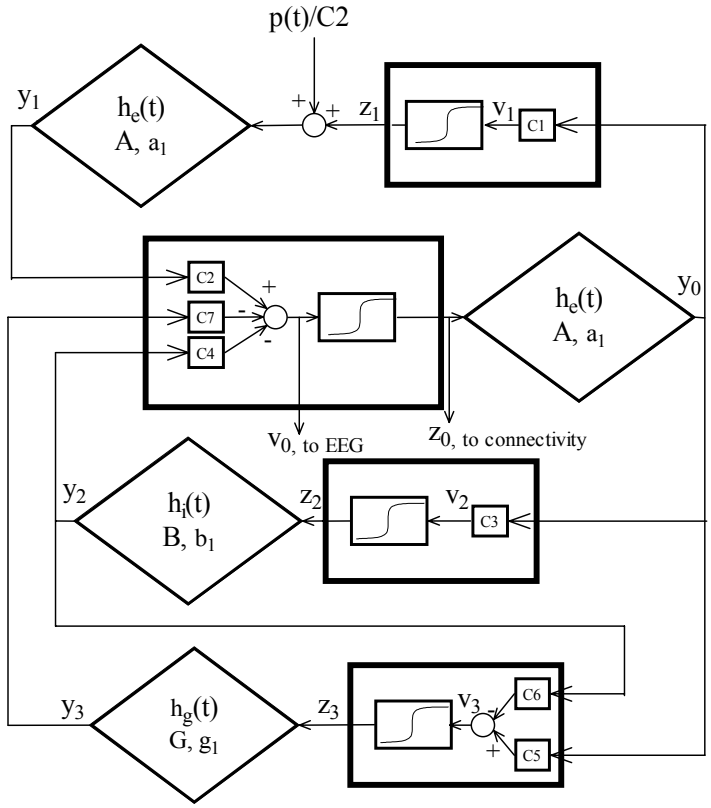

b)

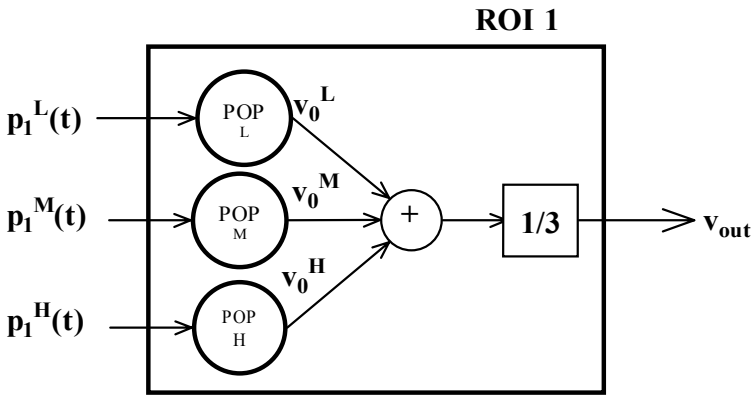

Figure 1.1 - a) Layout of a single population model. b) Parallel arrangement of three populations used to describe a region of interest (ROI).

Each neural group receives an average postsynaptic membrane potential from the other groups, and converts the average membrane potential into an average density of spikes fired by the neurons. This conversion is simulated via a static sigmoidal relationship. The effect of the synapses is described via second order linear transfer functions, which convert the presynaptic spike density into the postsynaptic membrane potential. Three different kinds of synapses, with impulse response h_e, h_i and h_g, (see Fig. 1.1a), are used to describe the synaptic effect of excitatory neurons (both pyramidal cells and excitatory interneurons), of slow inhibitory interneurons and of fast inhibitory interneurons, respectively.

According to Fig. 1.1a, model equations can be written as follows:

Pyramidal neurons

$$\frac{dy_0(t)}{dt} = y_5(t) \tag{1.1}$$

$$\frac{dy_5(t)}{dt} = A \cdot a_1 \cdot z_0(t) - 2 \cdot a_1 \cdot y_5(t) - a_1^{\,2} \cdot y_0(t) \tag{1.2}$$

$$z_0(t) = \frac{(2 \cdot e_0)}{1 + e^{r \cdot (s_0 - v_0)}} \tag{1.3}$$

$$v_0(t) = C_2 \cdot y_1(t) - C_4 \cdot y_2(t) - C_7 \cdot y_3(t) \tag{1.4}$$

Excitatory interneurons

$$\frac{dy_1(t)}{dt} = y_6(t) \tag{1.5}$$

$$\frac{dy_6(t)}{dt} = A \cdot a_1 \cdot (z_1(t) + \frac{p(t)}{C_2}) - 2 \cdot a_1 \cdot y_6(t) - a_1^{\,2} \cdot y_1(t) \tag{1.6}$$

$$z_1(t) = \frac{(2 \cdot e_0)}{1 + e^{r \cdot (s_0 - v_1)}} \tag{1.7}$$

$$v_1(t) = C_1 \cdot y_0(t) \tag{1.8}$$

Slow inhibitory interneurons

$$\frac{dy_2(t)}{dt} = y_7(t) \tag{1.9}$$

$$\frac{dy_7(t)}{dt} = B \cdot b_1 \cdot z_2(t) - 2 \cdot b_1 \cdot y_7(t) - b_1^2 \cdot y_2(t) \tag{1.10}$$

$$z_2(t) = \frac{(2 \cdot e_0)}{1 + e^{r \cdot (s_0 - v_2)}} \tag{1.11}$$

$$v_2(t) = C_3 \cdot y_0(t) \tag{1.12}$$

Fast inhibitory interneurons

$$\frac{dy_3(t)}{dt} = y_8(t) \tag{1.13}$$

$$\frac{dy_8(t)}{dt} = G \cdot g_1 \cdot z_3(t) - 2 \cdot g_1 \cdot y_8(t) - g_1^2 \cdot y_3(t) \tag{1.14}$$

$$z_3(t) = \frac{(2 \cdot e_0)}{1 + e^{r \cdot (s_0 - v_3)}} \tag{1.15}$$

$$v_3(t) = C_5 \cdot y_0(t) - C_6 \cdot y_2(t) \tag{1.16}$$

In these equations, the symbols v_i represent the average membrane potentials (i = 0, 1, 2, 3 for the four groups). These are the input for the sigmoid function which converts them into the average density of spikes (z_i, i = 0, 1, 2, 3) fired by the neurons. Then, these outputs enter into the synapses (excitatory, slow inhibitory or fast inhibitory), represented via the second order linear functions. Each synapse is described by an average gain (A, B and G for the excitatory, slow inhibitory and fast inhibitory synapses, respectively) and a time constant (the reciprocal of a_1, b_1 and g_1, respectively). The outputs of these equations, which can be excitatory, slow inhibitory or fast inhibitory, represent the postsynaptic membrane potentials (y_i, i = 0, 1, 2, 3). Interactions among neurons are represented via seven connectivity constants (C_i). Finally, p(t) represents a Gaussian white noise

with assigned mean value, m, and variance, σ^2. This noise summarizes all exogenous contributions, both excitation coming from external sources and the density of action potentials coming from other connected regions.

Model of a region of interest (ROI)

The previous model was used to simulate a single population, the dynamic of which ensues from the interactions of the four neural subgroups. As shown in David et al. (David and Friston 2003), however, and confirmed by our simulations, a single population can produce just a unimodal spectrum (i.e., a spectrum with a single peak), whose position and bandwidth can be finely adjusted, but cannot mimic the overall complexity of EEG in an entire cortical area. For this reason, the model of an overall ROI can be composed by N populations deployed in parallel. We assumed that these populations are connected in a simple feedforward schema (see Fig.1.1b), with the same weight for all populations. This is a very simple choice, adopted to avoid inclusion of additional parameters describing the direction and degree of internal coupling in the model. A different role for each population has been assigned, in the best fitting procedure, by changing the variance of the noise stimulating each population. The limitations of this approach, and the possibility to adopt more physiological internal connections within a ROI in future work are discussed in the last section of this chapter.

Each population is characterized by different values of time constants (i.e., of parameters a_1, b_1, g_1) and so can produce a different rhythm. The number, N, depends on the complexity of the EEG, i.e., on the number of different peaks in its spectrum. Analysis of data obtained using a motor or cognitive task (see section 1.2.2) suggests that the use of just three populations is sufficient to simulate cortical activity. In the following, these populations will be indicated with the superscript L, M and H, to represent rhythms at low, medium and high frequency. The cortical EEG of a ROI (say $v_{out}(t)$) is obtained as the mean value of the membrane potentials of pyramidal neurons in the three populations (i.e., averaging quantity v_0). We have

$$v_{out}(t) = \frac{1}{3} \sum_{k=L,M,H} v_0^k(t) \tag{1.17}$$

1.2.2 Acquisition of experimental data

Experimental data were acquired from two different tasks: one related to a self-paced finger movement of the right hand, and the second one related to the execution of a working memory task. In the following the two acquisition procedures are briefly presented.

Subject and Experimental Design

Finger tapping task:

Two normal subjects participated in the experiment, which took place in the laboratories of the Santa Lucia Foundation, Rome, after the informed consent was obtained. Subjects were comfortably seated in an armchair with both arms relaxed, in an electrically shielded, dimly lit room. They were requested to perform repetitive right finger movements. The task was repeated every 2 seconds, in a self-paced manner. A 96-channel EEG system (BrainAmp, Brainproducts GmbH, Germany) was used to record electrical potentials by means of an electrode cap, accordingly to an extension of the 10-20 international system. Structural MRIs of the subject's head were taken with a Siemens 1.5T Vision Magnetom MR system (Germany). During motor task, subject was instructed to avoid eye blinks, swallowing, or any movement other than the required finger movements.

Event related potential (ERP) data were recorded with 96 electrodes; data were recorded with a left ear reference and submitted to the artifact removal processing. About 500 single trials were recorded for each subject and averaged for the linear inverse estimation described below. A/D sampling rate was 250 Hz. The surface electromyographic (EMG) activity of the muscle was also collected. The onset of the EMG response served as zero time. After the EEG recording, the electrode positions were digitized using a stereophotogrammetric procedure. The analysis period for the potentials, time-locked to the movement execution, was set from 300 ms before to 300 ms after the EMG trigger (0 time).

Working memory task:

A subject was seated in a comfortable reclining armchair placed in a dimly lit, sound-damped, and electrically shielded room. They kept their forearms resting on armchairs, with right index finger resting between two

buttons spaced 6 cm apart. A computer monitor was placed in front of the subjects (100 cm). The working memory task comprised a sequence of baseline stimulus (0.7 degrees cross at the center of the monitor for 1 s), visual warning stimulus, visual cue stimulus (two vertical bars large 2 degrees and height 2.5–7 degrees for 2 s), delay period (blank screen for 3.5–5.5 s), go stimulus (a green circle appeared for 1 s), and right finger movement to press the proper button of a custom made device. This device had two large buttons approximately 10 cm distant from one another, which were electronically connected to the mouse of the computer giving the visual stimuli. Subjects had to click the left button if the taller bar (cue stimulus) was at the left monitor side, whereas they had to click the right button if the taller bar was at the right monitor side. In the no working memory condition (not used here) the visual cue stimulus was delivered up to the go stimulus. The zero time was the onset of the cue stimulus. Two trial blocks for each condition were pseudorandomly intermingled (block; 50 single trials; 2 min pause). In this task the EEG data were recorded (0.1 – 60 Hz bandpass; 256 Hz sampling frequency) with a 46-tin electrode cap referenced to linked ears. The electrodes were disposed according to an augmented 10-20 system and electrode impedance was kept lower than 5 kV. The positions of the electrodes and landmarks were digitized. The EEG data analyzed was those obtained from the period in which the subject has to hold in memory the pattern of the bars, lasting half a second before the overt muscular responses. Also in this case trials were averaged.

The Head Models and the Cortical Source Estimation

A 3-shell Boundary Element Model (BEM) of the head was used to estimate the cortical current density (CCD) distribution. The scalp surface, the external and internal surfaces of the skull were used to separate the four compartments of the model (brain, skull, scalp and air). A triangle tessellation made up of about 1000 triangles was fitted to match the geometric shape of the surface, as determined from the MRIs of each subject.

The cortical sources were described by using a distributed source model with realistic cortical shape (Grave de Peralta and Gonzalez Andino 1999;Dale et al. 2000). With this approach, once the cortical surface is tessellated with a procedure similar to the one described for the BEM

surfaces, a current dipole is placed at each vertex of the tessellation, yielding about 3000 source locations. The orientation of each dipole is constrained to be perpendicular to the surface, to model the alignment of the pyramidal neurons with respect to the cortical mantle. The adopted source model allow to estimate the cortical activation with a lower number of unknowns with respect to tomographic 3D source models, yielding a better numeric stability. This hypothesis is assumed not to produce mixing errors, since we do not expect relevant sources to be located outside the cortical mantle (i.e. subcortically). BEM and source model tessellations were obtained with the help of the Curry 4.6 software (Compumedics Neuroscan Ltd., El Paso, Texas).

The actual strength of these sources is then estimated by using a linear inverse procedure (Uutela et al. 1999;Babiloni et al. 2005).

Several Regions of Interest (ROIs) were selected for the estimation of cortical activity from high resolution EEG measurements on the basis of Talairach coordinates and anatomical landmarks available. In Fig. 1.2, some of the ROIs are shown, on a realistic reconstruction of the cortex and head of an experimental subject. Different ROIs are represented in different colours. The ROIs employed in this study were the left (L) and right (R) Brodmann areas 5, 3-1-2 (primary somato-sensory area), 6 anterior (6A) coincident with the supplementary motor area proper and the Brodmann area 46.

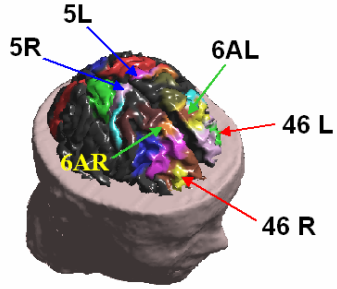

Figure 1.2 – Disposition of the six regions of interest (ROIs) used to fit EEG power spectral densities during a finger motor task. The ROIs are represented in different colours, on a realistic reconstruction of the subject's head. Cortical EEG in each region was computed, from high-resolution scalp EEG, using the inverse propagation model described in (Babiloni et al. 2005).

The degree of involvement of the ROI in the experimental task is measured by the average estimated cortical activity in the region. To measure this quantity, those dipoles of the source model (introduced in the previous section) that are geometrically included in a ROI are grouped in a subset of the source space, one subset for each ROI. By averaging the estimated dipole moment within each subset, the time course of the activity on the ROI can be computed.

These ROI waveforms, related to the event-related changes of the cortical current density, were successively subjected to the spectral analysis in order to produce the spectra used for the estimation of the model parameters.

1.2.3 Best fitting procedure

A best fitting between model simulated EEG of a ROI ($v_{out}(t)$) and real data has been achieved in the frequency domain, by minimizing a least square criterion function of the difference between the power spectral densities in the range 3-50 Hz. As explained in "Results, section 1.3", parameters estimated by the minimization algorithm are the mean values (m^L, m^M and m^H) and standard deviations (σ^L, σ^M and σ^H) of exogenous noise, and the fast inhibitory average gains of synapses (G^L, G^M and G^H), see Eq. 1.14, in the three populations. In order to eliminate possible differences in amplification all power spectra have been preliminary normalized to have unitary area in the same frequency range (3-50 Hz). Power spectra have been computed by using the Welch's average modified periodogram method (Welch 1967). In particular, when computing model power spectra, we produced a 30 s output, and averaged 50% overlapping sections each with duration 1 s. The use of a 30 s simulated signal is justified by the necessity to reduce the variance of the estimated spectrum to an acceptable level. We verified, using a random repetition of the same simulation by changing the input noise, that these spectra are only scarcely affected by the single noise realization. By contrast, just eight overlapping sections have been used to compute spectra from real data, since these signals were previously mediated over different trials to reduce noise variance (see section 1.2.2). Sections have been zero-padded to 1 s to have the same resolution (1 Hz) in the experimental and model spectra.

1.3 Results

1.3.1 Analysis of a single population

A single population produces a signal with a unimodal spectrum. By contrast, analysis of cortical EEGs obtained during the motor or cognitive task revealed the presence of one, two or three peaks in the frequency spectrum, located in different positions within the range 3-50 Hz. Moreover, the frequency position of these peaks is not constant, but may vary from one region to another, or during the task. In our model, as in David et al. (David and Friston 2003), we assume that these peaks derive from individual populations, each with a different synaptic kinetics. According to this idea, the first stage of our study intends to analyze the behaviour of a single population and, in particular, to determine the parameters which affect the position of the individual rhythm generated by the population . The main questions are: how is it possible to generate different peaks in the low, medium or high frequency range? How is it possible to tune the position of these peaks subtly, acting on physiological parameters? In order to answer these questions, we assumed that the position of the peak primarily depends on the synaptic kinetics (i.e., on parameters a_1, b_1 and g_1 in Eqs. 1.2, 1.6, 1.10 and 1.14). However, this position can also be finely tuned, acting on the balance between excitatory and inhibitory synapses within the population. We also presuppose that the parameters describing synaptic kinetics (a_1, b_1 and g_1) are fixed for each population, i.e., cannot change during the task or from one region to another. By contrast, we assume that the average gain of the synapses (i.e., parameters A, B and G in Eqs. 1.2, 1.6, 1.10 and 1.14) can vary, either spatially or temporally, due to plasticity of the synaptic strength. In the following, however, only parameter G will be changed, to avoid fitting an excessive number of parameters.

A basal value for the parameters in the three populations have been given to have peaks which approximately lie in the theta and alpha band (4-12 Hz), in the beta band (12-30 Hz) and in the gamma band (greater than 30 Hz). These values are reported in Table 1.1. As illustrated in Fig. 1.3, with these parameters, and using a random input noise (mean value = 60, variance = 100), each population can produce a well-defined peak within its typical frequency-band.

Table 1.1

Model basal parameters in common for the three populations.

C_1	C_2	C_3	C_4	C_5	C_6	C_7	s_0	e_0	r
135	108	33.75	33.75	40.5	13.5	108	6	2.5	0.56

Model basal parameters different for the three populations.

(Parameters a_1, b_1, g_1 are in s^{-1})

	A^L	B^L	G^L	a_1^L	b_1^L	g_1^L	$(\sigma^L)^2$	m^L
POP LF	2.7	3.2	39	40	20	300	60	100

	A^M	B^M	G^M	a_1^M	b_1^M	g_1^M	$(\sigma^M)^2$	m^M
POP MF	5.2	4.5	43	85	30	350	60	100

	A^H	B^H	G^H	a_1^H	b_1^H	g_1^H	$(\sigma^H)^2$	m^H
POP HF	5.6	3.8	75	110	40	790	60	100

As specified above, subtle adjustments in the position of the peaks can be obtained by modifying the average gain of excitatory vs. inhibitory synapses in the model. In particular, we found that the position of the peak finely depends on the average gain of fast inhibitory synapses (parameter G in Eq. 1.14). For this reason, throughout the present work we will act on this synaptic parameter only. Such a choice is justified by the necessity to reduce the number of free parameters in the model. By changing this parameter we can control the position of the peak in a subtle way within the corresponding frequency band, as illustrated in Fig. 1.4.

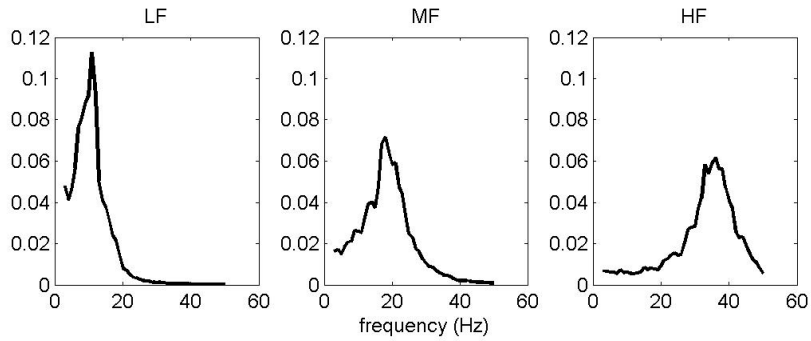

Figure 1.3 – Normalized power spectral density obtained with the three individual population models, using the parameter values reported in Tab. 1.1. A single population produces a signal with a narrow frequency band. The first population mimics a rhythm in the theta-alpha band (4-12 Hz), the second a rhythm in the beta band (12-30 Hz) and the third in the gamma band (greater than 30 Hz). The power spectral densities have been normalized, to have an area equal to one in the range 3-50 Hz.

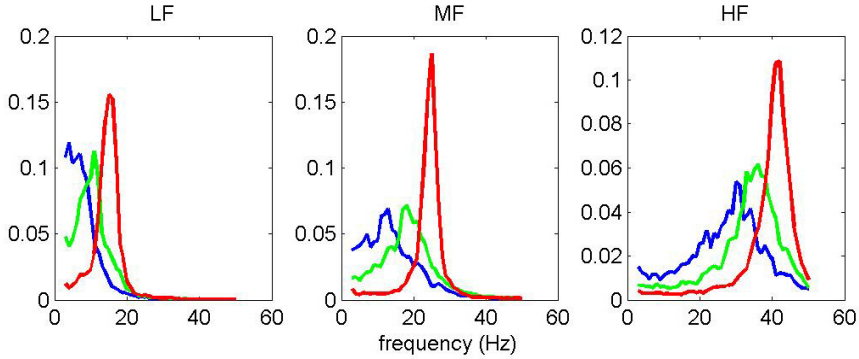

Figure 1.4 – Examples of how the position of the peak generated by each population can be finely tuned, by acting on the average gain of the fast inhibitory synapses (i.e., on parameter G in Eq. 1.14). All panels represent power spectral densities normalized in the range 3-50 Hz. The left panel describes changes in the first population peak, obtained by giving parameter G^L the values 22.3, 39.0 and 62.5. The middle panel describes changes in the second population peak, obtained by giving parameter G^M the values 28.6, 43.0 and 65.9. Finally, the right panel describes changes in the third population peak, obtained by giving parameter G^H the values 62.5, 75.0 and 93.8.

1.3.2 Fitting of EEG spectra in different regions

The previous analysis demonstrated that peaks within the three frequency bands can be quite finely adjusted by considering three populations and modifying a single parameter, G, in each population. The subsequent step is to build a three-population model (or three-kinetic model) and to check whether its output ($v_{out}(t)$ in Eq. 1.17) can be fitted to cortical EEG in different regions. Our idea is that the position of the peaks can be determined by acting on parameter G in each population, whereas the amplitude of the peaks depends on the excitation received by the population (i.e., on the mean value, m, and standard deviation, σ^2, of the noise term p(t) in Eq. 1.6). We are aware that exogenous input may above all reflect connectivity among regions. However, the problem of connectivity is voluntarily neglected in this chapter. As commented in the final section, analysis of connectivity will represent a pivotal application of the present model in other studies described in Chapter 2.

Accordingly, in order to fit real EEGs in different regions, we acted on 9 parameters: they are the mean values (m^L, m^M and m^H) and standard deviations (σ^L, σ^M and σ^H) of exogenous noise, and the fast inhibitory average gains (G^L, G^M and G^H) in the three populations. These parameters have been fitted on real data, as described in section 1.2.3. All other parameters are fixed at the value reported in Tab. 1.1.

A first example of the results obtained by the minimization algorithm is presented in Fig. 1.5, with reference to the six different regions depicted in Fig. 1.2. For each ROI, cortical EEG was computed, starting from EEG measurements performed on the scalp during a finger movement task, as described in section 1.2.2. Each cortical signal has a duration of 0.6 s and was sampled at 250 Hz. The values of estimated parameters are reported in Table 1.2 (see I subject). As it is clear form Fig. 1.5, cortical EEG in different ROIs exhibits a different frequency content: while some ROIs (ROI 5R) exhibit a well defined peak in the beta range, others exhibit a single peak in the alpha band (ROI 5L) or in the gamma band (ROI 6AR and ROI 46R). ROI 6AL does not exhibit any specific peak, with most of its power spectrum at very low frequencies. Finally, ROI 46L exhibits two peaks in the beta and gamma ranges, together with a significant low-frequency content. The model is able to mimic this variety of spectra very well, by acting on the

9 estimated parameters. In particular a peak can be suppressed by reducing the mean value of the input noise, while the use of a larger or smaller variance further modulates the amplitude of the peak.

A second example is shown in Fig. 1.6, while the corresponding estimated parameter values are reported in Table 1.2 (see II subject). In this case too the model is able to fit spectra quite well. We can just observe that the peak in ROI 46L is narrower in the model than in the real data. This difference, however, might be due to the short duration of the real EEG used to compute PSD (0.6 s) which might cause a broadening of the frequency band.

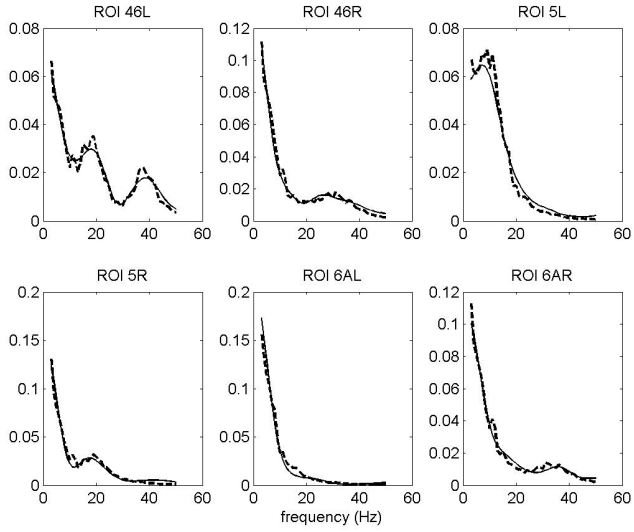

Figure 1.5 - Fitting of experimental EEG power spectral densities from the six regions of interest (ROIs) shown in Fig. 1.2, during a finger movement task (I subject). The model used for the automatic fitting procedure was obtained by arranging three single population models in parallel. Dashed line represents power spectral denisity simulated by the model of a ROI. Continuous line represents experimental PSDs, evaluated on a signal with 0.6 s in length, averaged over more than five hundred of artefact-free trials. All PSDs are normalized to have unitary area in the range 3-50 Hz. Parameters used during the minimization are the mean values (m^L, m^M and m^H) and standard deviations (σ^L, σ^M and σ^H) of exogenous noise, and the fast inhibitory average gains (G^L, G^M and G^H) in the three populations (see Table 1.2, I subject). Hence, the three populations in each ROI have the same time constants and differ as to the value of fast inhibitory synapses and gaussian white noise.

Table 1.2

Estimated parameters for six regions of interest (ROIs), during the right finger movement in two subjects.

	G^L	G^M	G^H	$(\sigma^L)^2$	$(\sigma^M)^2$	$(\sigma^H)^2$	m^L	m^M	m^H
I Subject									
ROI 46L	14.9	47.6	75.0	28.7	45.8	33.1	43.6	154.8	117.5
ROI 46R	14.9	57.1	56.3	42.0	19.0	84.5	59.6	-20	88.2
ROI 5L	39.1	33.0	51.1	10.0	5.2	6.6	85.8	-43.7	-59.6
ROI 5R	14.2	37.3	75.0	72.7	38.8	9.9	105.1	87.1	-43.3
ROI 6AL	17.4	31.8	56.3	59.4	9.7	9.0	112.5	-50.1	-45.0
ROI 6AR	17.4	45.1	66.2	0.5	16.9	10.4	102.5	-57.1	121.3
II Subject									
ROI 46L	4.8	25.1	66.2	5.01	2.7	25.5	56.3	-3.6	103.2
ROI 46R	14.2	29.6	59.2	75.5	23.2	63.6	67.8	-21.4	91.2
ROI 5L	24.0	57.1	56.3	61.0	30.5	69.0	60.1	-20.6	115.9
ROI 5R	20.8	35.7	66.2	61.0	19.7	47.7	100.8	100.8	103.0
ROI 6AL	18.4	33.0	75.0	58.3	9.6	9.7	111.2	-47.4	-47.1
ROI 6AR	18.4	31.8	160.7	49.6	10.8	9.6	79.9	-55.0	0.0

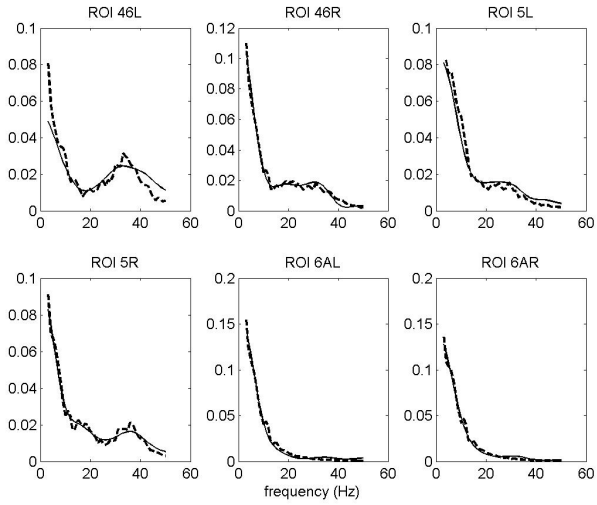

Figure 1.6 - Fitting of experimental EEG power spectral densities from the six regions of interest (ROIs) shown in Fig. 1.2, during a finger movement task (II subject). The significance of the panels is the same as in Fig. 1.5. Estimated parameter values can be found in Table 1.2 (see II subject).

1.3.3 Fitting of temporal changes in EEG spectra

A further important point is the capacity of the model to simulate the temporal changes in EEG power spectral density in one region, during prosecution of a task. To this end, we used a long EEG tracing in the same region (overall duration 12 s) during a working memory task (see section 1.2.2) and subdivided it into consecutive segments of 1 s duration each. For each segment, model parameters were fitted to individual spectra. An example of the obtained results, concerning the last four consecutive seconds from region a312L, is reported in Fig. 1.7, while estimated parameters are reported in Table 1.3. In this case too, the model is able to fit spectra reasonably well, by describing the multiplicity of peaks and the alterations in

their position. Changes in the estimated parameters provide information on the variations in the exogenous input and on internal synapses occurring in the temporal period examined. Analysis of this information may open new possibilities to characterize the behaviour of individual regions during the task, which may represent future model application (see ''Discussion, section 1.4'').

Table 1.3

Estimated parameters for one region of interest (ROI a312L), during a working memory task in one subject (from IX to XII second).

	G^L	G^M	G^H	$(\sigma^L)^2$	$(\sigma^M)^2$	$(\sigma^H)^2$	m^L	m^M	m^H
IX Second	5.9	53.6	40.2	53.1	12.8	23.4	117.5	7.4	3.3
X Second	9.8	37.3	75.0	46.9	27.8	9.8	139.3	90.1	-28.0
XI Second	44.6	40.8	62.5	68.2	9.3	16.9	127.4	0.0	140.4
XII Second	34.7	42.9	75.0	14.1	0.2	2.8	87.0	92.5	150.0

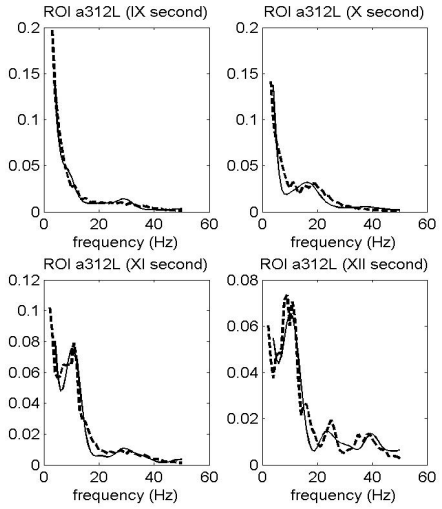

Figure 1.7 - Fitting of experimental EEG power spectral densities in the region of interest a312L at different seconds during a working memory movement task. Each panel represents EEG power spectral density evaluated during a 1 second window. The model used for the automatic fitting procedure was obtained by arranging three single population models in parallel. Dashed line represents power spectral density simulated by the model of a ROI. Continuous line represents experimental PSD, evaluated during a 1 second window. All PSDs are normalized to have unitary area in the range 3-50 Hz. The estimated parameter values can be found in Table 1.3.

1.4 Discussion

The use of mathematical models for the interpretation of functional neuroimaging data has been advocated by several authors in the last years. In particular, information contained in the EEGs risks to be insufficiently understood without a neuro-physiological interpretation of the underlying physiological mechanisms. This interpretation mainly comprehends understanding synaptic changes in different regions, different kinetics of the neuronal populations involved, the input coming from the external world and from other regions in the brain (effective connectivity) during specific tasks. On the other hand, detailed models, which simulate individual neuron dynamics, are often too complex, and contain too many variables and parameters, for being of a practical value in the interpretation of macroscopic events.

A class of models, frequently used starting from the mid-seventies, are neural mass models, which can mimic electrical activity of large neural populations by using a reduced number of state variables. In perspective, these models may be very useful to simulate brain electrical activity in regions of interest, and to assess the effect of changes in brain connectivity during cognitive or motor tasks. Although these models have been largely used to simulate EEG rhythms (Jansen and Rit 1995;Rodriguez et al. 1999;Wendling et al. 2002), and have been recently modified to analyse the effect of connectivity among regions (Jansen and Rit 1995;Wendling et al. 2002;David et al. 2004;David et al. 2005), we are not aware of their use until now to reproduce real patterns of electrical activity in the cortical surface, via a best fitting procedure (see Chapter 2).

The objective of the study presented in this chapter was to analyze whether a neural mass model, consisting of several populations arranged in parallel, can actually be used to interpret and mimic real cortical EEG spectra, by accounting for differences among brain regions involved in the same task, and for temporal differences within the same region. Furthermore, we wished to investigate whether differences in the observed EEG spectra could be ascribed to alterations in the average gain of synapses within the region and in the excitation of populations by external input. These are essential requisite to use these models within the framework of brain neuroimaging, with future emphasis on effective connectivity.

The model for a single population used in our work was originally proposed by Wendling et al. (Wendling et al. 2002) to represent the electrical activity recorded in the hippocampus. Indeed, inhibitory gabaergic interneurons with fast kinetics are well documented in hyppocampal slices of the rat (Bartos et al. 2001;Bartos et al. 2002). Nevertheless, several studies mention that fast inhibitory synapses are also common in the neocortex (Traub et al. 1999). Recently, Traub et al. (Traub et al. 2005) published a complete thalamocortical model, including fast inhibitory synapses from basket cells to cortical interneurons. On the basis of these works, we can assume that the model by Wendling et al. is relevant not only for the hippocampus, but also to represent a single population in the neocortex.

In order to realize a model of a ROI, we arranged three populations in parallel. This is basically the same approach used by David et al. in a recent paper on Neuroimage (David and Friston 2003), although the authors used a different parallel arrangement. We are aware that this choice does not reflect physiology, and that the real arrangement of internal synapses in a region is more complex and a-symmetric (including also feedback connections) than that used here. The possibility to build a more physiological model, reflecting the internal arrangement of synapses among a variety of neural populations may certainly be of the greatest value, but it is at present extremely difficult and beyond the aim of the present study. Data contained in a recent paper by Traub et al. (Traub et al. 2005) may be used to this aim, but such a more physiological model would probably include too many free parameters, and too many internal synaptic gains. Our idea was to concentrate on the input-output relationship of a ROI, (i.e., what input should be given to ROI to produce a given output) since this relationship is fundamental to infer connectivity. We are aware that the present model cannot be used to improve our physiological knowledge on the internal structure of a ROI, but it may be helpful in improving our knowledge about the connectivity patterns among different ROIs. The model has been designed with this purpose, and will be used with this purpose in future works.

There is also another empirical consideration which justifies the use of a parallel arrangement of populations. EEG rhythms are considered a measure of the synchronism among neural populations and representative of the existence of non-linear phase coupling among different oscillators (Ebersole

and Milton 2002). Synchronism generally depends on the presence of strong coupling terms between inhibitory and excitatory populations which are engaged in the same oscillatory activity (Ursino et al. 2003). Hence, according to a parallel arrangement, it is reasonable to assume that populations which participate to the same rhythm are more strongly reciprocally interconnected than population engaged in different rhythms.

The present simulation results suggest a few new considerations that should be taken in mind in order to use these models in conjunction with cortical EEG data, at least during the considered tasks:

i) three populations arranged in parallel (i.e., a three kinetics model) are sufficient to account for the complexity of the observed EEG spectra in the range 3-50 Hz sufficiently well. Although the use of a greater number of populations might be useful to improve some aspects of the EEG spectra in the most difficult conditions (for instance, to simulate the spectrum depicted in the bottom panels of Fig. 1.7), we deemed the introduction of a fourth population unnecessarily cumbersome.

ii) The three populations may produce different rhythms in the EEG, which correspond to peaks in the power spectral density. The amplitude of these peaks mainly depends on the level of activity in each population. In particular, a population may be silent or strongly active depending on the mean value and variance of the input noise. This aspect may become important in future applications of the model, devoted to the investigation of brain connectivity among different regions. In fact, in real conditions the different regions do not receive external noise only, but part of their input may derive from other regions participating to the same task. Hence, changes in connectivity may result in well-detectable changes in population activity and in the consequent EEG spectrum.

iii) The position of the individual peaks may be finely tuned acting on the average gain of the excitatory and inhibitory synapses within a region, without modifying the synaptic kinetics. Of course, a complete analysis might consider a change in the average gains of both excitatory and slow inhibitory as well in fast inhibitory ones (i.e., in parameters A, B and G simultaneously in Eqs. 1.2, 1.6, 1.10 and 1.14). However, we do not think that all these parameters can be individually estimated looking at EEG only. Our preliminary simulations (not reported here for brevity) suggested that it is especially the ratio of fast inhibitory vs. slow excitatory-inhibitory

synapses which modulates the position of the peaks. In order to reduce the number of free parameters, in the present work we modified only the average gain of fast inhibitory synapses. As suggested by Horwitz et al. (Horwitz et al. 1999), more complete information on synaptic changes might be obtained by coupling EEG signals (which are a measure of excitatory activity in pyramidal neurons) with data obtained with other neuroimaging techniques (such as fMRI or PET) which measure metabolic changes, more closely related with the overall (inhibitory + excitatory) synaptic activity. In this regard, the use of physiological models may have an important function to link data obtained with different techniques into a single theoretical framework.

Among the estimated parameters, we included the mean value and variance of input random noise. This choice and the values of estimated parameters deserve some considerations. During a real cognitive task the input to a population is a time-varying dynamical process. In the present work we tried to capture the time varying properties of the changing input by subdividing the task into different epochs (of 1 second each, see Tab. 1.3), and by estimating the mean value and variance of the input noise in each epoch. It would be possible to reduce the duration of the epochs (to better capture the time varying properties of the input noise) but this would worsen the resolution of the computer power density spectra. Our objective in future works (see Chapter 2) is to replace the random noise with a signal coming from other ROIs, according to a connectivity circuit. A time-varying input noise will be used just to mimic the excitation to the ROIs initiating the target (such as the ROI 5L in the motor task), whereas inputs to the remaining ROIs will be derived from the connectivity circuit.

It is worth noting that that the estimated mean value for the input noise, reported in Tab. 1.2 and 1.3, may assume negative values. This may be surprising since this noise represents an average density of afferent action potentials. A negative mean value for the input noise was necessary to maintain some populations in the ROI silent (that is, almost completely inhibited). There are two possible explanations for this finding. a) the population receives inhibition from other populations or from the thalamus, and a negative mean value for the noise can be interpreted as a prevalence of inhibition over excitation. This might be explicitly included in the model by adding a further noise term as input to inhibitory neurons, but this would

increase the number of estimated parameters. b) the position of the sigmoidal relationship may be translated to the right, so that a population would be in a silent state (i.e., in the lower plateau of the sigmoid) by using a noise with zero mean value. We prefer the first solution, since we think that a population may be maintained silent by inhibition exceeding excitation.

An interesting aspect, which deserves some comments, is the value of time constants (inversely related to parameters a_1, b_1, g_1) used for the three populations. Such values changed according to the frequency bands considered (theta-alpha, beta and gamma). Although the relationship between time constants and frequency-band can be in part argued "a priori", there are several non-linear factors which complicate the final result and keep away from a purely analytical solution. The position of the peak is dramatically affected not only by the time constant, but also by the average gain of the fast inhibitory synapses. By increasing the average gain of fast inhibitory synapses, the peak moves to the right (see Fig. 1.4). This phenomenon interferes with the choice of the synaptic time constants. Moreover, in order to have appropriate frequency bands, we must modify not only the time constants of fast inhibitory synapses, but also those of slow inhibitory interneurons and of the excitatory cells.

For excitatory time constants we obtained from 25 ms in the theta and alpha frequency ranges up to 9 ms in the gamma band. Such values for the time constant are usually found for glutamatergic synaptic transmission mediated by NMDA (N-methyl-D-aspartate) receptors, found in the cerebral cortex as well as in the cerebellar nuclei. For the slow inhibitory we got from 50 ms in the theta band up to 25 ms in the gamma band. The values obtained in the theta band for such inhibitory time constants are consistent with those obtained experimentally from in vivo studies of brain of mice related to the GABA neurotransmitter (Molyneaux and Hasselmo 2002). The interest in this lyies in the fact that other independent computational modeling suggests that phasic changes in strength of synaptic transmission could allow separate phases of encoding and retrieval in the hippocampal formation (Hasselmo et al. 1996;Wallenstein and Hasselmo 1997a;Wallenstein and Hasselmo 1997b;Hasselmo et al. 2002). The value of fast inhibitory synapses of the third population appears very small (down to 1.2 ms). However, there are some arguments which justify this choice. First, with the use of higher time constants it is very difficult to obtain a peak of EEG activity in the

gamma-band; consequently, fitting of the high frequency portion of the spectra significantly worsens. Second, inhibitory post-synaptic currents with very fast time constants have been observed by Bartos et al. (Bartos et al. 2001;Bartos et al. 2002) in the rat hippocampal slices. The time constants were 1.2 and 1.8 ms in CA3 and CA1, respectively. Although these data refer to the hippocampus (see also the comment above) they demonstrate that fast time constants may actually characterize inhibitory synapses. Furthermore, in a recent model Traub et al. (Traub et al. 2005), used a time course for GABA conductances of the kind $c \cdot e^{-t/\tau}$ with $\tau = 3$ ms for basket cell to cortical interneuron connections. It is worth noting that the previous equation assumes an instantaneous rising time, and a slower decay time. Our equations for synaptic dynamics lead to an impulse response of the type $c \cdot t \cdot e^{-t/\tau}$, with a peak at $t = \tau$ and a subsequent decay with time constant τ. The equation by Traub et al. can be simulated quite well with our synaptic kinetics if the time constant in settled in the range 1.0-1.5 ms. Furthermore, Treves (Treves 1993) demonstrated that the time constant of synaptic integration in a mean-field model (i.e., a model without an explicit description of spikes) can be chosen much smaller than the membrane time constant, in conditions where a neuron receives much input.

Taken together, the results obtained for the time constants of the modeled populations are compatible with the class of the neurotrasmitters usually found at the cortical level, in the Brodmann regions considered.

The results summarized above may open some new perspective in the use of neural mass models in conjunction with EEG measurements. First, activity in different regions can be summarized using a few parameters for each region, describing the activity level of populations with a different kinetic, and (although partially) the modulation in their internal excitatory-inhibitory synaptic loops. Even more important, our results indicate that the present model of a single ROI may become the brick for building more sophisticated networks of interconnected brain regions. A subsequent improvement in that direction will be to replace the exogenous noise into the different ROIs, used in the present study, with a more complex input term, which accounts for possible connections among the different regions involved in the simulated task (see Chapter 2). This will be a fundamental advance, for funding the analysis of effective connectivity on physiological models, rather than on empirical algorithms. A first step in that direction was

presented by David et al. (David and Friston 2003) recently. In their work, the authors investigated how connectivity among two ROIs may affect peaks in the spectrum and the coherence between signals. The authors, however, did not use their model to fit real EEGs. A fitting to real EEG signals was achieved by Rowe et al. (Rowe et al. 2004), using a biophysical model of brain activity. Their model, however, aspires to simulate the effect of overall brain activity on scalp EEG. By contrast, our study was mainly concerned with electrical activity in individual restricted regions in the cortex. In our work, scalp EEG was propagated to the brain surface using an inverse propagation model, and attention was focused on an internal representation of brain regions. Hence, our study aspires to evolve toward brain connectivity analysis in individual ROIs. By contrast, the model of Rowe et al. aspires to simulate the effect of the overall brain activity on EEG at a particular site in the scalp (in particular, the authors used the central site Cz in their study).

Finally, it may be interesting to analyze lines for future works and possible applications of the present model.

A first important point is that, in the present study, we did not try to provide a physiological explanation of the obtained results, but just to demonstrate that the model is able to fit real cortical EEG power spectral densities in a variety of spatial and temporal conditions. The values of synaptic weights and of the excitatory input in selected ROIs may be exploited in future works to reach a deeper understanding of electrical activity changes occurring during a task. This description may represent a simple way to summarize the distribution of EEG power spectral density in a quantitative fashion, based on a few parameters only, and a simple way to follow its temporal and spatial changes.

A second point may concerns the relations of the present model not only with cortical EEGs, but also with data obtained by other techniques, more related with metabolic activity (such as fMRI and PET). For instance, Horvitz et al. (Tagamets and Horwitz 1998) developed a multi-layer neural mass model to simulate a delayed match-to-sample task, and used this model to mimic PET data obtained in the prefrontal cortex. Metabolic data can be obtained, with our model, by computing a quantity related with the sum of all synaptic activities.

Perhaps the most interesting evolution of this study may consist in building network of functionally connected ROIs, by replacing the external noise with terms reproducing effective connectivity (see Chapter 2). The final purpose of this network may be to realize new methods to assess connectivity from EEG data, based on non-linear models and neuro-physiological relationships among quantities.

CHAPTER 2

USE OF A NEURAL MASS MODEL FOR THE ANALYSIS OF EFFECTIVE CONNECTIVITY AMONG CORTICAL REGIONS BASED ON HIGH RESOLUTION EEG RECORDINGS

2.1 Introduction

Brain processing, even during simple cognitive tasks, is the result of the interaction among several cortical regions, which are reciprocally interconnected and functionally integrated. In this context, a crucial role in the neurophysiology is played by the concept of brain connectivity. Knowledge of connectivity is considered essential today to understand how the brain works, and to assess the role of different regions in the achievement of specific cognitive functions. However, connectivity can be defined in several alternative ways (Wendling et al. 2002;Lee et al. 2003a;Lee et al. 2003b), which have a different theoretical and practical impact: anatomical, functional and effective connectivity. In particular, while functional connectivity has been defined as "the temporal correlation between spatially remote neurophysiological events" (Friston et al. 1993), effective connectivity is concerned with "the influence that one neural system exerts on another one" (Friston et al. 1993). An improved definition, provided recently, considers effective connectivity as "the simplest brain circuit that would produce the same temporal relationship as observed experimentally between cortical sites" (Horwitz 2003). Although both functional and effective connectivity are of physiological relevance, they have a different meaning and subtend different theoretical ideas. The definition of functional connectivity is "model free", whereas effective connectivity requires the formulation of a causal model connecting several brain regions of interest (ROIs). Connectivity has been evaluated, in several recent studies, both starting from neuroimaging data (such as PET or fMRI) (Rowe et al. 2005;Erickson et al. 2005) and from high-resolution scalp

electroencephalograms (EEG) or magnetoencephalograms (MEG) (David et al. 2005).

A considerable number of approaches has been proposed for the estimation of functional connectivity on EEG signals: among these, one of the first to exploit the concept of directed functional connectivity was the directed coherence (DC), introduced by Saito and Harashima (Saito and Harashima 1981) and generalized by Baccalà and Sameshima (Baccalà and Sameshima 1998). Later, multivariate methods were developed, like the partial directed coherence (PDC), the directed transfer function (DTF) and the direct DTF (dDTF) (Kaminski and Blinowska 1991;Kaminski et al. 1995;Kaminski et al. 1997; Kaminski et al. 2001; Baccala and Sameshima 2001; Korzeniewska et al. 2003; Astolfi, Cincotti et al., 2004; Astolfi et al. 2005). The most diffuse method to estimate effective connectivity in neuroscience is the structural equation modelling (SEM) (McIntosh and Gonzalez-Lima 1994).

Despite the large number of studies appeared in last years for assessment of connectivity from EEG/MEG data, there is no definite consensus today on the method that provides optimal results, nor on the significance of the results obtained, and on the possible causes of error.

An interesting new opportunity, still at the pioneering stage, consists in the use of neurophysiological models (i.e., models based on biology) to derive effective connectivity from real data. These models may be useful to establish causal relationships among remote cortical regions, to gain a deeper insight into the underlying neural processes, and to establish some basic mechanisms for signal generation (including non-linearities).

As we discussed in Chapter 1, section 1.1, two main classes of models are used in neurophysiological simulation: detailed models and mascroscopic models; in our study we considered only the latter.

A neural mass model was used by Tagamets, Horwitz et al. (Tagamets and Horwitz 1998;Horwitz et al. 1999;Tagamets and Horwitz 2000) to simulate a delayed match-to-sample task. To this end, the authors defined a simple local circuit that reflects the role of local connectivity in producing neuroimaging data, and in accomplishing the proposed task, while connections among regions were based on primate neuroanatomical data. Hence, in these studies connectivity is not derived from data, but the model

presupposes a given connectivity to simulate a functional neuroimaging study.

As we briefly discussed in Chapter 1, David et al. (David and Friston 2003) used the Jansen model to simulate how the MEG/EEG spectrum can be modified by changing a few parameters which describe population kinetics, and investigated how these spectra are altered by a simple connection between two coupled cortical areas, or including different hierarchical arrangements (David et al. 2005). The authors reached the conclusion that both the coupling strength and propagation delay have a critical impact of MEG/EEG spectra. Then, the authors used signals generated by the same model to test the validity of different measures of functional connectivity (David et al. 2004). Although these studies have a great importance to show how connectivity may affect spectra, and what kind of information can be extracted, they did not attempt estimation of model parameters based on real data, i.e., the models are not used to explain real waveforms, nor to infer effective connectivity from data.

Also Robinson, Rowe et al. recently proposed a model to generate scalp EEG signals (Robinson et al. 2003), and used this model to estimate neurophysiological parameters from EEG (Rowe et al. 2004) in a broad range of frequency (0.25-50 Hz). These works represent a significant advancement in EEG modelling, and provide an understanding of EEG spectra in terms of cortical and thalamo-cortical mechanisms. However, they are not explicitly devoted to the problem of effective connectivity assessment among ROIs.

The study presented in this chapter continues on the same route, with the aim of using a neural mass model (Wendling et al. 2002) to infer connectivity from data.

In the study described in Chapter 1 we modified the model proposed by (Wendling et al. 2002) to simulate cortical EEGs in some regions of interest (ROIs) during simple tasks (finger movement or working memory tasks). In particular, we showed that a single neural mass model is able to produce a unimodal spectrum, and that different EEG rhythms (in the alpha, beta or gamma frequency range) can be mimicked by the same model acting on the time constants of the synapses. More complex EEG patterns in the range 3-50 Hz, similar to those experimentally observed (containing up to three simultaneous rhythms), could be simulated quite well using the parallel

arrangement of three neural mass models with different synaptic kinetics, each excited with white noise with proper mean value and variance.

While the previous work demonstrated the capacity of simple neural mass models to simulate real cortical EEGs, it was not concerned with the problem of brain connectivity. In particular, in the previous work the input to each ROI was an exogenous input quantity, simulated as a white noise term. By contrast, in a real situation the input to ROIs derives largely from the other interconnected regions, i.e., a realistic model should consider several ROIs which simultaneously excite each others.

The aim of work presented in this chapter is to substantially advance our previous study, by considering the problem of connectivity among several ROIs within the framework of neural mass models. A possible model of connectivity, which accounts for several simultaneous rhythms, and distinguish among different frequency bands, is first presented. Then, examples of the effect of connectivity on EEG power spectral density are shown. Finally, an algorithm is proposed, to infer possible patterns of connectivity from data during finger motor tasks.

Two main objectives are pursued. First, we wish to investigate the effect of different patterns of connectivity among ROIs (each described via the previous model), by using a sensitivity analysis on the parameters specifying this connectivity. The target is to reach a deeper understanding of how EEG spectra are affected by connections among ROIs. Second, we investigate which patterns of connectivity among ROIs can be derived, by using a best fitting procedure between model and data. To this end, high-resolution EEG activity measured on the scalp is propagated to the cortex with a realistic back-propagation model (Babiloni et al. 2005), in order to generate reliable cortical EEGs during the task. The best fitting procedure tries to minimize the square difference between model spectra and real ones, using the strengths of connectivity as estimated parameters.

Results show that the proposed neural mass model can be used to infer a connectivity circuit from high-resolution scalp EEGs. Of course, reliability of the circuit obtained requires further validation studies and comparison with other techniques, as well as a comparison with neuroanatomical and neurophysiological data. Limitations, possible causes of errors of the method and lines for future studies are thus discussed at the end.

To our knowledge, this is the first attempt to estimate connectivity, using a neurophysiological model fitted to real data. Although the results obtained are clearly preliminary, and still require further validation, they may open a promising route in the problem of effective connectivity estimation via physiological models.

2.2 Method

2.2.1 Mathematical model

The description of the model of a single population and of a region of interest, as well as model equations, can be found in Chapter 1, section 1.2.1.; for this reason they are not reported here.

Model of connectivity among ROIs

A critical problem in this study concerns the choice of the model for connectivity among different ROIs. In fact effective connectivity is model-dependent, and different choices may lead to different results. David et al., in a recent paper (David et al. 2005), simulated various types of connectivity among two cortical areas: "bottom-up", top-down" and "lateral". In all these patterns the output is the spike density of pyramidal cells, but the targets depend on the type of connection.

In this chapter we assumed that all connections among ROIs are "bottom-up" in type. This choice is justified by the fact that in this study we will apply our model to a motor task, without entering into a hierarchical organization of the different zones involved. Of course, different types of connections can be included in future works (see also "Discussion, section 2.4") depending on the neuroanatomical and neurophysiological knowledge of the problem under examination.

As described and justified in Chapter 1 the model of an overall ROI has been constructed by using three populations arranged in parallel. In order to simulate connectivity among different ROIs, we computed the average spike density of all pyramidal cells in the three populations (say $z_{out}(t)$). We have:

$$z_{out}(t) = \frac{1}{3} \sum_{k=L,M,H} z_0^k(t) \tag{2.1}$$

where z_0 is spike density of pyramidal neurons (see Eq. 1.3 in Chapter 1, section 1.2.1). Parameters in the three populations have been chosen to obtain peaks in the theta and alpha band (4-12 Hz), in the beta band (12-30 Hz) and in the gamma band (greater than 30 Hz), respectively. These values are reported in Table 2.1. To simulate connectivity, we assumed that the average spike density of pyramidal neurons (i.e., the quantity $z_{out}(t)$ in Eq. 2.1) affects excitatory interneurons in the target region via a weight factor, W, and a time delay, T. This is achieved by modifying the input quantity p(t) in Eq. 1.6 of Chapter 1, section 1.2.1. In the following, in order to deal with several ROIs simultaneously, we will use the subscripts i (or j) to denote a quantity which belongs to the ith (or jth) ROI, while the superscript k will be used to denote the kth population in the same ROI. Hence, the input $p_i^k(t)$ to the kth population in the ith ROI can be computed as follows

$$p_i^k(t) = n_i^k(t) + \sum_j W_{ij}^k z_{out,j}(t-T) \qquad \text{k} = \text{L, M, H} \tag{2.2}$$

where W_{ij}^k is the weight of the synaptic link from the jth (pre-synaptic) ROI to the kth population of the ith (post-synaptic) ROI, T is the time delay (assumed equal for all synapses), $n_i^k(t)$ represents a gaussian white noise with mean value m_i^k and standard deviation σ_i^k, and the sum in the right hand member of Eq. 2.2 is extended to all ROIs, j, which target into the ROI i.

An example of connectivity among two ROIs is illustrated in Fig. 2.1. In the present study, all time delays among ROIs have been taken equal to 10 ms. The weights have been assigned different values, in order to simulate various patterns of connectivity and analyze their influence on the EEG of the downstream region.

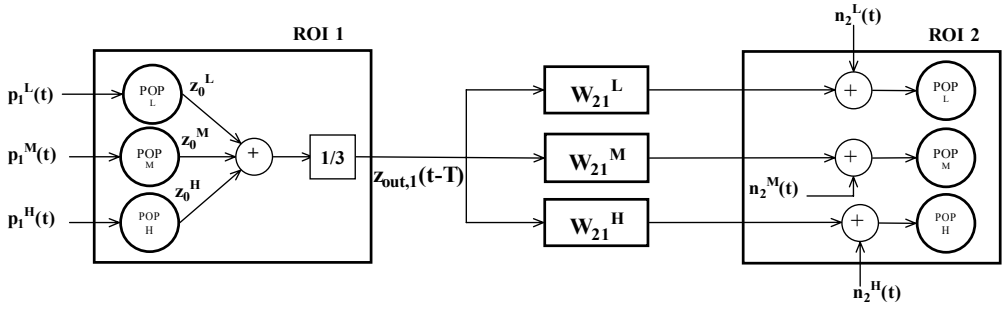

Figure 2.1 - Example of connectivity from one ROI to another one, according to the present model.

Table 2.1

Model basal parameters in common for the three populations.

(see Chapter 1 for the meaning of symbols)

C_1	C_2	C_3	C_4	C_5	C_6	C_7	s_0	e_0	r
135	108	33.75	33.75	40.5	13.5	108	6	2.5	0.56

Model basal parameters different for the three populations.

(Parameters a_1, b_1, g_1 are in s^{-1})

	A^L	B^L	G^L	a_1^L	b_1^L	g_1^L
POP LF	3.3	3.9	25	40	20	300

	A^M	B^M	G^M	a_1^M	b_1^M	g_1^M
POP MF	7.4	6.36	60	85	30	350

	A^H	B^H	G^H	a_1^H	b_1^H	g_1^H
POP HF	6.9	4.7	90	110	40	790

2.2.2 Acquisition of experimental data

In this study we considered the finger tapping task described in Chapter 1, section 1.2.2; for this reason the section ‘’acquisition of experimental data’’ is not reported here.

2.2.3 Best fitting procedure

The best fitting between model simulated EEG of the ith ROI ($v_{out,i}(t)$) and real data has been achieved in the frequency domain, by minimizing the square difference between the power spectral densities in the range 3-50 Hz. Parameters estimated by the minimization algorithm are the connectivity weights, (W_{ij}^k in Eq. 2.2) as shown in section “Results, section 2.3”. The best fitting procedure is the same described in Chapter 1, section 1.2.3; for this reason it is not reported here.

2.3 Results

Effect of connectivity on power spectral density

In the study presented in Chapter 1, the populations in a ROI were stimulated by different levels of external input noise. In the reality, this input noise reflects not only external stimuli, but above all activity coming from other regions participating to the same task and functionally integrated. To account for this aspect, in a first set of simulations we considered a network of three ROIs, and studied how their power spectral densities can be modified by the pattern of connectivity among them. The use of only three ROIs is justified by the necessity to maintain a moderate level of complexity in this initial study, and by the observation that these ROIs may represent the regions of the left hemisphere mainly concerned with the right finger movement task described in Chapter 1, section 1.2.2. In particular, we will assume that the first ROI (subscript i = 1) receives significant input noise but does not receive connections from the other regions. Parameters of the input noise (mean values and variances) has been chosen to mimic the power spectral density in the region ROI 5L of Fig. 1.2, Chapter 1. The results are presented in Fig. 2.2 , where parameters used for the noise are reported in the legend. By contrast, we assumed that the other two ROIs (i = 2, 3) receive negligible excitation ($m^L=m^M=m^H=-50$; $(\sigma^L)^2=(\sigma^M)^2=(\sigma^H)^2=20$) and are activated mainly as a consequence of connections from the other regions. In the rest of this chapter, these two regions are considered representative of regions ROI 6AL and ROI 46L in Fig. 1.2. The previous choice is the same as to assume that region ROI 5L receives most of the external stimulus which triggers the motor task, and drives the other two regions. The latter may further modulate their activity by recurrent connections. This assumption is justified by the observation that, during the performed motor task there is also an anticipatory function that is usually promoted by the superior parietal cortex in humans, here represented by the ROI 5L.

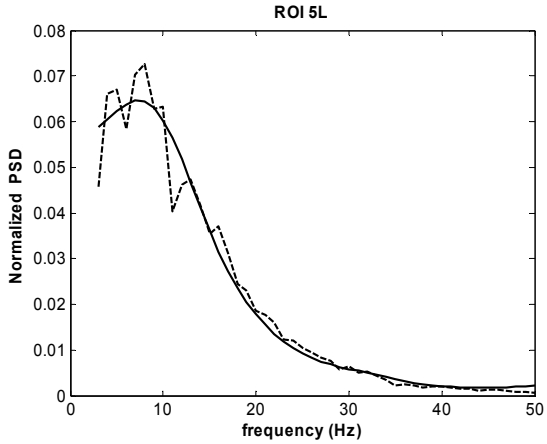

Figure 2.2 - Example of fitting of an experimental ROI (continuous line). The power spectral density of the model output (dashed line) has been obtained using the following values for the mean and variance of the noise in the three populations: m^L=10, m^M=200, m^H=-50, $(\sigma^L)^2=(\sigma^M)^2=(\sigma^H)^2$=20.

Four simple examples of how feedforward connectivity can modify the EEG power spectral density in ROIs 2 and 3 are displayed in Fig. 2.3. This figure illustrates that the pattern of connectivity is reflected into evident and well-detectable changes in the EEG spectrum.

The real situation, however, is more complex than the feedforward examples delineated in Fig. 2.3, due to the presence of reentrant connections among ROIs. Hence, a more complex example is shown in Fig. 2.4. This example differs from the previous for the presence of a feedback between the ROI 2 and the ROI 3. Here we assume that the ROI 3 receives significant connections from the second regions in the medium frequency and high frequency populations, and sends a connection to the low frequency population of the ROI 2. Moreover, ROI 3 is also directly activated by the first ROI.

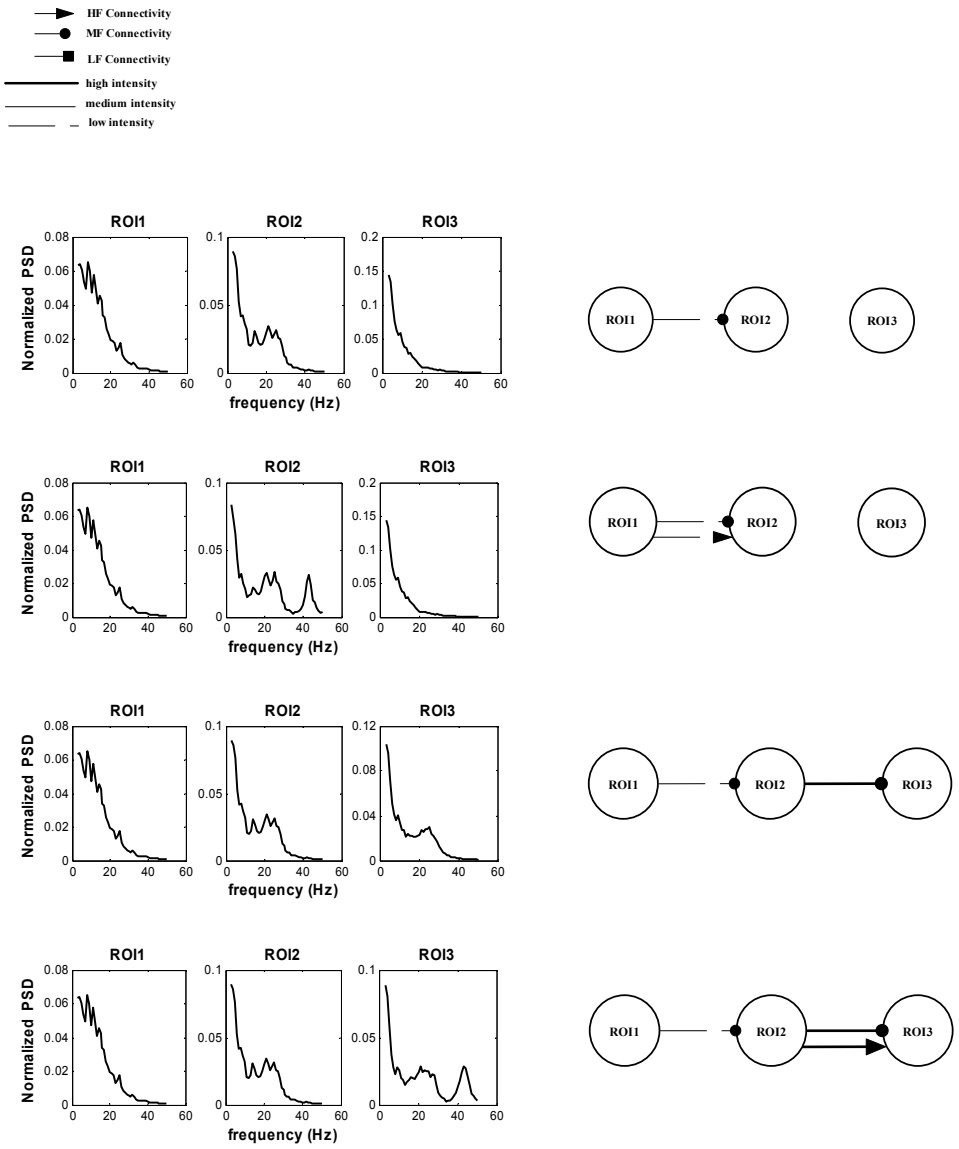

Figure 2.3 – Four examples of hypothetical feed forward connectivity among three regions, simulated by the model of a ROI described before. The values of connectivity used in these examples are: First example: W^{M}_{21}=10. Second example: W^{M}_{21}=10, W^{H}_{21}=10. Third example: W^{M}_{21}=10, W^{M}_{32}=50. Fourth example: W^{M}_{21}=10, W^{M}_{32}=50, W^{H}_{32}=50. Connectivity causes evident peaks in the power spectral density of the ROIs.

In order to clarify the situation, Fig. 2.4 shows the power spectral density of the three ROIs and the temporal activity of all populations involved. As it is evident from Fig. 2.4, the ROI 1 exhibits significant activity only in the low frequency and medium frequency populations, while the high frequency population is almost silent. ROI 2 exhibits significant activity only in the low frequency population. This activity reflects incoming connections from the ROI 1 and ROI 3. Finally, the third ROI exhibits significant activity in the medium frequency and high frequency populations, whereas the low frequency population is silent.

Looking at Fig. 2.4, we can underline an aspect of ROI 3 which deserves particular attention: while the activity of the third population exhibits a large variance, which is reflected in a large peak in the power spectral density, activity in the second population exhibits only a mild variance. This is reflected in a moderate peak in the power spectral density at mid frequencies. The reason is that neurons in the second population of ROI 3 work almost completely in saturation, as a consequence of the strong activation coming simultaneously from ROI 1 and ROI 2. Indeed, power density in neural mass models does not reflect the average level of activation of a population, but rather the variations in activity. In order to better illustrate this point, we repeated the same simulation using a network identical to that in Fig. 2.4, but decreasing the strength of the two connections arriving to the medium frequency population of ROI 3. Results are shown in Fig. 2.5. In this case, neurons in the medium frequency population of ROI 3 are not in saturation, and their activity exhibits a large variance, which is reflected in a large peak of power spectral density at medium frequencies. This example illustrates the apparently paradoxical case in which a decrease in connectivity strength induce an increase in power density, by allowing neurons to exit from a saturation state. This is a direct consequence of the non-linear sigmoidal relationship used in these models to describe the spiking activity of neurons.

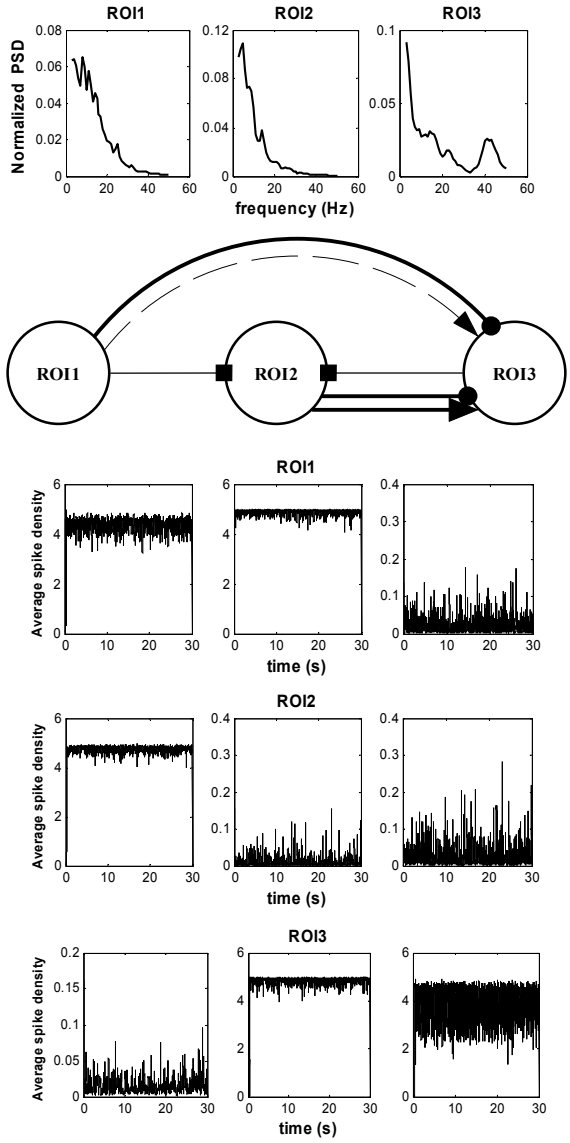

Figure 2.4 – Example of a hypothetical feedback connectivity among three regions, simulated by the model of a ROI described before. The panels show the presynaptic spike density of the three populations (L, M and H respectively) which build the ROIs and the normalized power spectral density of each ROI. The values of connectivity used in these examples are: W_{21}^{L}=20; W_{31}^{M}=50; W_{31}^{H}=10; W_{32}^{M}=50; W_{32}^{H}=50; W_{23}^{L}=20. This example is more complex than the previous ones and the connections cause evident peaks in the ROIs and some saturations in spike activities. The saturation obscures the peaks (see the second population in ROI 3).

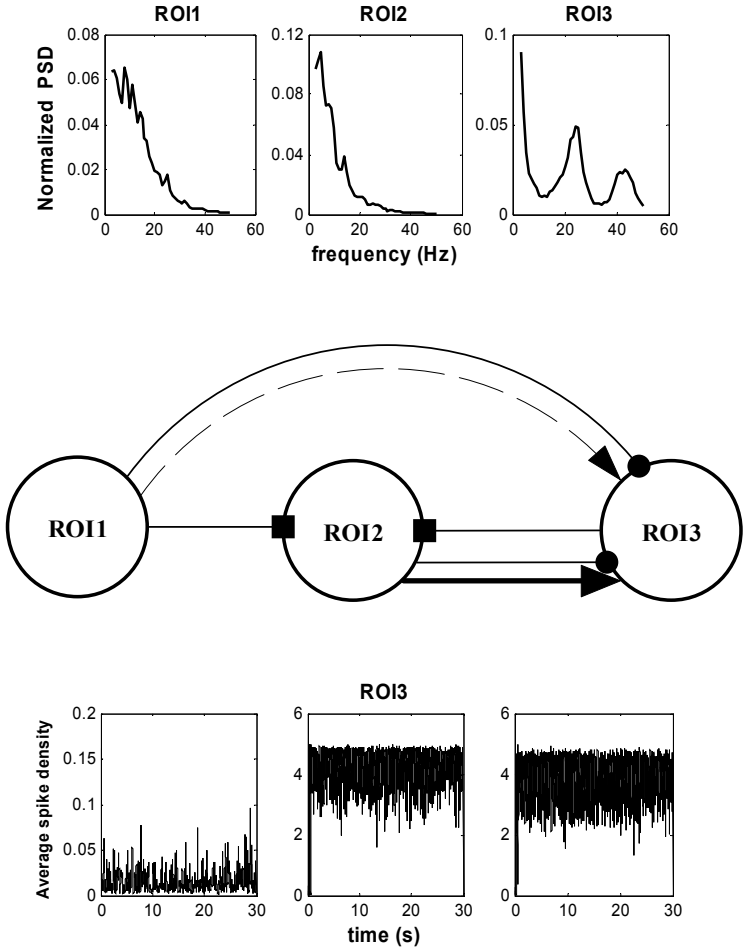

Figure 2.5– Example of a hypothetical feedback connectivity among three regions, simulated by the model of a ROI described before. This example differs from the one shown in Fig. 2.4 since we decreased the connection strength to the medium frequency population of the third ROI, i.e., we have: W_{31}^{M}=20; W_{32}^{M}=20. The effect of this reduction in connection strength is that the peak in the beta frequency range of the power spectral density in ROI 3 is more evident than in the previous example, since the medium-frequency population of ROI 3 is no longer in a saturation state. The panels show the normalized power spectral density of each ROI and the presynaptic spike density of the three populations (L, M and H respectively) which build the third ROI. The presynaptic spike densities of the other ROIs are not shown, since their activity is similar to that in Fig. 2.4.

Estimation of connectivity strength on real data

The last step in this study concerns estimation of parameters W_{ij}^{k} in Eq. 2.2, starting from real data. As described in Chapter 1, section 1.2.2, these data concern cortical EEG in several ROIs obtained from measurement on the scalp with the inverse propagation algorithm, during a finger movement task. As described in "Method, section 2.2", best fitting has been achieved by minimizing a least square criterion function of the difference between model and experimental power spectral density, in the range 3-50 Hz with a resolution of 1 Hz. In performing the minimization algorithm we assumed, as in the previous subsection, that ROI 1 does not receive any connection from the other regions, but receives a significant input noise, whereas the ROI 2 and ROI 3 receive negligible input noise but may receive all possible connections from the other ROIs, including self connections. Thus unknown parameters for the algorithm are all connectivity weights W_{ij}^{k}, with i = 2, 3, j = 1,2, 3, and k = L, M, H. The total number of estimate parameters is 18. However, as shown below, most of these parameters will be given a value close to zero by the algorithm, i.e., only a small number of connections is sufficient to mimic the observed power spectral density.

Results obtained by the minimization algorithm are presented in Fig. 2.6, where a block diagram of the estimated connections is also shown. The numerical values of parameters W_{ij}^{k} are given in Table 2.2 (see I subject). It is noticeable that just 6 connections weights are significantly different from zero at the termination of the algorithm. All other connections, including all self connections, assume negligible values. The algorithm suggests the presence of a feedforward connection from ROI 1 to ROI 2 at low frequencies, and from ROI 1 to ROI 3 at high frequencies. Moreover, the algorithm puts in evidence the presence of significant recurrent connections between ROI 2 and ROI 3: from ROI 2 to ROI 3 at medium and high frequencies, and from ROI 3 to ROI2 at low and high frequencies. Although the present results are just preliminary, they show that power spectral density can be mimicked using a simple circuit simulating effective connectivity. The same algorithm has been applied to the second subject performing the same task, obtaining quite similar values of estimated parameters (see Tab. 2.2, II subject). We can just observe the presence of a new (weak) connection from ROI 1 to ROI 3 at medium frequencies, and the absence of

the (weak) connection from ROI 2 to ROI 3 at high frequencies. All other connections remain quite similar, suggesting a quite repetitive result.

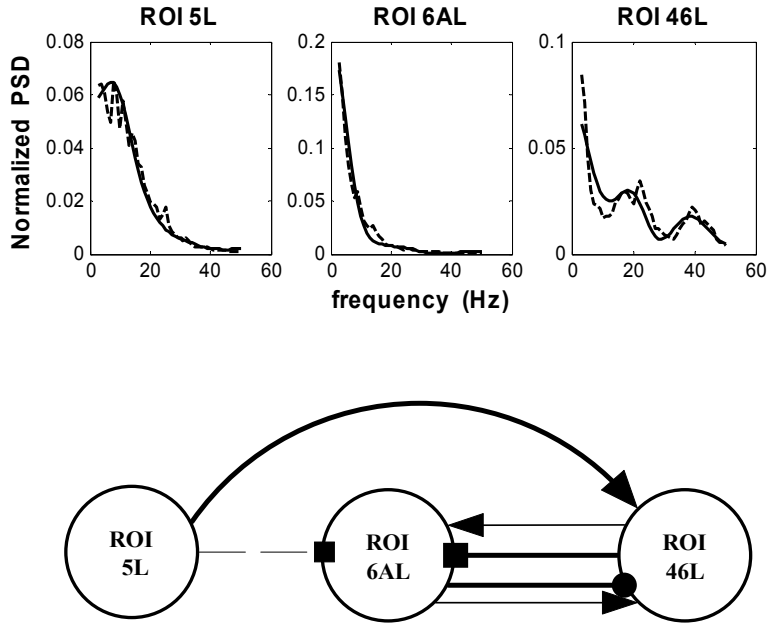

Figure 2.6 – Example of model fitting to three real power spectral densities, belonging to regions ROI 5L, ROI 6AL and ROI 46L of Fig. 1.2, Chapter 1. Fitting has been achieved by estimating the connection strengths among populations (see text for details). Continuous lines represent experimental Power Spectral Densities, while dashed lines are model ones. All spectra have been normalized, to have unitary area in the range 3-50 Hz. Estimated parameters are shown in Table 2.2.

Table 2.2

Estimated connection strengths parameters for three ROIs (5L, 6AL, 46L) connected during the right finger movement in two subjects.

	W_{21}^{L}	W_{23}^{L}	W_{31}^{M}	W_{32}^{M}	W_{31}^{H}	W_{32}^{H}	W_{23}^{H}
I Subject	0.35	1364.50	0.00	110.13	53.12	2.17	6.96
II Subject	0.37	1268.60	5.17	3.65	35.19	0.00	7.40

2.4 Discussion

The study of brain connectivity represents a fundamental aspect of neurophysiology today. In fact, an integrate understanding of human brain function requires not only knowledge of the different areas involved in a given task, but also of their reciprocal connections and functional links. Various authors in past years suggested that neural mass models may represent a promising tool for the analysis of this problem, in association with data obtained with functional neuroimaging techniques (fMRI or PET) and/or high resolution EEG or MEG (Horwitz et al. 1999;David et al. 2005;Rowe et al. 2005;Erickson et al. 2005). In this chapter we aspire at analyzing the possible use of an update neural mass model, for the study of brain connectivity. The study was developed in different phases, which represent necessary steps toward a deeper understanding of the potential benefits and limitations of the proposed model.

The first simple step was accomplished in the previous chapter; it consisted in the realization of a model for a ROI which represents a good compromise between computational simplicity and completeness. More specifically, our purpose was to arrive at a model able to simulate the main characteristics of cortical EEG power density in the range 3-50 Hz, by simply acting on its input. To this end, we adopted a model composed of three subpopulations arranged in parallel, each population simulated as in Wendling et al. (Wendling et al. 2002), but with different values of parameters (in particular, with different synaptic kinetics). In the previous chapter we verified that the proposed model for a ROI is able to simulate different EEG PSDs, by simply assuming a different input noise. This was a necessary requisite to use the model as an instrument to generate reliable signals and/or to infer connectivity from data.

The work presented in this chapter significantly advances the previous one concerning two main aspects. First, we proposed a new model of connectivity, and tested how connectivity may modify EEG power density. The following questions were analyzed. Does connectivity result in a clear change in EEG PSD? Does this change reflect the imposed connectivity in a simple and straightforward way, at least in case of feedforward connections? Can the model be used as a simulation tool to show how different patterns of connectivity result in different PSD spectra? (that is a direct use of the model

as a data generator). Although in the present chapter we displayed just a few exemplary simulations (but many others can be performed) these clearly show that connectivity induces evident changes in spectral content.

The example of feedforward connectivity among ROIs, depicted in Fig. 2.3, resemble those shown in David et al. (David and Friston 2003). However, there are significant differences between our model of connectivity and that used by these authors. These differences may be reflected in different circuits for the interpretation of data. First, in David et al. connectivity from one ROI to another is described only by means of a constant gain factor and a time delay. By contrast, we used three gain factors, assuming that the connection strength may vary depending on the sub-population involved (i.e., with slow, medium or fast kinetics). The main consequence of this choice is that, in our model, a presynaptic ROI may induce a rhythm in a different frequency-band of the target ROI, i.e., it is not necessary that the pre-synaptic ROI contains the same rhythm that it induces downstream. This is evident, for instance, in Fig. 2.3, where a rhythm at medium frequencies appears in the ROI 2, although this was not evident in ROI 1. We judge that this possibility is important to arrive at a proper understanding of connectivity. In fact, looking at the PSD in the six ROIs during finger movement, we observed the presence of some peaks in the frontal region (46L) which were not present in the other ones. A further advantage of our approach, is that connectivity may be described in the frequency domain: it is not a simple scalar number, but a more complex entity which depends on the particular rhythm (or frequency band) considered.

A second major difference between our model of connectivity and that by David et al. is that these authors maintained a constant average input to each ROI, i.e., they preserved mean value and standard deviation of presynaptic input independent of the connection strength (in their work coupling among two ROIs just modifies the ratio of the input attributable to the source area vs. the extrinsic noise). In other words, coupling does not modify the equilibrium activity of each population. By contrast, in our approach a strong connection may significantly modify the average activity. This has strong consequences, which are underlined in Fig. 2.4. In certain cases, increasing connectivity may lead to a saturation of the post-synaptic population. This saturation may be reflected in a decreased variance of all

quantities in the population and so in a reduced power density in the given frequency band. Hence, in our study non-linear effects become much more evident than in former ones.

The previous steps confirmed that the model can be used as a simulation tool, able to produce reliable signals with different patterns of EEG power spectral density, and to mimic the effect of different imposed patterns of connectivity. The use of the model as a simulation tool can be useful, for instance, to provide artificial signals to test methods actually adopted to infer connectivity from data. The cortical signals generated with the model, assuming a given connectivity, may be propagated to the scalp (using realistic anatomical models of the skull and interposed tissue) and corrupted with noise. These artificial scalp signals can then be used to test algorithms commonly adopted to infer connectivity from scalp EEG (for instance the PDC, see Astolfi et al. (Astolfi et al. 2004)). This use of the model will be exploited in future works.

The last, and more ambitious step of the work described in this chapter, was to check whether the present model, trained with a minimization algorithm, can "discover" a simple pattern of connectivity, starting from real data, under a few basic hypotheses. Is it possible, using a model of interconnected ROIs, to infer a simple pattern of connectivity with an automatic algorithm, so that each ROI produces the same cortical EEG spectrum as data obtained from in vivo measurement?

Results obtained with the minimization algorithm are encouraging. The algorithm found a simple pattern of connectivity, which explains EEG power spectral density carefully, and seemed quite repetitive in the second subject. Moreover, several connections (including all self-connections) assume a negligible strength. Although the estimation algorithm used 18 parameters, just 6 of them was given a value significantly different from zero. Hence, a model with 6 connectivity parameters is able to mimic PSD in the three ROIs of the left hemisphere, during the finger movement task.

Although the results are of value, and may open new possibilities in the study of brain connectivity, they should be considered with caution. First, the obtained results depend on the the "a priori" assumptions introduced. In this work, our main assumption was that the region named ROI 5L receives a significant exogenous noise (which may represent the input signal which triggers the task) and drives the other two regions in the left hemisphere

(named ROI 6AL and ROI 46L). The latter two ROIs are reciprocally connected, and receive small exogenous noise (this exogenous noise may represent input from other regions). Of course, a different "a priori" choice for the connectivity circuit may lead to alterative results (for instance, if one includes connections with ROIs in the right hemisphere, or assumes a feedback connection to the ROI 5L too). The possibility to simulate a larger number of interconnected ROIs, and limitations on the number of free parameters, will be discussed more extensively below.

A second important point is that, even using a priori assumptions, multiple equivalent solutions may exist, and the algorithm discovers just one of them. This is a clear limitation of all minimization algorithms for non-linear problems, i.e., the solution is not unique, and alternative solutions may be found depending on the initial guess. In our problem, this means that other values for the connection strengths among the three ROIs might exist, able to produce similar EEG power spectral density.

Finally, we must consider that, in the present work, we used a constant time delay for all connections among ROIs. Of course, time delays might represent additional parameters for the fitting procedure. As shown in David et al. (David and Friston 2003), time delays may modify the position of the peak in the power spectral density. This problem may be the subject of additional studies with the model. However, we think that additional information (such as cross-correlation) should be required to estimate time delays from data (see below).

According to the previous considerations, we wish to stress that, in this work, we did not aspire to find "true" connectivity from data (indeed, the connectivity concept is strongly model dependent) but to show how the proposed model, trained with real signals, can discover "one possible" solution which describes data quite well.

In the present work we assumed just three interconnected ROIs. Of course, a limitation of the proposed approach consists in the number of parameters, which should be simultaneously estimated, in case of a greater number of interconnected ROIs. Assuming that all self connections can be given a value zero (as confirmed by the present results) and considering N totally interconnected ROIs, the number of free connectivity strengths would be 3 N (N-1) (i.e., each ROI may receive three connections from the other ones). The number would further increase considering time delays.

In order to overcome the typical limitations delineated above (i.e., the dependence of the solution on the "a priori" hypothesis, the uniqueness of solution and the excessive number of parameters) we think that the proposed algorithm should be enriched with additional information. This may comprehend: i) anatomical and neurophysiological "a priori" knowledge. Such information may provide additional constraints on which connections should be included in the model, and which connections should be forced to zero. ii) The minimization algorithm might exploit not only information on power spectral density, but also additional information extracted from data (such as cross-correlation and cross-spectra). This information may be useful to limit the number of possible alternative solutions for the algorithm, and to allow estimation of time delays. iii) As suggested by Horwitz et al. (Horwitz et al. 1999), models may be valuable to integrate data obtained with different techniques (not only EEG or MEG, but also data more related with metabolism, such as those obtained with fMRI or PET, which are especially expression of synaptic activity). Fitting synaptic activity to metabolic data may provide additional constraints for the model. Viceversa, the model may be used as a simulation tool, to interpret fMRI/PET data during cognitive tasks involving different ROIs (but see Horwitz (Horwitz et al. 1999;Horwitz et al. 2000;Horwitz 2003) for excellent examples of this model use).

The problem of multiple solutions might also be overcome, in future works, with the use of more sophisticate optimization methods (such as Monte Carlo techniques, or simulated annealing), that involve a search from a population of solutions, not from a single point. Among these methods, evolutionary algorithms (EAs) (Goldberg 1989) are particularly promising. EAs are search methods that are inspired by Darwinian evolution, i.e., natural selection and survival of the best in the biological world. The solutions with high fitness are recombined with other solutions and mutated by making a small change to them. Recombination and mutation are used to generate new solutions that are biased towards regions of the space for which good solutions have already been obtained. Of course, the counterpart of this technique is the high computational time required to run the minimization algorithm several times, with different values of the initial guess.

In conclusion, the present chapter was focused on the possibility to use neural mass models to analyzing data on brain function, in the same direction as that previously investigated by other groups (Horwitz et al.

1999;Horwitz 2003;Rowe et al. 2004;David et al. 2005). The emphasis of this chapter is on the possibility to use these models to infer information on connectivity, either using the model as a simulator, to generate signals and/or to gain a deeper insight into to possible effect of connectivity on measured data, or as a part of an algorithm, to derive connectivity from data. Although the last step is still at a preliminary stage, the present work represents a first promising attempt in that direction.

CHAPTER 3

THE EFFECT OF CONNECTIVITY ON EEG RHYTHMS, POWER SPECTRAL DENSITY AND COHERENCE AMONG COUPLED NEURAL POPULATIONS: ANALYSIS WITH A NEURAL MASS MODEL

3.1 Introduction

Analysis of neural signals (such as electroencephalography (EEG), magnetoencephalography (MEG), functional magnetic resonance imaging (fMRI) or positron emission tomography (PET)), is playing a fundamental role in Neuroscience today, to monitor brain function in humans and to gain a deeper understanding on how the brain works. However, interpretation of these signals in terms of neural activity is difficult and not completely understood yet, for several concomitant reasons.

First, fMRI and PET provide a measurement of metabolic activity in the brain, with high spatial resolution and only poor temporal resolution. As we discussed in Chapters 1 and 2, it is generally assumed (Kadekaro et al. 1985;Nudo and Masterton 1986;Jueptner and Weiller 1995) that this measurement is mainly related with synaptic activity (both excitatory and inhibitory) in the detected zone. Unfortunately, synaptic activity is not linearly correlated with the spike rate of pyramidal neurons, which represents the essential information used in brain processing. By way of example, an increase in synaptic activity (hence in metabolism) may induce only modest changes in spike rate, if both excitatory and inhibitory synapses are simultaneously involved (Almeida and Stetter 2002).

Second, EEG power spectral density is used to infer information on brain activity in different cortical areas, and to study functional links among brain regions. As well known, EEG exhibits several rhythms (in the alpha, beta, gamma or delta ranges): alterations in power density of these rhythms is associated with modification in behavior (such as attentional effects, sleep, cognitive processes, etc.. (Singer 1999;Kubota et al. 2001;Jiang 2005;Strelets et al. 2006)) and may be exploited in the brain-computer

interface (Pfurtscheller and Lopes da Silva 1999;Wolpaw et al. 2002;Pfurtscheller et al. 2004). However, the mechanism which causes changes in EEG rhythms is not fully understood.

As we discussed in previous chapters, a further central problem in modern Neuroscience is integration among the different methods to monitor brain function. EEG/MEG have a higher temporal resolution but less spatial resolution compared with fMRI or PET.

All the problems delineated above may benefit from the use of mathematical models based on a physiological description of neural activity in brain regions. As we clarified in the previous two chapters, mathematical models may help to elucidate the relationship between neural activity, synaptic activity (FMRI, PET) and brain electric potentials (EEG/MEG), and may allow a quantitative analysis of the effect of connections among distal regions. Among the various models proposed in the literature, the so called "neural mass models" or "mean-field models" (Wilson and Cowan 1972;Freeman 1978;Jansen and Rit 1995;Horwitz et al. 1999;Wendling et al. 2002) are particularly suitable to describe activity in large brain areas, since they exhibit an adequate compromise between simplicity and physiological reliability.

Although there are many works in literature which deal with the problem of connectivity and represent significant steps in the use of neural mass models to deepen our understanding of brain activity and clarify neural signal generation mechanisms, there are some major issues which are not addressed. As we discussed in Chapter 1 and 2, cortical EEG spectra, measured during motor and/or cognitive tasks, often exhibit a multimodal pattern, in which different rhythms coexist: in some cortical regions, both peaks in the alpha and beta, as well as in the gamma range are simultaneously present. By contrast, classical neural mass models based on the feedback interaction of excitatory and inhibitory populations reveal a single rhythm at the resonance frequency of the circuit: the corresponding power spectral density (PSD) exhibits a unimodal pattern. Hence, a fundamental problem arises: which model should be used to generate multimodal spectra, as those observed in real scenarios? And which are the mechanisms responsible for the appearance, disappearance or modification of a given rhythm in a cortical region? How can a model account for a change in PSD in different frequency bands? A single neural mass model,

with assigned synaptic kinetics, seems intrinsically unable to deal with these problems. As suggested by David and Friston (David and Friston 2003), models including multiple synaptic kinetics should be used.

We think that addressing these major questions is essential for developing models of neural activity in entire brain areas, which may be exploited to link EEG and functional imaging data, and to found the problem of connectivity on more physiological bases.

Some of the questions raised above have been investigated in recent papers by David et al. (David and Friston 2003;David et al. 2004;David et al. 2005), and in Chapter 1 and 2.

In Chapter 1, we used the parallel arrangement of three neural populations, with different synaptic kinetics, to simulate the simultaneous presence of alpha, beta and gamma rhythms in the same region. We showed that real cortical EEGs, measured during cognitive or motor tasks, can be reproduced quite well with that model, by modifying the exogenous input noise and the intrinsic excitation/inhibition ratio. In a subsequent extension of the same model (see Chapter 2), real EEG power spectral densities were simulated by replacing the external noise with an excitatory input coming from other interconnected regions, thus providing some preliminary indications on how connectivity could be estimated from EEG data.

In the model presented in Chapter 1, as well as in the model by David and Friston (David and Friston 2003), the presence of different rhythms was caused by different populations, which oscillate at their specific resonance frequency. Although this hypothesis is plausible, it has the disadvantage to engender a great number of parameters and equations if one wishes to simulate multiple interconnected areas. Any cortical region encopasses multiple neural populations, each with its own parameters and connection strength. In the present chapter we wish to test an alternative more parsimonious hypothesis: we assume that a single region is composed of only a single population with assigned synaptic kinetics (instead of the parallel arrangement of N populations). As a consequence, if stimulated with exogenous white noise, it oscillates at its own resonance frequency and cannot produce a multimodal spectrum. However, if this population receives excitatory input from another connected region, which oscillates at a different frequency, it may exhibit both its intrinsic rhythm, and the exogenous one. In this manner, spectra with multiple rhythms might

originate inside a single population, avoiding the presence of several synaptic kinetics in the same region.

These conditions are investigated in the present chapter, by considering two or three connected regions, each with its own dynamics. With this model, we show that a single population can exhibit two or three peaks, and that the characteristics of these peaks depend on the internal parameters of the population (such as its synaptic kinetics) and on connectivity with other populations. The model is validated with reference to cortical EEGs evaluated in the controlateral cingulated cortex of 4 human volunteers during a right foot movement task.

3.2 Method

3.2.1 Mathematical model

The description of the model of a single population as well as model equations can be found in Chapter 1, section 1.2.1.; for this reason they are not reported here.

Model of connectivity among populations

In order to study how the populations interact, we then considered a model composed of N populations (in the following examples, $N = 2$ or $N = 3$) which are interconnected through long-range excitatory connections. As in the example shown in Fig. 3.1, connections can include both feed forward and feedback links among populations, with different weights. To simulate the connectivity among populations, we assumed that the average spike density of pyramidal neurons (z_0) acts on the target population via a weight factor, W, and a time delay, T. This is achieved by modifying the quantity $p(t)$ in Eq. 1.6, Chapter 1. In the following, in order to deal with several populations simultaneously, we will use the subscripts i (or j) to denote a quantity which belongs to the ith (or jth) population.

Hence, the input $p_i(t)$ in the ith population can be computed as follows

$$p_i(t) = n_i(t) + \sum_j W_{ij}\, z_{0,j}(t - T) \tag{3.1}$$

where W_{ij} is the weight of the synaptic link from the jth (pre-synaptic) population to ith (post-synaptic) population, T is the time delay (assumed equal for all synapses), $n_i(t)$ represents a gaussain white noise with mean value m_i and standard deviation σ_i, and the sum in the right hand member of Eq. 3.1 is extended to all populations, j, which target into the population i.

In the present study, the time delay and weights among populations have been assigned different values, in order to simulate various patterns of connectivity and analyze their influence on the EEG of the downstream population.

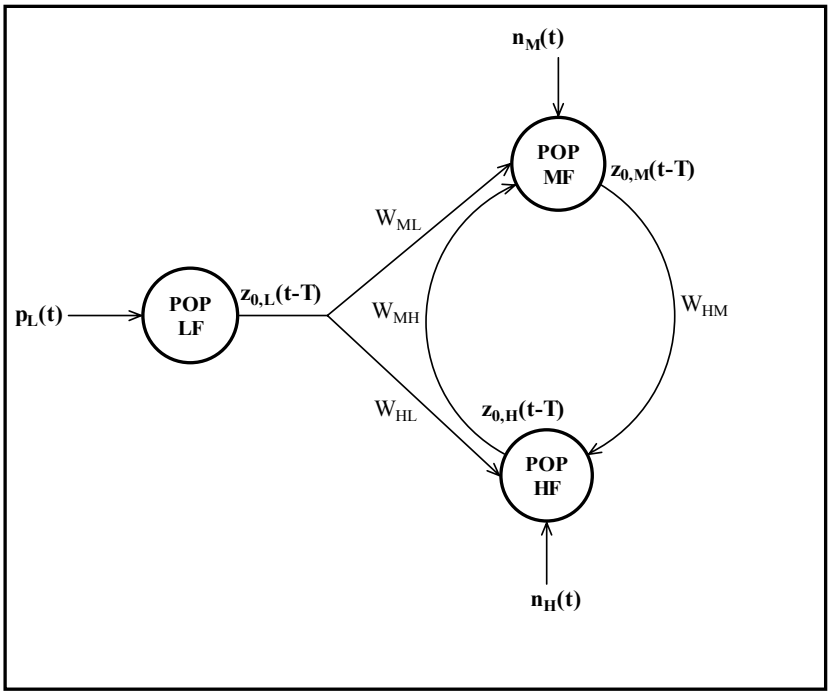

Figure 3.1 – Example of connectivity among three populations, according to the present model. The populations are indicated with LF, MF and HF, to represent rhythms at low, medium and high frequency.

3.2.2 Acquisition of experimental data

Four normal subjects participated in the experiment, which took place in the laboratories of the Santa Lucia Foundation, Rome, after the informed

consent was obtained. Subjects were comfortably seated in an armchair with both arms relaxed, in an electrically shielded, dimly lit room. They were asked to perform a brisk protrusion of their lips (lip pursing) while they were performing a right foot movement. A 58-channel EEG system (BrainAmp, Brainproducts GmbH, Germany) was used to record electrical potentials by means of an electrode cap, accordingly to an extension of the 10-20 international system. A/D sampling rate was 200 Hz. During motor task, subject was instructed to avoid eye blinks, swallowing or any movement other than the required foot movements. Structural MRIs of the subject's head were taken with a Siemens 1.5T Vision Magnetom MR system (Germany). The surface electromyographic (EMG) activity of the muscle was also collected. The onset of the EMG response served as zero time. All data were visually inspected, and trials containing artifacts were rejected. After the EEG recording, the electrode positions were digitized using a 3D localization device with respect to the anatomic landmarks of the head (nasion and two preauricular points). The analysis period for the potentials, time-locked to the movement execution, was set from 1500 ms before to the EMG trigger (0 time).

Finally, A 3-shell Boundary Element Model (BEM) of the head was used to estimate the cortical current density (CCD) distribution in a region of the cortex (the cingulated cortex) starting from activity measured on the scalp. The procedure used is described in (Babiloni 2005) and in Chapter 1, section 1.2.2. From the CCD, the average estimated cortical activity in the region has then been evaluated. The latter has been successively subjected to spectral analysis in order to produce the spectra used for the estimation of the model parameters.

3.2.3 Data analysis

In order to investigate the behaviour of the model both in time and frequency domain, and compare it with real data, the average membrane potentials of pyramidal neurons (considered representative of EEG) were used to calculate the power spectral density (PSD), the cross-correlation functions, the cross-spectra and the coherence. In all the simulations we used a model sample rate of 1 kHz.

Model validation has been performed in the frequency domain, by

comparing the EEG power spectral densities of simulated and real data. In order to eliminate possible differences in amplification all power spectra have been preliminary normalized to have unitary area in the frequency range (6–50 Hz). Parameters individually modified to achieve a good fitting are the connectivity strengths, *Wij*, and the reciprocal of the time constants of excitatory synapses in the three populations, a_1. This fitting was performed with a manual procedure to show that the model can simulate real spectra with only moderate parameter changes. An automatic minimisation procedure would produce a better fitting, but with larger changes in parameters.

The signal processing procedure is the same described in Chapter 1, section 1.2.3; for this reason it is not reported here.

The cross-spectra among different populations in the model have been computed using the discrete Fourier transform (DFT) of the cross-correlation function (cross-covariance) which is calculated normalizing the sequence so that the covariances at zero lag were identically 1.0. Finally, the magnitude squared coherence between two signals (say x and y) is given by

$$Cxy = \frac{|Pxy|^2}{Pxx \cdot Pyy} \tag{3.2}$$

where Pxx and Pyy are the PSD of x and y respectively, and Pxy is the cross spectral density estimate of x and y. All terms in (3.2) were estimated using Welch's averaged, modified periodogram method. Coherence is a function of frequency with values between 0 and 1 that indicates how well the input x corresponds to the output y at each frequency.

3.3 Results

3.3.1 Analysis of a single population model

We considered the three populations modelled as described in Chapters 1 and 2; they have peaks which approximately lie in the theta and alpha band (4-12 Hz), in the beta band (12-30 Hz) and in the gamma band (greater than 30 Hz). In the following, these populations will be indicated as POP LF, POP

MF and POP HF, to represent rhythms at low, medium and high frequency. The corresponding values of parameters are reported in Table 3.1.

Table 3.1

Model basal parameters in common for the three populations.

(See Chapter 1 for the meaning of symbols)

C_1	C_2	C_3	C_4	C_5	C_6	C_7	s_0	e_0	r
135	108	33.75	33.75	40.5	13.5	108	6	2.5	0.56

Model basal parameters different for the three populations.

(Parameters a_1, b_1, g_1 are in s^{-1})

	A^L	B^L	G^L	a_1^L	b_1^L	g_1^L
POP LF	2.7	3.2	22.3	20	20	300

	A^M	B^M	G^M	a_1^M	b_1^M	g_1^M
POP MF	5.2	4.5	57.1	85	30	350

	A^H	B^H	G^H	a_1^H	b_1^H	g_1^H
POP HF	5.6	3.8	173.1	110	40	790

The example shown in Fig. 3.2 illustrates that more subtle adjustments in the position of the peaks can be obtained by acting on a single parameter, in particular on the time constant of excitatory synapses. By changing this parameter we can have a fine control of the position within the corresponding frequency band.

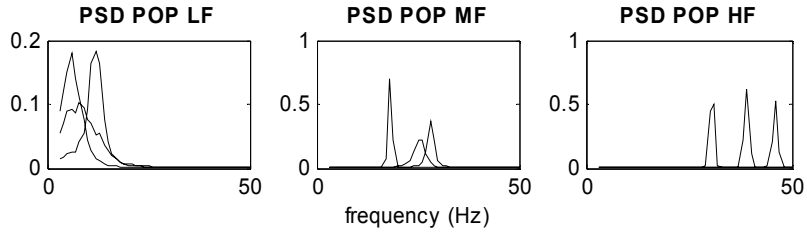

Figure 3.2 – Examples of how the position of the peak generated by each population can be finely tuned, by acting on the inverse of time constant of excitatory cells (i.e., on parameter a_1 in Eqs. 1.2 and 1.6, Chapter 1). All panels represent power spectral densities normalized in the range 3-50 Hz. The left panel describes changes in the first population peak, obtained by giving parameter a_1^L the values 20, 30 and 40. The middle panel describes changes in the second population peak, obtained by giving parameter a_1^M the values 40, 85 and 100. Finally, the right panel describes changes in the third population peak, obtained by giving parameter a_1^H the values 50, 80 and 110.

3.3.2 Analysis of the connectivity model: two populations

Although a single population can produce just a single peak due to its intrinsic resonance frequency, is it possible that it produces a multimodal spectrum if it receives a connection from other populations which have a different frequency.

Hence, we considered the effect of a simple connectivity among two populations, the first at medium (MF), the second at high (HF) frequency. We first investigated the role of the connection strength and then we examined time delay.

Connection strength

Figures 3.3 and 3.4 show the temporal patterns of spikes density and membrane potential (considered representative of cortical EEGs) of pyramidal neurons in each population, the PSDs of the membrane potentials, the cross-correlation function, the cross-spectra and the coherence between the two populations.

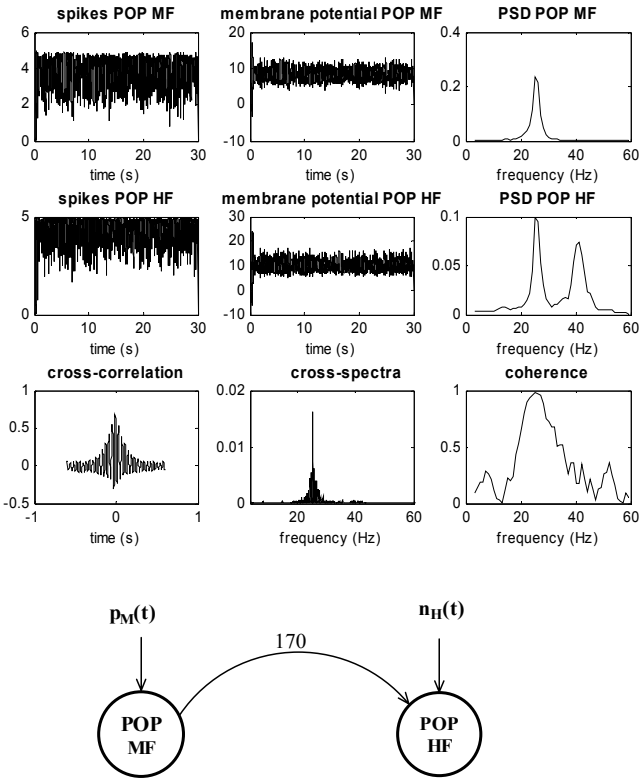

Figure 3.3 – Example of hypothetical feed forward connectivity between two populations (POP MF and POP HF) simulated with the model. The values for mean and variance of the noise and for the connectivity are: m_M =50, m_H=-50, $(\sigma_M)^2=(\sigma_H)^2=20$, W_{HM} =170. The panels in the first and second line show the spike density, the membrane potential and the power spectral density of POP MF and POP HF respectively. The panels in the last line show the cross-correlation function, the cross-spectra and the coherence between the two populations. The power spectral densities have been normalized, to have an area equal to one in the range 3-50 Hz. Connectivity causes evident changes in the power spectral density of the target population.

In Fig. 3.3, POP MF does not receive any connectivity but a strong Gaussian white noise. Hence, it shows its peak at medium frequency due to its internal dynamics. By contrast, POP HF receives a negligible Gaussian white noise but is activated by the other population. As a consequence of this

connection, POP HF shows both its own typical peak at high frequency and a peak at medium frequency caused by POP MF. Accordingly, the coherence function shows a high value (almost 1) in correspondence of the medium frequency band. The cross-correlation function shows a maximum in correspondence of the time delay of connection (10 ms), suggesting that there is a population (POP MF) which anticipates and activates the other one (POP HF).

The previous result confirms that a multimodal spectrum can actually be obtained, even by a single population model, provided that this model is not activated by white noise, but it receives an input signal with a well defined-rhythm different from its intrinsic rhythm.

Figure 3.4a considers a different pattern of connectivity between POP MF and POP HF, in which both populations receive a connectivity from the other one. In particular POP MF receives a strong Gaussian white noise and activates POP HF (W_{HM} = 100). The latter receives a negligible Gaussian white noise and sends back a weaker input to POP MF (W_{MH} = 40), causing a peak at high frequency in its PSD. As well expected, the coherence function and cross-spectrum demonstrate a strong correspondence between the two populations at high frequencies. In this case, however, due to the presence of a feedback connection, it is much more difficult to understand which population anticipates the other by analysis of the cross correlation function.

It is interesting to observe that, with this particular value of parameters, the population HF does not oscillate at medium frequency, i.e., the rhythm received from the first population (about 30 Hz) just triggers the activity of the second at its resonant frequency (≅ 45 Hz) but does not induce a synchronisation. By contrast, oscillation of the second population causes a synchronisation of the activity of the first, which exhibits both rhythms (endogenous and exogenous).

A dual situation can be observed if the strength of the connection which goes from the first population to the second is increased (W_{HM} = 170, Fig. 3.4b). With this value, the second population now exhibits both rhythms, while the first exhibits only its intrinsic rhythm at medium frequency. Hence, we can speculate that, depending on the strength of the re-entrant connections, one population can impose its rhythm to the other.

a)

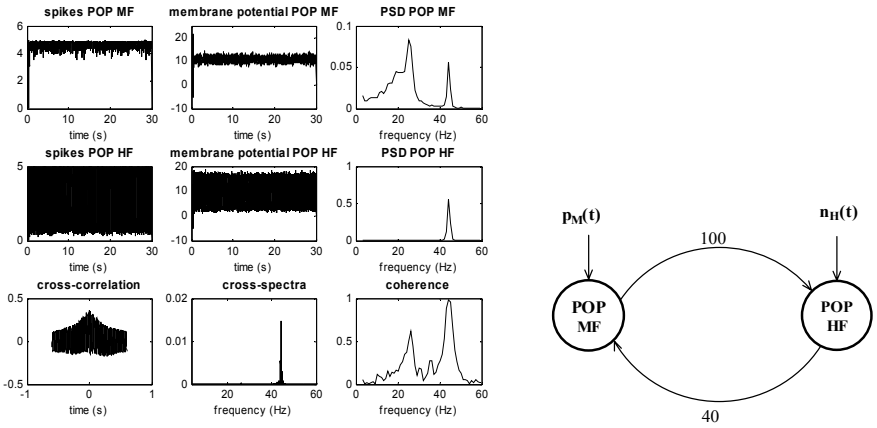

b)

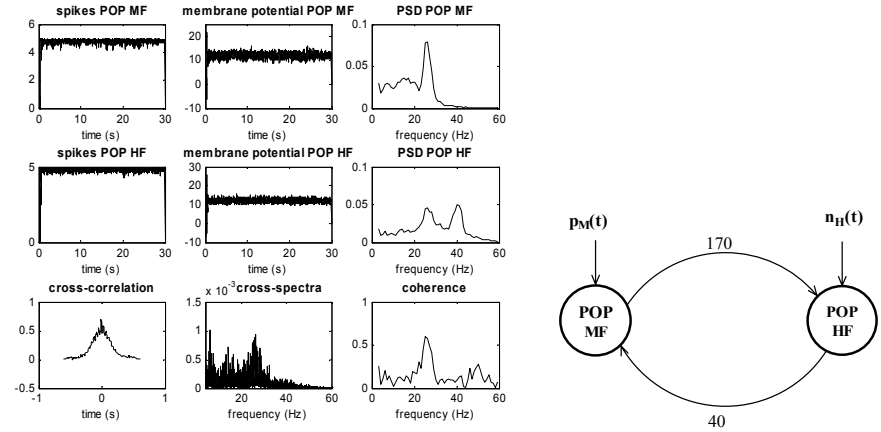

Figure 3.4 – Example of hypothetical feedback connectivity between two populations (POP MF and POP HF) simulated with the model. The values of connectivity used are: Fig. 3.4a: W_{HM} =100 and W_{MH} = 40. Fig. 3.4b: W_{HM}=170 and W_{MH}=40. Mean and variance of the noise in both examples are: m_M=50, m_H=-50, $(\sigma_M)^2=(\sigma_H)^2$=20. The panels show the same quantities as in Fig. 3.3.

In order to investigate this problem more systematically, we performed a sensitivity analysis on parameters representing the connection strengths. The results are summarized in Figs. 3.5 and 3.6. These figures show the values of

the PSD of the two populations, and the value of the coherence function, computed at the two frequencies (about 25 Hz and about 45 Hz) of the two rhythms.

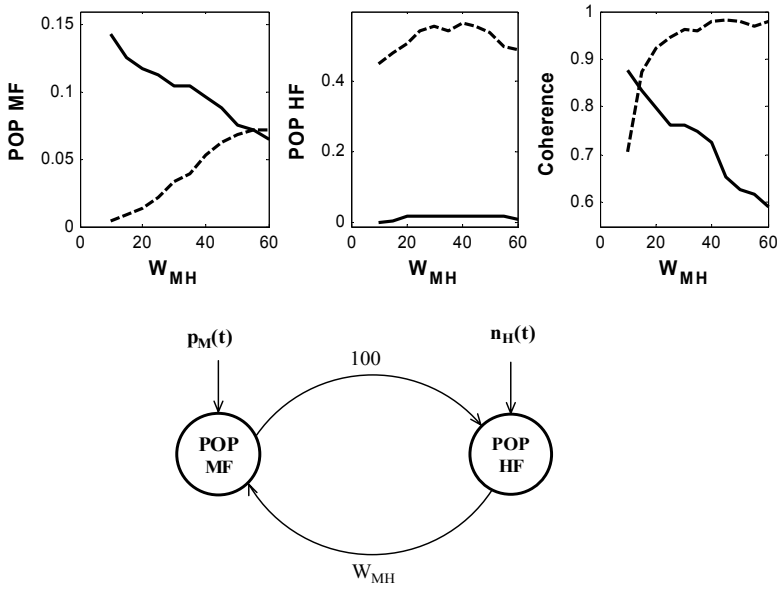

Figure 3.5 – Results of the sensitivity analysis on the parameter W_{MH}, representing the connectivity weight from POP HF to POP MF. The figures have been obtained by giving the parameter W_{MH} the values from 10 to 60; the parameter W_{HM} is the same as in Fig. 3.4a (W_{HM} = 100). The panels represent the value of the peak at medium frequency (continuous line) and high frequency (dashed line) in the power spectral density of POP MF (left panel), of POP HF (middle panel), and in coherence function (right panel). In these simulations mean and variance of the noise in the two populations are: m_M =50, m_H =-50, $(\sigma_M)^2=(\sigma_H)^2$=20.

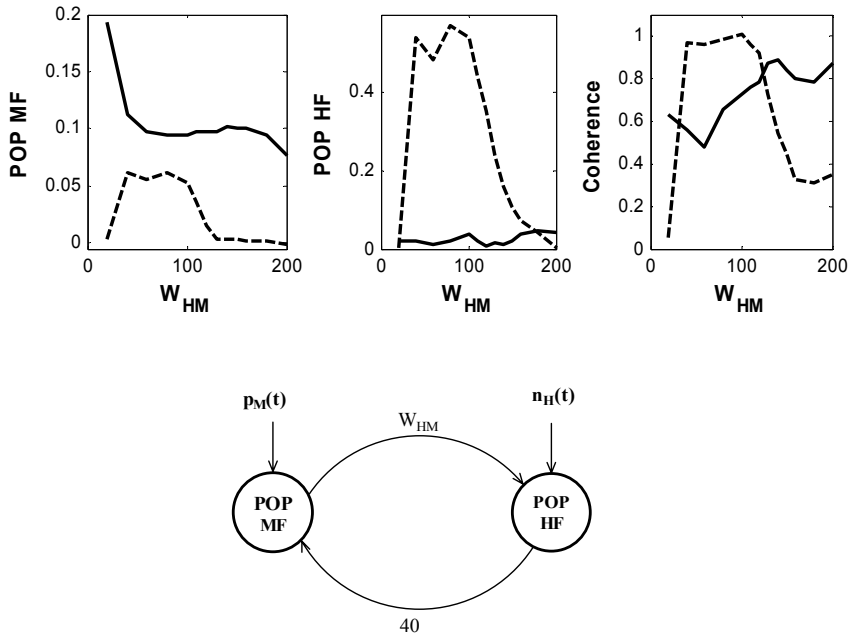

Figure 3.6 – Results of the sensitivity analysis on the parameter W_{HM}, representing the connectivity weight from POP MF to POP HF. The figures have been obtained by giving the parameter W_{HM} the values from 20 to 200; the parameter W_{MH} is the same as in Fig. 3.4 (W_{MH} = 40). The panels represent the same quantities as in Fig. 3.5. In these simulations mean and variance of the noise in the two populations are: m_M=50, m_H=-50, $(\sigma_M)^2=(\sigma_H)^2$=20.

In Fig. 3.5 parameter W_{MH} is varied between 10 and 60, with W_{HM} = 100. Results show that, increasing parameter W_{MH} (which represents the connection strength from the second population (POP HF) to the first (POP MF)) causes the appearance of a high-frequency rhythm in the first population. This rhythm increases in amplitude until, at high values of W_{MH}, the first population exhibits two rhythms of comparable amplitude. The second population does not change its behaviour: it shows only its intrinsic rhythm, which does not appreciable change in amplitude. The coherences vary with the parameter change: coherence is higher at medium frequencies if W_{MH} is low. Increasing W_{MH} causes a decrease in medium frequency coherence and an increase in high frequency coherence, which tends to 1.

Hence, the ratio of coherences seems to contain information on relative weight of the two connections in the feedback loop.

The behaviour is more complex in Fig. 3.6, where W_{HM} (i.e., the connection strength from the first population to the second) is varied in the range 20-200, by maintaining $W_{MH} = 40$. Results show that, when parameter W_{HM} is lower than 20, the first population exhibits its individual rhythm, whereas the second population is not activated, and so it does not exhibit any evident rhythm. When parameter W_{HM} is in the range 40–120, POP MF shows a second rhythm at high frequency, besides its intrinsic rhythm. This is the condition shown in Fig. 3.4a. This is a particular result: an increase in the connection from the first to the second population causes appearance of a new rhythm in the first population. The reason is that this higher connection strength causes an increased activity in the second population (which was only marginally activated by external noise). The increased activity of the second population, in turn, is able to communicate its rhythm to the first via the feedback connection. At higher values of W_{HM} (above 120), the first population loses the high frequency rhythm, while the second population exhibits a particular behaviour: the amplitude of its high-frequency rhythm significantly decreases, and a second small rhythm (at medium frequency) appears. At values of W_{HM} around 180 the second population exhibits two rhythms of small amplitude (this is the situation depicted in Fig. 3.4b). Looking at the coherence, we can say that at lower values of W_{HM} (40-120) coherence is greater at high frequency, and smaller at medium frequency. Increasing the synaptic strength from the first to second population causes a fall in the high-frequency coherence, and an increase in medium-frequency coherence which tends to 1. Once again, the ratio of coherences seems to reflect the relative importance of the two synaptic weights in the feedback loop, coherence is higher in the connection which induces a rhythm in the target population.

Time delay

We repeated several of the previous simulations by changing the connection time delay between 5 and 80 ms. Since the anatomical distance between the two populations is the same, we assumed that the time delay is the same in the two connections of the feedback loop. The case of two different time delays was not investigated. Contrarily to the results by David

et al. (David and Friston 2003), in our simulations time delay has only minor effects on the PSDs. We noticed just a moderate and not systemic increase in coherence with time delay.

3.3.3 Analysis of the connectivity model: three populations

The subsequent set of simulations considers a model with three populations. In this case we assumed that POP LF receives a significant white noise and activates the other two populations, but does not receive any connectivity from them. On the contrary, POP MF and POP HF receive a negligible Gaussian white noise but can be activated by connections from all other populations. This choice has been adopted to simulate a possible simple task (such as the finger motor task examined in Chapter 1 and 2 and the simultaneous lips-foot movement task used in the present validation) in which a starting command initiates from a centro-parietal region, and then is transmitted to mid-frontal regions, which are involved also in memory task as well as motor or behavioural planning. Of course, this is just an exemplary situation, and different arrangements might be simulated, with different connectivity patterns.

In particular in Fig. 3.7 we can see the effect of a simple feed forward connection: POP LF activates POP MF which, in turn, activates POP HF. As a consequence, POP MF exhibits significant power at low frequency, while POP HF shows two peaks at medium and high frequency. The existence of these connections among populations can be seen in the coherence functions (we have a coherence approximately as high as 0.4 between the first two populations in the low frequency range, and a coherence greater than 0.5 at medium frequency between the second and the third population). Negligible coherence appears between the first and the third population.

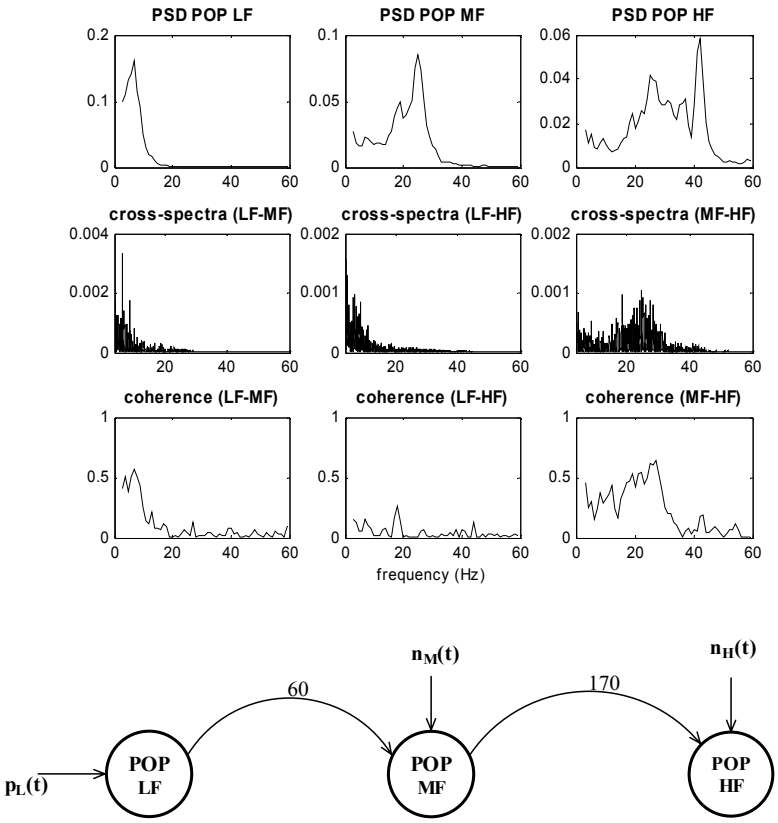

Figure 3.7 – Example of hypothetical feed forward connectivity among three populations (POP LF, POP MF and POP HF) simulated with the model. The values for mean and variance of the noise and for the connectivity are: m_L=0, m_M=-50, m_H=-50, $(\sigma_L)^2=(\sigma_M)^2=(\sigma_H)^2$=20, W_{ML}=60, W_{HM} =170. The panels in the first line show the power spectral densities of the three populations respectively. The power spectral densities have been normalized, to have an area equal to one in the range 3-50 Hz. The panels in the second and third line respectively show the cross-spectra and the coherence functions between POP LF and POP MF, between POP LF and POP HF, between POP MF and POP HF. Connectivity causes evident changes in the power spectral density of the target populations.

In Fig. 3.8 and Fig 3.9 POP LF activates POP MF, which, in turn, is connected by a feedback loop with POP HF. Hence, POP MF receives two inputs from two different populations. As a consequence of this connection,

its PSDs shows three well defined peaks, at low, medium and high frequencies (see Fig 3.9) and also a less evident peak at low-medium frequency (Fig. 3.8). Coherence functions reflect the connectivity pattern very well. In particular, the coherence between POP LF and POP HF is low, suggesting that there is no direct relation between the spectra of these populations. Coherence between POP LF and POP MF is greater than 0.5 at low frequency, reflecting the fact that the low-frequency population stimulates the second one in this frequency range. Coherence between POP MF and POP HF is about 0.3 at medium frequency (in fact the second population does not impose its rhythm to the third) and almost 1.0 at high frequency, where the third population induces its rhythm on the second one.

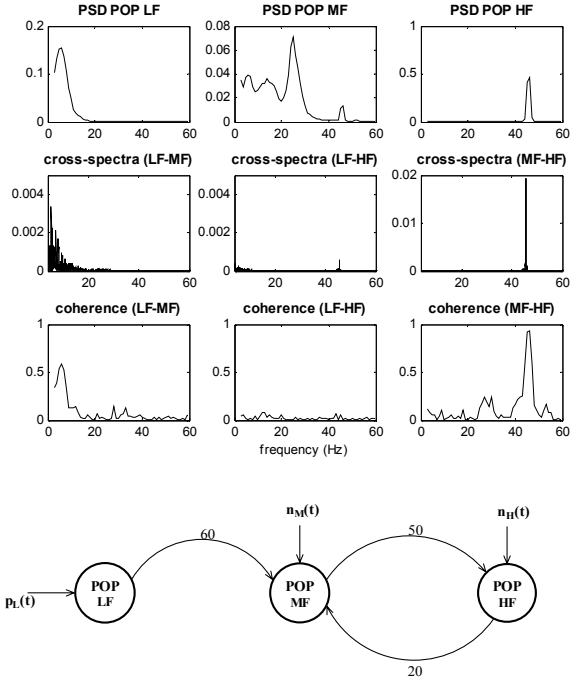

Figure 3.8 – Example of hypothetical feed forward connectivity among three populations (POP LF, POP MF and POP HF) simulated with the model. The values for mean and variance of the noise and for the connectivity are: m_L=0, m_M=-50, m_H=-50, $(\sigma_L)^2=(\sigma_M)^2=(\sigma_H)^2$=20, W_{ML}=60, W_{HM} =50 and W_{MH} =20. The panels represent the same quantities as in Fig. 3.7.

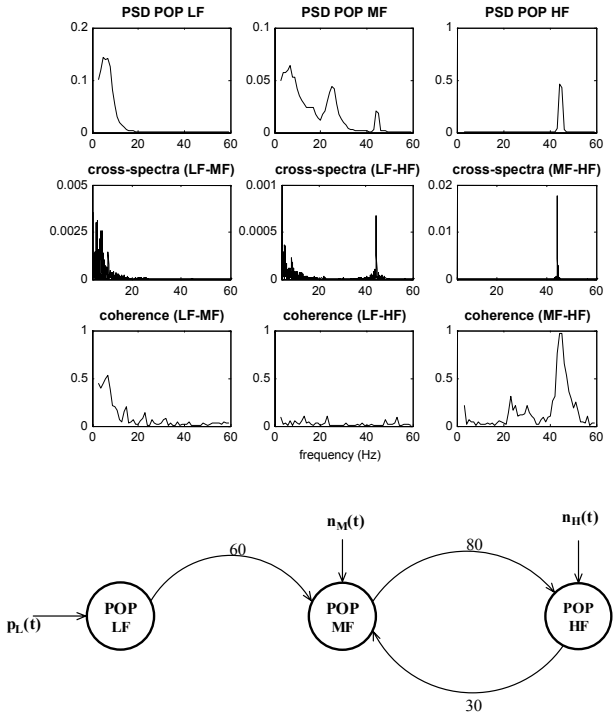

Figure 3.9 - Example of hypothetical feed forward and feedback connectivity among three populations (POP LF, POP MF and POP HF) simulated with the model. The values for mean and variance of the noise and for the connectivity are: m_L=0, m_M =-50, m_H =-50, $(\sigma_L)^2=(\sigma_M)^2=(\sigma_H)^2$=20, W_{ML} =60, W_{MH} =30 and W_{HM}=80. The panels represent the same quantities as in Fig. 3.7.

In Fig. 3.10 POP LF activates both POP MF and POP HF, which are connected to each other by a feedback loop. This situation differs from that in Figs. 3.8 and 3.9, since both POP MF and HF receive two inputs, the one coming from POP LF and the other from the target population. As a consequence of these connections PSD of POP HF shows a complex spectrum, with a low frequency content, a low-amplitude band which covers a wide frequency range around medium frequency and a well defined peak at high frequency. PSD of POP MF shows its well defined peak at medium frequency and a broad band at low-medium frequencies. The peak at high frequency is very low because the connectivity from POP HF is not strong enough. Coherence between POP LF and POP MF and between POP LF and

POP HF is greater than 0.5 at low frequency, this underlines the relationship between the populations, in which the first (POP LF) triggers the other ones (POP MF or POP HF). Coherence between POP MF and POP HF is more complex and shows peaks of medium amplitude (about 0.3-0.4) at low, medium and high frequencies, confirming the minor importance of this feedback loop.

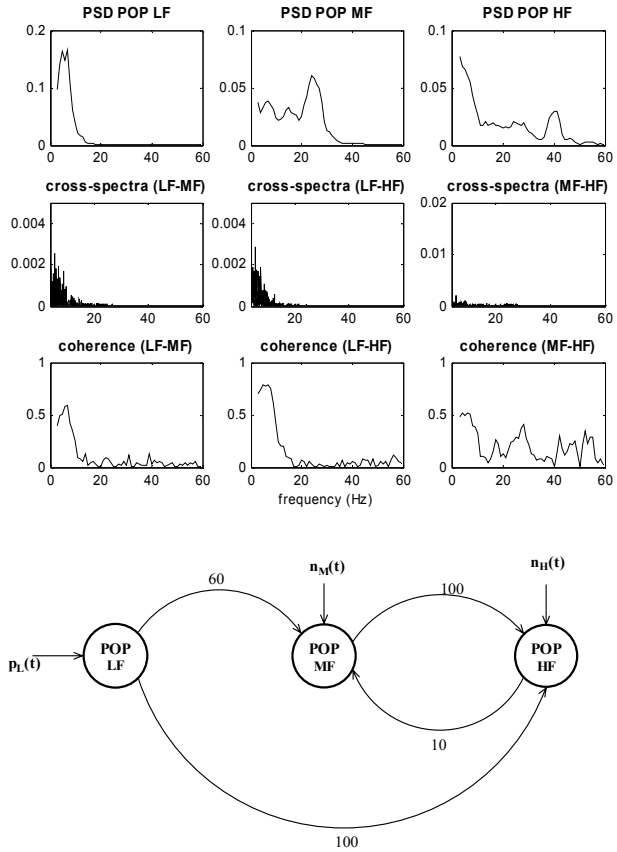

Figure 3.10 – Example of hypothetical feed forward connectivity among three populations (POP LF, POP MF and POP HF) simulated with the model. The values for mean and variance of the noise and for the connectivity are: m_L=0, m_M=-50, m_H=-50, $(\sigma_L)^2=(\sigma_M)^2=(\sigma_H)^2$=20, W_{ML}=60, W_{HL}=100, W_{MH}=10,W_{HM} =100. The panels represent the same quantities as in Fig. 3.7.

In Fig. 3.11 POP LF activates POP HF, which is connected by a feedback loop with POP MF. This situation differs from that in Fig. 3.10, since POP MF receives only an input (from POP HF). As a consequence of these connections PSD of POP HF shows three peaks. Coherence between POP MF and POP HF shows significant values at medium and high frequencies, confirming the importance of the feedback loop; but we have a significant value also in coherence between POP LF and POP HF at low frequency; this underlines the relationship between the two populations, in which the first triggers the other.

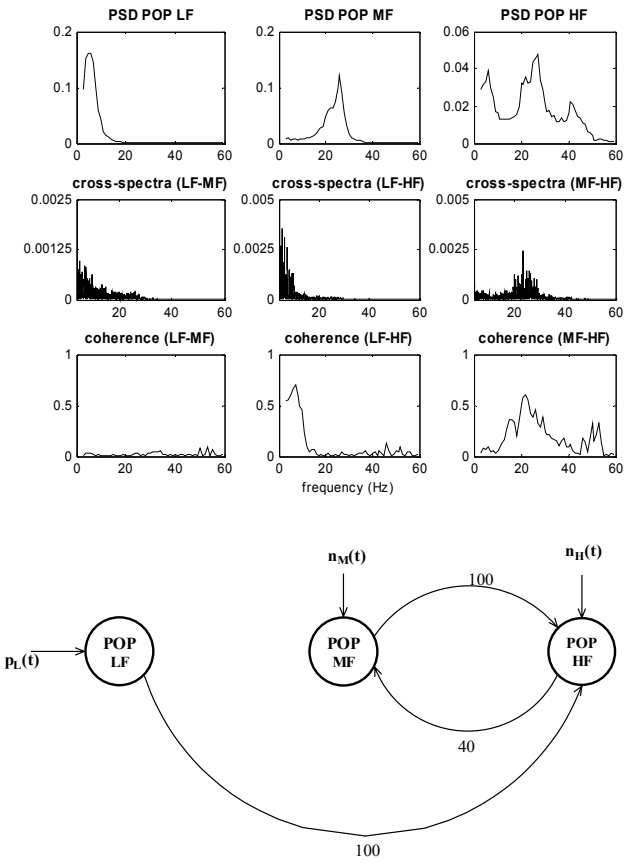

Figure 3.11 - Example of hypothetical feed forward and feedback connectivity among three populations (POP LF, POP MF and POP HF) simulated with the model. The values for mean and variance of the noise and for the connectivity are: m_L=0, m_M=-50, m_H=-50, $(\sigma_L)^2=(\sigma_M)^2=(\sigma_H)^2$=20, W_{HL} =100, W_{MH} =40 and W_{HM} =100. The panels represent the same quantities as in Fig. 3.7.

In Fig. 3.12 we simulated the same connectivity pattern as in Fig. 3.11 but using different weights in the feedback loop. This choice leads up to different PSDs; in this case in fact POP MF shows three peaks. The strong input sent by POP HF to POP MF is confirmed in the coherence function, which grows up to 1 at high frequency.

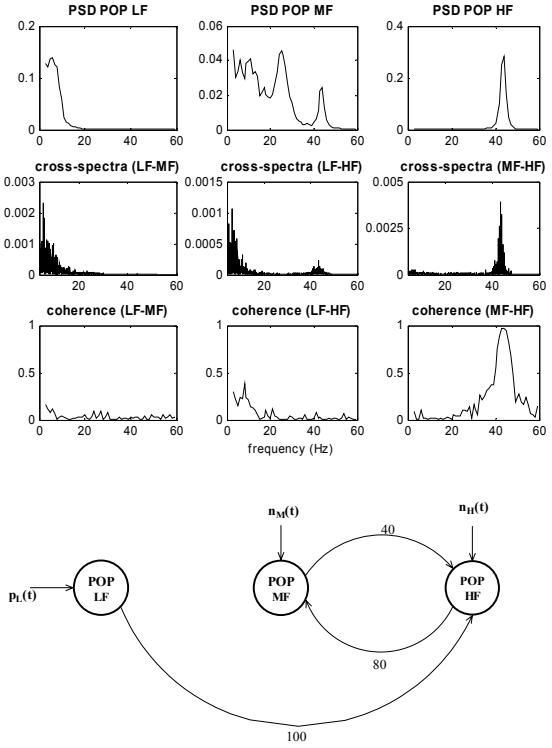

Figure 3.12 - Example of hypothetical feed forward and feedback connectivity among three populations (POP LF, POP MF and POP HF) simulated with the model. The values for mean and variance of the noise and for the connectivity are: m_L=0, m_M=-50, m_H=-50, $(\sigma_L)^2=(\sigma_M)^2=(\sigma_H)^2$=20, W_{HL} =100, W_{MH} =80 and W_{HM} =40. The panels represent the same quantities as in Fig. 3.7.

3.3.4 Fitting of model spectra with cortical activity in the cingulated cortex

To simulate real spectra computed in the cingulated cortex, we adopted the connectivity pattern illustrated in Figs. 3.8 and 3.9. In particular, we assumed that the cingulated cortex corresponds to POP MF in that figure,

and receives external input from two other populations (POP LF and POP HF). Parameters used for the fitting are the connection strengths among populations (W_{ML}, W_{MH}, W_{HM}) and the time constant of excitatory synapses in the three populations (inversely related to a_1^L, a_1^M and a_1^H). We noticed that a change in these time constants is sufficient to position the corresponding peak in the spectrum quite finely, without the necessity to modify the time constants of inhibitory synapses.

The comparison between model and real PSDs, obtained on 12 trials (4 subjects, 3 trials per subject) is shown in Fig. 3.13. The corresponding values of the parameters are reported in Table 3.2.

Table 3.2

Estimated parameters for the cingulated cortex, during a right foot movement task in four normal subjects (three trials per subject).

(Parameters a_1^L , a_1^M , a_1^H are in s^{-1})

	W_{ML}	W_{HM}	W_{MH}	a_1^L	a_1^M	a_1^H
SUBJECT 1						
TRIAL 1	125.0	86.0	15.0	21.0	66.5	50.0
TRIAL 2	84.0	86.0	15.0	20.5	75.0	63.5
TRIAL 3	100.0	86.0	15.0	23.5	85.0	70.0
SUBJECT 2						
TRIAL 1	85.0	86.0	20.0	20.5	85.0	80.0
TRIAL 2	90.0	86.0	20.0	20.5	75.0	50.0
TRIAL 3	120.0	86.0	15.0	20.5	70.0	50.0
SUBJECT 3						
TRIAL 1	125.0	80.0	30.0	20.0	65.0	45.0
TRIAL 2	125.0	80.0	35.0	20.0	65.0	45.0
TRIAL 3	90.0	85.0	20.0	20.0	85.0	43.0
SUBJECT 4						
TRIAL 1	100.0	86.0	25.0	20.5	75.0	55.0
TRIAL 2	130.0	86.0	35.0	20.5	62.0	39.8
TRIAL 3	97.0	86.0	25.0	20.5	78.0	60.0

Results show that the model is able to simulate real PSDs quite well in all examined cases. Furthermore, the parameter values are quite repetitive within the same subject. One can just observe that, in some trials (see for instance trial 2 of subject 2, trials 2 and 3 of subject 4 and all the trials of subject 3) real PSD is greater in the range 30-40 Hz compared with model one. In other words, the real spectra exhibit a broader frequency content in the medium-high frequencies, whereas our spectra falls to zero more rapidly above 30 Hz. Inclusion of a fourth external population, with a peak at about 35-40 Hz may improve fitting, but making the model more complex.

It is worth noting that the values of time constants of excitatory synapses for the population POP HF ($1/a_1^H$) used during the fitting procedure are significantly higher than those adopted in the exemplary simulations of Figs. 3.7-3.12 (we chose $a_1^H = 110\ s^{-1}$ in Table 3.1, whereas the values reported in Table 3.2 lie in the range 40-80 s^{-1}). The reason is that the third peak in real PSDs normally occur between 25 and 35 Hz, while, in our previous examples, this peak was positioned above 40 Hz.

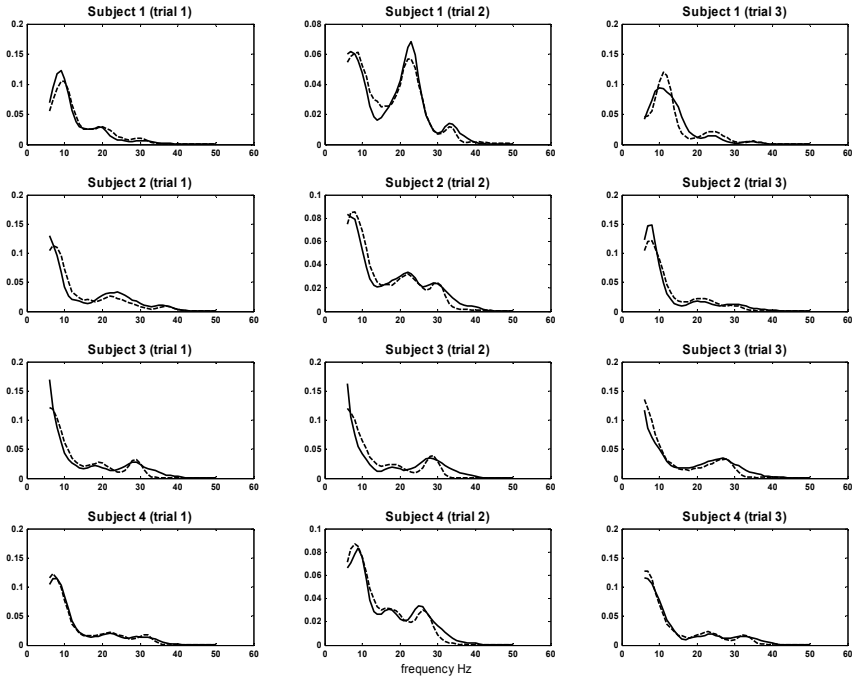

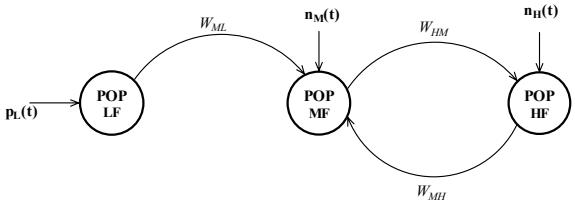

Figure 3.13 - Example of model fitting to 12 real power spectral densities, belonging to cingulated cortex in 4 subjects (3 trials per subject). Fitting has been achieved by estimating the connection strengths among populations and the time constant of excitatory synapses in the three populations. The values for mean and variance of the noise are: m_L=0, m_M=-50, m_H=-50, $(\sigma_L)^2=(\sigma_M)^2=(\sigma_H)^2$=20. Continuous lines represent experimental Power Spectral Densities, while dashed lines are model ones. All spectra have been normalized, to have unitary area in the range 6-50 Hz. Estimated parameters are shown in Table 3.2.

3.4 Discussion

The purpose of the work presented in this chapter was to investigate the meaning of information extracted from cortical EEGs, using a neural mass model of interconnected populations. In particular, we focused attention on two strictly related problems: Which are the mechanisms causing different rhythms in EEG spectra? How are these rhythms modified by connectivity among populations?

Although these questions have been already dealt with in previous papers by David et al. (David and Friston 2003;David et al. 2004), and in previous chapters, the present study introduces a substantial novelty: different rhythms (up to three in our figures) can be obtained within the same population model without the need to use different synaptic kinetics. Conversely, in Chapter 1, as well as in the model by David and Friston (David and Friston 2003), PSD was produced by using the output of a multiple population model, in which different kinetics arranged in parallel contribute to signal generation.

As a general rule, we can state that a single population model, composed of four interacting sub-units (pyramidal neurons, excitatory interneurons, slow inhibitory interneurons, and fast inhibitory interneurons) stimulated with white noise, can generate a unimodal spectrum (i.e., a central rhythm, with a narrower or larger frequency band depending on parameter values and on the variance of the noise). Moreover, the position of this rhythm can be quite finely tuned acting on synaptic kinetics. The rhythm is induced by the internal feedbacks of the population, and by non-linearities represented by sigmoidal relationships. However, the same population can also exhibit additional rhythms (i.e., other peaks in the spectrum) if they are furnished by an external source. In this case, one (intrinsic) rhythm is produced inside the model, while the others are derived from external forcing inputs which cause partial synchronization. By contrast, in our previous model (see Chapter 1 and 2) all rhythms were generated internally by a unique multiple population system.

Of course, since EEG considers a large portion of the cortex (i.e., it has poor spatial resolution) it is very difficult at present to discriminate between a single-kinetic population model, as the one proposed here, and a multiple-kinetic model (as in previous works) on the basis of EEG data only. It is

equally possible that several populations with different kinetics contribute in parallel to the detected EEG signal in a single region, or that this signal reflects the behaviour of a single population only, stimulated by external rhythms coming from more distal regions. A measurement method with higher spatial resolution is necessary to isolate a single population and verify its behaviour. However, in the case of EEG technique, it is clear that the detectable neural populations are generally located at the cortical level, since such cortical assemblies are close to the recording sensors, and the morphology of the cortical layers allows the generation of open (rather than closed) electromagnetic fields. The importance of the presented modelling lies in the fact that with the EEG we are dealing only with the synchronized neural activity. In fact it is often poorly understood that the EEG cannot detect appropriately those cortical assemblies that do not fire synchronously together. In fact, in a dipole layer composed by M coherent sources and N incoherent ones, the potentials due to individual coherent sources are combined by linear superposition, while the combination of the incoherent sources is only due to statistical fluctuations. The ratio between the contributions of coherent to incoherent source can be expressed by $M\ N^{-0,5}$ (Nunez 1995). Hence, if N is very large, say about 10 million of incoherent neurons that fire continuously, and M is a small percentage of such neurons (say 1%; about 100,000 neurons) that instead fire synchronously, we obtain that the potential measured at the scalp level will be determined by $10^5\ 10^{-7/2}$, with a net result of about 30. Hence, only 1% of the active sources produce a potential larger than the other 99% by a factor of 30 just because of the synchronicity property.

In the present chapter, all simulations have been performed to reproduce spectra in normal subjects, performing a motor task. It is worth noting, however, that the same model might also be used to simulate epileptic patterns, either characterized by isolated spikes or seizures. Simulation of these patterns is beyond the aim of the present chapter, but a detailed analysis can be found in the pivotal papers by Wendling et al. (Wendling et al. 2002). In particular, these authors showed that epileptic-like signals can be obtained in a single population by reducing the gain of inhibitory synapses. In perspective, the present model, including connectivity among different populations, may also be used to analyze how epileptic patterns can propagate from one region to another, and to study the possible effect of

connectivity on observed EEG signals during epilepsy.

In the present study we verified the possibility to generate (or to suppress) multiple rhythms within the same population and we performed an extensive analysis on the role of connection weights. Although the wealth of factors and parameters which may affect the results makes it difficult to infer quantitative indices of connectivity from EEG signals, there are some encouraging aspects which emerge from our study. First, in most cases coherence between two signals reflects the existence of some direct connection among the relative populations. This result, previously documented in David and Friston (David and Friston 2003), is confirmed by our results. Second, although the simultaneous analysis of peaks in PSDs and of coherence cannot furnish unique values for connectivity weights (since spectra are affected by many other factors) this analysis may help understanding which population dominates in a feedback loop, and which may be the relative weights of the two re-entrant connections. For instance, looking at the sensitivity analyses reported in Figs. 3.5 and 3.6, we can understand whether a weight in a feedback loop is increasing compared with the other: for instance, if the weight W_{HM} increases, or the weight W_{MH} decreases, POP MF forces its rhythm to POP HF and the coherence increases in the medium frequency range. The opposite is true if W_{HM} decreases and/or W_{MH} increases. In this case, the population HF is forcing its rhythm into the MF population, with an increase in high frequency coherence. Hence, relative changes in the synaptic gains may be discovered, particularly if spectra and coherences are compared with a previous situation, assumed as basal.

The patterns of coherence, illustrated in Figs. 3.7-3.12, also deserve some comments. A high coherence is generally indicative of a strong connection between two populations, as predicted by traditional linear models. However, in linear models coherence always occurs between signals in the same frequency band. Conversely, in the present model one can observe that the resonance power in one population can be modulated as a function of the input from another population, which oscillates at a different frequency. This effect is a consequence of the strong non-linearities in the model, induced by sigmoidal relationships. In fact, an input signal at a given frequency, passing through a sigmoidal relationship, can modify the average activity (i.e., the working point) of the downstream population. A change in the working point, in turn, can be reflected in significant changes in the

resonant loop. Hence, we can remark that, due to the presence of non-linearities, classical linear methods to derive connectivity from data may sometimes lead to erroneous conclusions when applied to neural problems.

Perhaps, the most impressive result of this chapter is that the model of Fig. 3.1 is able to mimic spectra calculated in a region involved in motor planning (i.e., the cingulated cortex) during a simple motor task. These spectra exhibit three peaks, which can be mimicked quite well by the present model within a single population. Furthermore, parameters of the model are quite repetitive, and exhibit only moderate changes within the same subject.

Parameters which exhibit the greater changes in Table 3.2 are the connectivity strength W_{ML} from the low-frequency to the medium-frequency population, the connectivity strength W_{MH} from the high frequency to the medium-frequency population, and the time constant of the excitatory synapses in the HF population. The first two parameters establish the strength of the inputs which activate POP MF (i.e., the cingulated cortex in our model); the second is related with the position of the last peak in the spectrum. The greater changes in these parameters are necessary to fit some spectra (like that in the second trial in subject 4) which are significantly different from the others. In perspective a quantitative analysis of these parameters may be of value to gain a deeper insight into the changes in the inputs to cortical areas which characterize the motor task. For instance, a potential important application of the model may be to compare spectra (and quantitative parameter values) between normal subjects performing the task, and paraplegic subjects who just imagine the task, or to compare spectral (and parameter) changes before and during movement imagination. These results might be exploited in the brain-computer interface problem, in which the use of relevant features of the recorded or modelled EEG signals is of paramount importance in order to raise the level of correct recognition of brain activity by using linear or non linear classifiers (Wolpaw et al. 2002).

Given the possibilities to simulate real EEG spectra pointed out by the previous analysis, it is now important to critically consider which may be the potential use of neural mass models at the present status of the neurophysiological research.

We claim that neural mass models, including connectivity among different populations, may have interesting potential applications. They may help to understand which are the putative mechanisms (internal to a

population, such as synaptic kinetics, or external, such as long range connectivity) which may cause a modification in EEG spectra. Since rhythms appear and disappear within the same region, depending on the specific task, attentional status, etc… this quantitative analysis may help neurophysiologists in the critical analysis of data. Furthermore, neural mass models can be exploited to help validation or rejection of existing hypotheses and to suggest new experiments. Finally, these models can be used to test the reliability of methods (such as the partial directed coherence (PDC), the directed transfer function (DTF) and the direct DTF (dDTF) (Kaminski et al. 2001;Korzeniewska et al. 2003;Astolfi et al. 2004) currently used to extract effective connectivity from data, and to link data obtained with different techniques. In the present chapter we focused attention or membrane potential of pyramidal neurons to mimic cortical EEG. Synaptic activity can be also included in the analysis, to have a signal more closely related to fMRI or PET (Tagamets and Horwitz 2001;Almeida and Stetter 2002), while spike activity can be used to mimic measurement performed on individual neurons (as in animal experiments).

In conclusion, the work presented in this chapter analyzes the possible mechanisms that generate multiple rhythms in cortical EEGs. An important new result, compared with previous studies (see Chapters 1-2), is that a single population with a given synaptic kinetics can oscillate with different rhythms, provided that some of these rhythms come from external sources (for instance, from remote regions). Analysis of coherence, and of the position of peaks in PSDs, reveals important information on the possible long-range connections among populations, especially useful to follow temporal changes in connectivity. Comparison with real data reveals that output of a single population is able to simulate cortical EEG in the cingulated cortex quite well, with only moderate parameter changes. In perspective, the results may be of value for a deeper comprehension of mechanism causing EEG rhythms, for the study of brain connectivity and for the test of neurophysiological hypotheses, and for integration of results obtained with different neuroimaging techniques into a definite theoretical framework.

CHAPTER 4

A MODEL OF RHYTHM GENERATION AND FUNCTIONAL CONNECTIVITY DURING A SIMPLE MOTOR TASK: PRELIMINARY VALIDATION WITH REAL SCALP EEG DATA

4.1 Introduction

Analysis of functional connectivity between different brain areas during the execution of motor or cognitive tasks has become a fundamental problem in computational neuroscience, which may have important theoretical and practical consequences. The problem is of the greatest value to deepen the present basic neurophysiological knowledge, while practical outcomes may be concerned with rehabilitation of patients with brain lesions, brain-computer interface and the design of innovative prostheses for driving voluntary movements.

Actually execution of a motor task and the consequent changes in cortical electrical activity and EEG are thought to be realized by the interaction among different regions of the brain, which are mutually connected and interact in complex non-linear ways. Functional connectivity is usually analyzed from electromagnetic measurement (such as scalp EEG or MEG) and using sophisticate processing algorithms (Astolfi et al. 2005;Astolfi et al. 2006;Astolfi et al. 2007). These techniques, however, are generally based on linear assumptions, whereas neural processing is intrinsically non-linear. Furthermore, data are generally corrupted by noise, which may affect algorithms for brain connectivity estimation in a complex and often unpredictable way. As discussed in previous chapters, the use of mathematical models and computer simulation techniques has been advocated to help the analysis of this information, to favor the conceptualization of knowledge, and the formulation of coherent and comprehensive theories (Horwitz et al. 1999;Horwitz et al. 2000). Furthermore, computer models can provide artificial data, which may be

used as input to test the accuracy and reliability of information processing algorithms.

Various mathematical models have been proposed during the past decades to simulate neural signals (see previous chapters). In recent years, we developed original neural mass models to simulate realistic EEG power spectral densities in some regions of the cortex during simple motor tasks, by acting just on a few model parameters which describe synaptic kinetics in the main regions and the connectivity among them (see Chapters 1 and 2). Furthermore, the model was used to identify simple connectivity circuits able to explain the EEG tracings in the scalp (see Chapter 2). Aim of the work presented here is to extend and improve the model described in Chapter 3, for simulating EEGs power spectral densities of a network of ROIs, and to propose its use for the estimation of connectivity relationships among ROIs from high-resolution EEG data taken on the scalp. Two main improvements are gained compared with Chapters 1-2: i) we use a simpler model of a single ROI, which allows simulation of EEGs power spectral densities with a smaller number of parameters and hypotheses; ii) parameters of brain connectivity are estimated, in a few exemplary cases, by accounting not only for the rhythms generated in the different ROIs and their relative power density, but also for some aspects of cross-power spectral density and coherence among regions.

The method is first presented in a synthetic form. Subsequently, some results, concerning a simple motor task (right foot movement) are shown. The discussion underlines the main virtues and limitations of the proposed method and points out the main aspects for future research.

4.2 Method

4.2.1 Mathematical model

Model of a single population

The description of the model of a single population as well as model equations can be found in Chapter 1, section 1.2.1.; for this reason they are not reported here.

Model of connectivity among populations

The description of the model of connectivity among populations as well as the model equations can be found in Chapter 3, section 3.2.1.; for this reason they are not reported here. However, in this study we considered a model composed of five populations.

4.2.2 Acquisition of experimental data

The description of the acquisition of experimental data and of data analysis is the same as in Chapter 3, section 3.2.2 and 3.2.3 respectively; for this reason it is not reported here. The only difference is that in this study we considered three regions of interest (ROI) of the cortex: the cingulated cortex (CMA_L), the primary motor area (M1F_L), and the supplementary motor area (SMA_p_L).

4.2.3 The model of the motor task

Simulations described in Chapter 3 demonstrate that a single population model, stimulated with input white noise, produces just a unimodal spectrum (i.e., a spectrum with a single well defined peak). The position of the peak primarily depends on the synaptic kinetics (i.e., on parameters a_1, b_1 and g_1). However, a single population can oscillate with different simultaneous rhythms, provided that some of these rhythms come from external sources (for instance, from remote regions).

According to these results, we assumed that the main populations which participate to the motor task (i.e., the cingulated cortex, the primary motor area and the supplementary motor area) exhibits an internal kinetics, corresponding to a rhythms in the medium frequency range (beta band, 12-30 Hz) but they also receive a low-frequency rhythm (in the alpha band (4-12 Hz)). The latter may come from subcortical region (like the thalamus) or from other regions in the cortex (like occipital lobes) not directly investigated here. Furthermore, we assumed that the cingulated cortex may also receive a high-frequency rhythm (greater than 30 Hz, gamma range) and, in turn, can affect this rhythm. In fact, a gamma rhythm is considered essential for binding information among different regions, and for high-level information processing.

The model is thus implemented through the connectivity pattern shown in Fig. 4.1, which is composed of five interconnected populations with different synaptic kinetics. The populations POP LF and POP HF exhibit an intrinsic rhythm at low and high frequency respectively. The other three populations (POP 1, POP 2 and POP 3) exhibit an intrinsic rhythm at medium frequency and simulate the cingulated cortex (ROI1), the primary motor area (ROI2) and the supplementary motor area (ROI3), respectively. The corresponding values of parameters are described in detail in Chapter 1 and Chapter 3, hence are not reported here for the sake of brevity.

In the present model, we assumed that POP LF receives a significant white noise and activates the other populations, but does not receive any connectivity from them. On the contrary, POP HF, POP1, POP2 and POP3 receive a negligible Gaussian white noise but can be activated by connections from all other populations as in Fig. 4.1. Hence, the motor command originates form region LF, and spreads toward the cingulated cortex. The latter, in turn, recruits a high-frequency rhythm, and drive the primary and supplementary motor areas. The latter are linked via a feedback loop.

4.2.4 Fitting procedure

In order to verify the ability of the model to mimic experimental data, the model has been fitted to real spectra computed in the cingulated cortex (ROI1), the primary motor area (ROI2) and the supplementary motor area (ROI3) during a right foot movement task in one normal subjects (three trials, see Chapter 3, section 3.2.2). The fitting was performed with an automatic procedure, by minimizing a least square criterion function of the difference between model and real data. Parameters estimated for the minimization are the connection strengths among populations (W_{1L}, W_{1H}, W_{H1}, W_{23}, W_{32}, W_{2L}, W_{3L}, W_{21}, W_{31}) and the time constant of excitatory synapses in the five populations inversely related to a_1^L, a_1^H, a_1^1, a_1^2 and a_1^3). The information used for building the criterion function includes the PSD in the range 4-50 Hz (evaluated with a frequency step = 1Hz) and the coherence among the population, ROI1-ROI2, ROI1-ROI3 and ROI2-ROI3 evaluated at the frequencies of peaks in the PSD of ROI1. In fact, according to the model (Fig. 4.1) the cingulated cortex drives the supplementary and

primary motor areas.

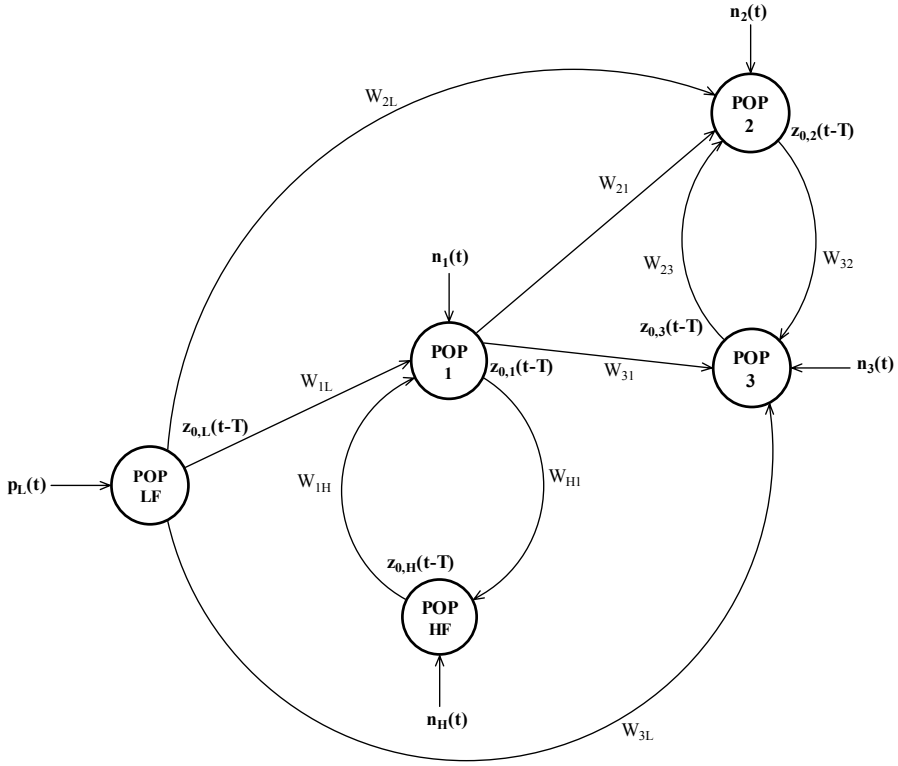

Figure 4.1 - Example of connectivity among five populations, according to the present model. The populations POP LF and POP HF exhibit intrinsic rhythms at low and high frequency respectively; POP1, POP 2 and POP 3 exhibit intrinsic rhythms at medium frequency.

4.3 Results

The results on the comparison between model and real PSDs, and between model and real coherence, obtained in three trials of one healthy subject are shown in Figs. 4.2, 4.3 and 4.4. The corresponding values of the parameters are reported in Table 4.1. Results show that the model is able to simulate real PSDs quite well in both examined cases and that the parameter values are quite repetitive within the subject. The results obtained with the coherence are encouraging and could be useful to establish causal

relationships among remote cortical regions connected during a task. However, it should be noted that in Figs. 4.2 and 4.3, the model overestimates the coherence between RO1 and ROI2, while it underestimates coherences between ROI3 and the other two regions.

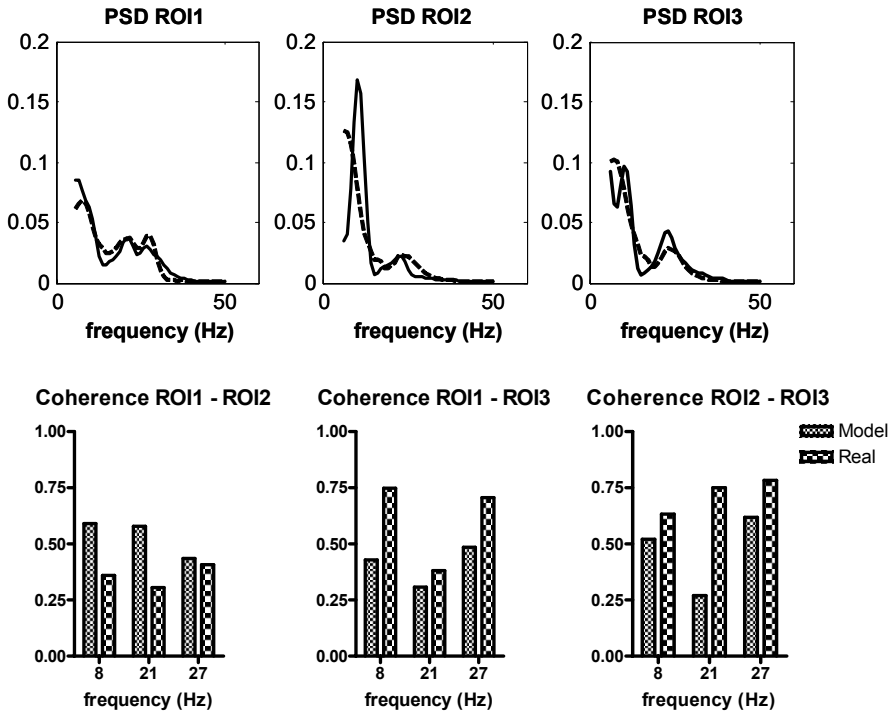

Figure 4.2 - Example of model fitting to three real power spectral densities (upper panels), belonging to cingulated cortex (ROI1), primary motor cortex (ROI2) and supplementary motor cortex (ROI3) in one subject (trial1). The fitting has been achieved by estimating the connection strengths among populations and the time constant of excitatory synapses in the five populations of Fig. 4.1. The values for mean and variance of the noise are: m_L=0, m_H=-50, m_1=-50, m_2=-50, m_3=-50 and $(\sigma_L)^2=(\sigma_H)^2=(\sigma_1)^2$ $(\sigma_2)^2=(\sigma_3)^2$=20. Continuous lines represent experimental Power Spectral Densities, while dashed lines are model ones. Estimated parameters are shown in Table 4.1. The three lower panels represent the comparison between model and real coherence computed at the frequency of the peaks of ROI1.

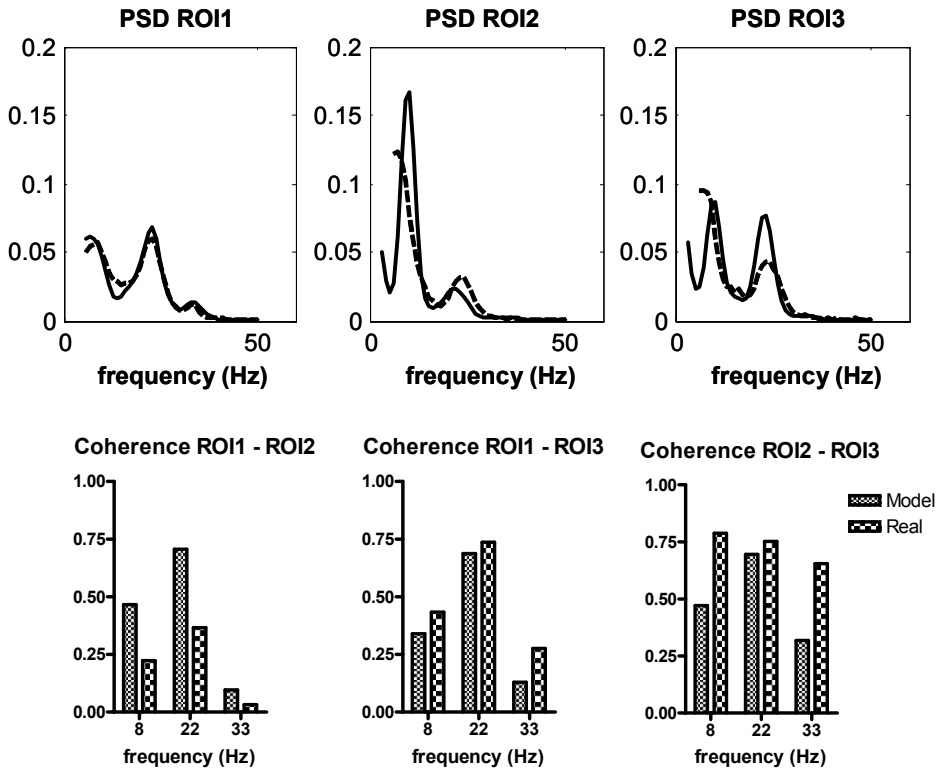

Figure 4.3 - Example of model fitting to three real power spectral densities (upper panels), belonging to cingulated cortex (ROI1), primary motor cortex (ROI2) and supplementary motor cortex (ROI3) in one subject (trial2). The fitting has been achieved by estimating the connection strengths among populations and the time constant of excitatory synapses in the five populations of Fig. 4.1. The values for mean and variance of the noise are: $m_L=0$, $m_H=-50$, $m_1=-50$, $m_2=-50$, $m_3=-50$ and $(\sigma_L)^2=(\sigma_H)^2=(\sigma_1)^2$ $(\sigma_2)^2=(\sigma_3)^2=20$. Continuous lines represent experimental Power Spectral Densities, while dashed lines are model ones. Estimated parameters are shown in Table 4.1. The three lower panels represent the comparison between model and real coherence computed at the frequency of the peaks of ROI1.

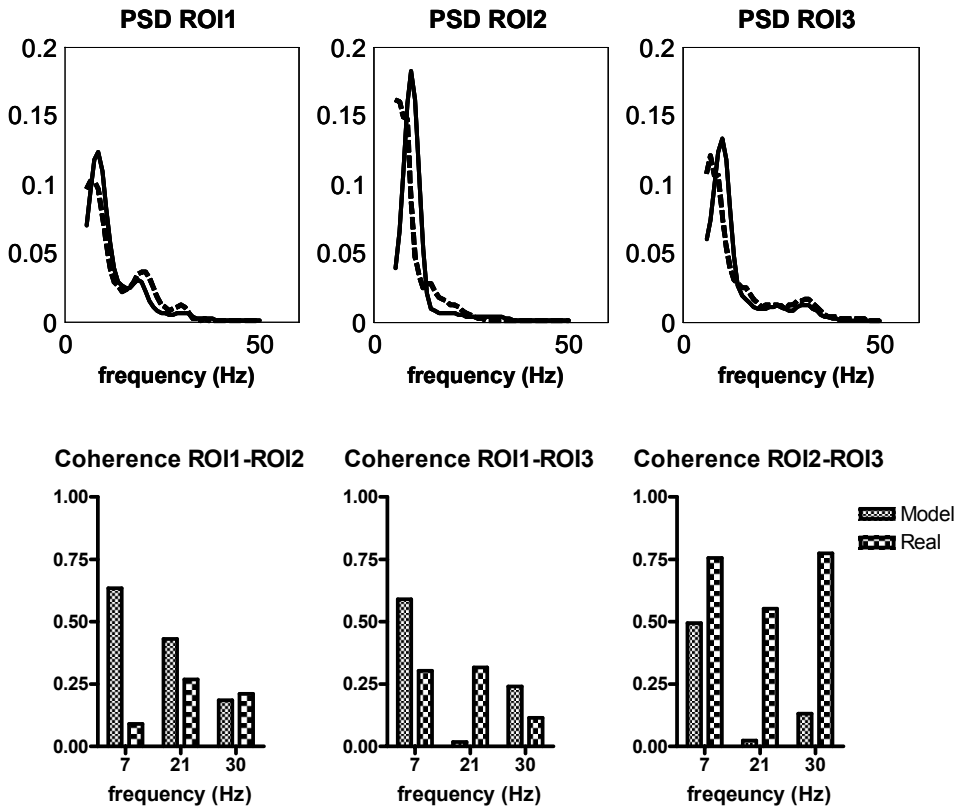

Figure 4.4 - Example of model fitting to three real power spectral densities (upper panels), belonging to cingulated cortex (ROI1), primary motor cortex (ROI2) and supplementary motor cortex (ROI3) in one subject (trial3). The fitting has been achieved by estimating the connection strengths among populations and the time constant of excitatory synapses in the five populations of Fig. 4.1. The values for mean and variance of the noise are: m_L=0, m_H=-50, m_1=-50, m_2=-50, m_3=-50 and $(\sigma_L)^2=(\sigma_H)^2=(\sigma_1)^2$ $(\sigma_2)^2=(\sigma_3)^2$=20. Continuous lines represent experimental Power Spectral Densities, while dashed lines are model ones. Estimated parameters are shown in Table 4.1. The three lower panels represent the comparison between model and real coherence computed at the frequency of the peaks of ROI1.

Table 4.1

Estimated parameters for the cingulated cortex, primary motor cortex and supplementary motor cortex in one subject (three trials) during a right foot movement task.

(Parameter a_1 is in s^{-1})

	W_{1L}	W_{H1}	W_{1H}	a_1^L	a_1^1	a_1^H
TRIAL1	*100.0*	*86.0*	*25.0*	*20.5*	*70.0*	*42.0*
TRIAL2	*84.0*	*86.0*	*15.0*	*20.5*	*75.0*	*63.5*
TRIAL3	*125.0*	*86.0*	*15.0*	*21.0*	*66.5*	*50.0*

	W_{21}	W_{31}	W_{23}	W_{32}	W_{2L}	W_{3L}	a_1^2	a_1^3
TRIAL1	*1.0*	*10.0*	*18.0*	*5.0*	*91.7*	*80.0*	*75.0*	*80.0*
TRIAL2	*1.0*	*47.0*	*11.0*	*0.0*	*96.0*	*47.0*	*78.0*	*83.4*
TRIAL3	*1.0*	*10.0*	*40.0*	*12.0*	*90.0*	*90.0*	*44.0*	*130.0*

4.4 Discussion

In the present chapter, a simple original model of five interconnected neural populations has been used to investigate the origin of EEG rhythms in the cerebral cortex during a simple motor task, and to point out the possible connectivity patterns linking the cingulated cortex, the primary motor area and the supplementary motor area. The main basic idea of our model is that each region receives a low-frequency rhythm from a common remote region (maybe the thalamus, and/or an occipital region). Moreover, the cingulated cortex drives the other two regions and is also involved in the synchronisation of a gamma rhythm with other areas in the brain. Indeed, the gamma rhythm is frequently involved in high mental activity. Then, we tested the possibility that the simple proposed schema is able to simulate real power spectra in the cortex, and to account for some aspects of the observed coherence among EEGs, by acting just on a few parameters which represent the strength of inter-area connections and the kinetics of excitatory synapses inside the regions.

The results are encouraging, both for what concerns the presence of multiple rhythms in the same region, the repeatability of parameter values in the same subject, and the coherence among EEG signals. However, some differences can be observed among model and real coherences. In particular, looking at Figs. 4.2, 4.3 and 4.4, one can observe that the model generally overestimates the coherence between ROI1 (the cingulated cortex) and ROI 2 (the primary motor cortex), while it underestimates the coherences of the cingulated cortex and primary motor cortex with the supplementary motor cortex (ROI3), with exception for the coherence between the cingulated cortex and the supplementary motor cortex in Fig. 4.4. The significance of these differences deserves further analysis.

The model may have several possible applications. First, it may be useful in neurophysiology to help understanding the functional links among the regions involved in a task and, in perspective, to analyze the changes in connectivity occurring during the temporal prosecution of a task, or as a consequence of an input change or a pharmacological treatment. Furthermore, the model may also be useful to investigate differences in functional connectivity and EEG rhythms generation between control subjects and paraplegic patients. These differences may be exploited in the computer-interface problem. The model may also be valuable to generate artificial cortical EEG data, with a pre-assigned pattern of connectivity. These data, propagated to the scalp according to anatomical knowledge, and corrupted with noise, may be used to test the accuracy and performances of the algorithms (such as the directed coherence or the partial directed coherence) commonly employed to derive connectivity from scalp EEG.

The present results, however, are just preliminary, and several additional steps should be performed to expand model applicability for the study of neural integration during motor tasks. A first important step is to perform a sensitivity analysis on model parameters, to discover which among the estimated parameters can be detected with sufficient accuracy based on available data, and which parameters should be considered with caution. A further important point is to improve the analysis of coherence and perhaps, replace the use of this index with other indices more suitable for the interpretation of non-linear systems. Indeed, power spectral density and coherence (i.e., cross spectra) are commonly used to estimate transfer functions in linear systems. Other indices (such as bi-spectra), explicitly

conceived to investigate interactions between non-linear systems, may be utilized in future works within the present automatic estimation procedure. Finally, it might be interesting in future works to encompass more detailed anatomical and/or physiological knowledge into the present model. This knowledge may be essential to account for a greater number of ROIs in the description of brain integration during the motor task, at the same time establishing some constraints on parameter values and on model structure, which may drive the estimation procedure. Indeed, one of the main problems in the present estimation procedure is the large number of parameters simultaneously involved, which precludes the possibility to incorporate a greater number of regions without enforcing some limitations in the parameter space.

PART 2

CHAPTER 5

VISUOTACTILE REPRESENTATION OF PERIPERSONAL SPACE: A NEURAL NETWORK STUDY

5.1 Introduction

In order to guide body movement through the space and allow interaction with the immediate surroundings, the brain must continuously monitor the location of the body parts across different postures and analyze the spatial relations between body parts and nearby objects. This process requires the integration of proprioceptive, tactile, visual and even auditory information regarding limb position. In the last few decades, much research has focused on how these various sensory cues may be combined and integrated to achieve perception of limb location and representation of the 'peripersonal' space immediately around the body. Research on this topic has accumulated a great amount of findings from a number of works involving different methodologies: single-cell recordings in animals (Hyvarinen 1981;Rizzolatti et al. 1981;Graziano and Gross 1995;Graziano et al. 1997;Duhamel et al. 1998;Avillac et al. 2007), neuropsychological studies in brain-damaged patients (Rizzolatti et al. 1981;Ladavas 2002;Holmes and Spence 2004), psychophysical and neuroimaging investigation in both healthy and pathological subjects (Tipper et al. 1998;Macaluso et al. 2000;Marzi et al. 2001;Kennett et al. 2001;Eimer et al. 2002;Taylor-Clarke et al. 2002;Sarri et al. 2006).

Neurons that respond both to tactile and visual stimuli have been found in several brain areas of macaque monkeys, both cortical (ventral premotor cortex (Rizzolatti et al. 1981;Graziano and Gross 1995;Fogassi et al. 1996;Graziano et al. 1997), ventral intraparietal area (Duhamel et al. 1998), parietal area 7b (Hyvarinen 1981)) and subcortical (putamen) (Graziano and Gross 1995). They respond to tactile stimuli located on specific body parts (such as hand, arm, face, shoulder) and to visual stimuli presented proximally to the body part. In particular, the following properties characterize these bimodal cells: i) The visual and tactile receptive fields

(RFs) are spatially aligned; ii) The response to a visual stimulus declines as the stimulus is moved away from the body; iii) The visual RF remains anchored to the body part, i.e. it moves as the body part is moved. On the contrary, when the eyes are moved, the visual RF remains fixed in space, near the corresponding tactile RF.

The previous findings suggest the existence of a distributed, visual-tactile system that codes the peripersonal space in a body part-centered frame of reference, and that may be involved in the representation and control of body position and movement.

The most influential evidence of a cross-modal spatial interaction between vision and touch in humans comes from studies in unilateral brain damaged patients suffering from extinction. Extinction patients can detect a single stimulus presented either in the ipsi- or contralesional side, but they miss a contralesional stimulus when presented concurrently with an ipsilesional stimulus. The presence of extinction only during bilateral stimulation is suggestive of an attentive competition mechanism between two neural representations (Duncan 1996;Mattingley et al. 1997;Marzi et al. 2001): unilateral lesion would chronically bias competition in favor of the ipsilesional event. Extinction can occur within each sensory modality (unimodal extinction), and has been recently observed crossmodally in right-brain damaged (RBD) patients with left tactile extinction (Di Pellegrino et al. 1997;Mattingley et al. 1997;Ladavas et al. 1998). In these studies, a visual stimulus presented near the ipsilesional (right) hand extinguished awareness of a tactile stimulus applied on the contralesional (left) hand (crossmodal visual-tactile extinction); the detection of the left touch improved significantly when the right visual stimulus was applied far from the hand. These results can be conceivably interpreted in terms of an integrated visual-tactile coding of the peripersonal space by bimodal neurons similar to those revealed by single-cell recordings in monkeys (Ladavas 2002;Holmes and Spence 2004). According to this interpretation, the activation of the bimodal neurons by a visual stimulus near a body-part boosts the corresponding somatosensory representation of that body part. The latter, however, may conflict with a simultaneous representation of the opposite body part. Conversely, a visual stimulus delivered far from the ipsilesional hand (outside the peripersonal space) does not boost the representation of the hand, and no competition occurs.

Besides cross-modal extinction, also cross-modal visual-tactile facilitation has been documented in RBD patients with left tactile extinction: under bilateral stimulation, patients were more accurate in detecting the left tactile stimulus when a visual stimulus was presented near the left hand (Ladavas et al. 1998;Ladavas et al. 2000). In other words, the combination of a tactile stimulus with a visual stimulus ameliorated the tactile perceptual deficit. A similar effect was observed by Halligan et al. (Halligan et al. 1996;Halligan et al. 1997) in patients with hemisensory loss of the upper limb: some of the examined patients felt the tactile sensation on the affected arm only if they were allowed to see the hand being touched.

Further evidence of crossmodal influences on unimodal sensory processing has been provided by recent studies in normal subjects (Tipper et al. 1998;Kennett et al. 2001;Taylor-Clarke et al. 2002): viewing the stimulated body site improves performances in tactile detection tasks (Tipper et al. 1998) and enhances tactile acuity (Kennett et al. 2001;Taylor-Clarke et al. 2002). A recent hypothesis (Driver and Spence 1998) suggests that the facilitatory crossmodal influences on unisensory processes may occur via feedback connections from multimodal areas to more specialized unimodal areas. Empirical support for such feedback is provided by recent event-related potential measures and functional imaging data showing that tactile events can alter activity in unimodal visual areas of the brain (Macaluso et al. 2000;Kennett et al. 2001) and viceversa (Taylor-Clarke et al. 2002;Macaluso and Driver 2005). However, this process appears to depend crucially on whether the tactile and visual stimuli are in spatial proximity (Macaluso et al. 2000).

Despite the multitude of data collected on the subject, a clear comprehension of the mechanisms underlying peripersonal space representation is still lacking. Enough information is presently available to attempt a theoretical description of these mechanisms and of the involved neural network by means of mathematical models. This effort is necessary to formulate plausible scenarios in quantitative terms, and to synthesize the knowledge obtained with different approaches into a unique, coherent structure. In particular, models can help interpretation of behavioral and psychophysical responses in terms of the reciprocal interconnections among neural mechanisms.

In the present work we propose a neural network model which mimics the visual-tactile representation of the peripersonal space around the right hand and around the left hand. The model considers the two hemispheres, each composed of three areas of neurons. The two upstream areas are unimodal and respond to visual and tactile stimuli, respectively. The third downstream area is multimodal and is devoted to multisensory integration. The connections between unimodal and multimodal neurons within the same hemisphere include both feedback and feedforward synapses. The two hemispheres are interconnected via inhibitory synapses. Neuronal activity is described by a sigmoidal function and a first order dynamics. By adopting the previous structure and by using a single set of parameters, the model is able to reproduce: i) the multisensory coding of the space around a hand; ii) the facilitatory influences of crossmodal stimuli on unisensory perception; iii) the competitive interaction between the right and left hand representations in normal subjects. Moreover, the network has been used to simulate the responses characterizing RBD patients (cross-modal visual-tactile extinction, cross-modal visual-tactile facilitation) by assuming plausible modifications in some model parameters.

5.2 Method

5.2.1 Model description

In this section, we will first provide a general qualitative description of the model. Then, all model equations will be presented and justified. Finally, criteria for parameter assignment will be reported.

General model structure

- The model is composed of two networks, one for each hemisphere, reciprocally interconnected (Fig. 5.1). The two networks share the same structure: each consists of three regions of neurons which communicate through synaptic connections.
- The two upstream regions are unimodal and respond to tactile and visual stimuli, respectively. They are organized in matrices of neurons. Both the tactile and visual areas are defined with reference to the hand of a hypothetical subject: in particular, neurons in the tactile area respond to

tactile stimuli applied on the hand, while neurons in the visual area respond to visual stimuli on the hand and around it.

- Each element of the unisensory areas has its own receptive field (RF) through which receives stimulation by an external input. Neurons in each unimodal area are arranged according to a topological organization, so that their RFs map the external space in an orderly manner. Accordingly, proximal neurons within each area respond to stimuli coming from proximal positions of the space. Moreover, the neurons in the same unimodal area interact via lateral synapses arranged according to a Mexican hat disposition (i.e., a circular excitatory region surrounded by a inhibitory annulus).
- The third downstream region is multimodal, devoted to visual-tactile integration. It consists of:

i) A matrix of multimodal excitatory neurons arranged according to a topological organization. They receive inputs from unisensory neurons in both areas via feedforward synapses and send back excitatory inputs to the unimodal neurons through feedback synapses. Thus, within the same hemisphere, detection of a multimodal stimulus may reinforce the perception of unimodal stimuli in the upstream areas. Moreover, these multimodal neurons send long-range projections towards the other hemisphere.

ii) Multimodal inhibitory interneurons. These neurons realize inter-hemispheric interaction. They receive visual-tactile information from the multimodal excitatory neurons in the other hemisphere and send inhibitory synapses locally to the unisensory neurons within the same hemisphere. Inclusion of these connections realizes a competition in case of the simultaneous activation of the right and left hand representations.

- All neurons in the network are normally in a silent state (or exhibit only a weak basal activity) and can be activated if stimulated by a sufficiently high input. The activity of each neuron is described through a sigmoidal relationship (with a lower threshold and an upper saturation) and a first order dynamics.
- A single neuron, in the model, should not be considered as representative of an individual cell only, but rather as a pool of cells which share the same spatial properties (i.e., approximately the same RF) and the same sensory modality. Similarly, synaptic weights should not be

considered as the strength of individual synapses, but rather summarize the overall effect of the synaptic strength multiplied per the number of cells involved.

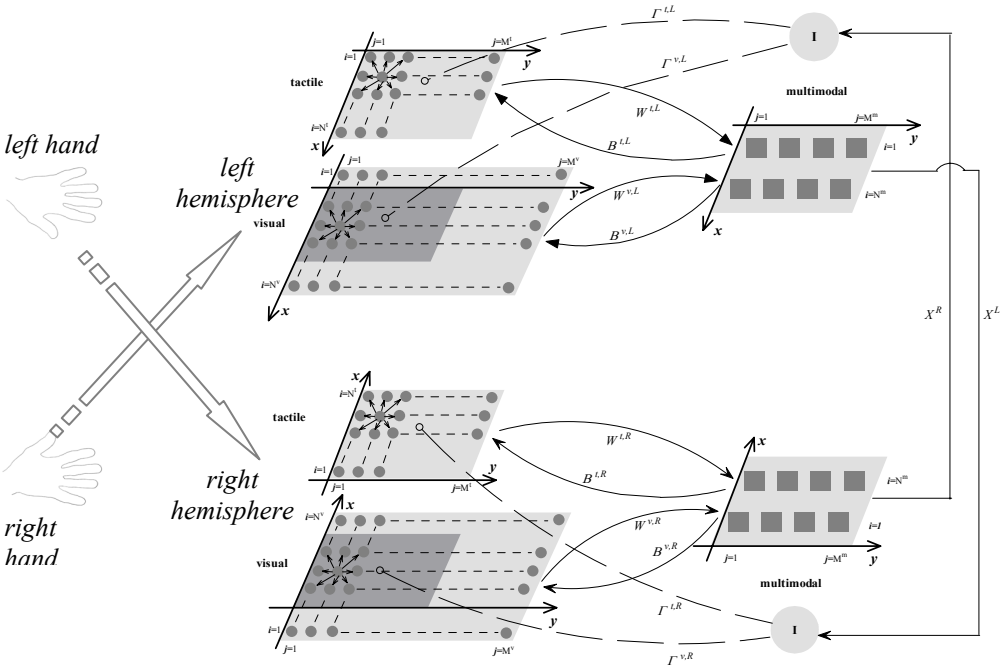

Figure 5.1 – Model structure. Schematic representation of the networks which compose the hemispheres and of synaptic connections among regions of neurons within the hemispheres and between them. Meaning of the symbols: superscript L, R=left and right hemisphere; superscript t, v, m=tactile, visual and multimodal area; I=inhibitory interneuron; Λ=lateral synapses within the unimodal areas; W=feedforward synapses from unimodal to multimodal neurons; B=feedback synapses from multimodal to unimodal neurons; Γ=inhibitory synapses from the inhibitory interneuron to unimodal areas; X=cross-connections between the hemispheres, linking the multimodal neurons within one hemisphere to the inhibitory interneuron in the other hemisphere. See text for details.

Mathematical description

Since the overall network has a symmetrical structure, only the equations for one hemisphere (the left one) will be presented. In the following, we will use: the superscripts t, v, and m to denote quantities referring to **t**actile, **v**isual and **m**ultimodal excitatory neurons, respectively; the superscript g indicates quantities referring to inhibitory (**G**ABAergic) interneurons; the superscripts L and R to distinguish the **l**eft and **r**ight hemisphere; the subscritps ij or hk to represent the spatial position of individual neurons.

i) Organization of the unimodal and multimodal regions

The unimodal areas are composed by N^sxM^s neurons (s = t, v), with N^t = 20, M^t = 40; N^v = 30, M^v = 140. In both areas, the RFs of neurons are arranged at a distance of 0.5 cm one from the other along both the x and y directions. Hence, the tactile area covers a space of 10 cm x 20 cm, representing the surface of one hand in an extremely simplified form, while the visual area covers a space of 15 cm x 70 cm, representing the visual space on the hand and around the hand (extending by 2.5 cm on each side and 50 cm ahead).

In the following, we will denote with x_i and y_j the centre of the RF of a generic neuron ij. By considering a reference frame rigidly connected with the hand (see Fig. 5.1), we can write:

$x_i^t = i \cdot 0.5$ cm (i = 1,2,…,N^t) $y_j^t = j \cdot 0.5$ cm (j = 1,2,…,M^t)

for the tactile neurons, and

$x_i^v = i \cdot 0.5$ -2.5 cm (i = 1,2,…,N^v) $y_j^v = j \cdot 0.5$ cm (j = 1,2,…,M^v)

for the visual neurons.

As to the multimodal region, we assumed that the overall visual-tactile space of the hand is covered by just 8 multimodal excitatory neurons (N^m= 2; M^m=4) whose RFs have a wider spatial extension compared with unimodal neurons. In particular, the centres of their RFs have a distance of 5 cm along the x axis and 4 cm along the y axis. Accordingly, for the multimodal neurons the following equations hold:

$x_i^m = i \cdot 5 - 2.5$ cm (i = 1,2) $y_j^m = j \cdot 4$ cm (j = 1,2,3,4)

Finally, for the sake of simplicity, a single inhibitory interneuron is considered in each hemisphere. The use of a smaller number of multimodal neurons compared with unimodal neurons is justified by their larger RF. Hence, just a few neurons are able to cover the entire space of the hand

(Rizzolatti et al. 1981;Iriki et al. 2001). The ratio of inhibitory interneurons vs. excitatory neurons (1/8) agrees with values commonly found in the cortex (inhibitory neurons are approximately 15-25 % of excitatory neurons) (Trappenberg 2002).

ii) The receptive fields of unisensory neurons

In the following, the RF will be denoted with the symbol Φ (Receptive **Fi**eld). The RF of unisensory neurons is described with a Gaussian function. Hence, for a neuron ij in the unisensory area s (s = t, v) - within the left hemisphere - the following equation holds:

$$\Phi_{ij}^{s,L}(x,y) = \Phi_0^{s,L} \cdot exp\left(-\frac{\left(x_i^{s,L} - x\right)^2 + \left(y_j^{s,L} - y\right)^2}{2 \cdot \left(\sigma_\Phi^{s,L}\right)^2} \right), \qquad s = t, v \qquad (5.1)$$

where x_i, y_j is the center of the RF, x and y are the spatial coordinates, and $\Phi_0^{s,L}$ and $\sigma_\Phi^{s,L}$ represent the amplitude and standard deviation of the Gaussian function (three standard deviations approximately cover the overall RF).

According to Eq. 5.1, an external stimulus applied at the position x, y excites not only the neuron centred in that point, but also the proximal neurons whose receptive fields cover that position.

iii) The activity of the unisensory neurons

The total input received by a generic neuron ij in the unisensory areas is the sum of four different contributions:

a) the contribution due to the external stimulus (say $\varphi_{ij}(t)$, since it depends on the RF Φ_{ij});
b) the contribution due to the lateral synapses linking the neuron with the other elements in the same area (say $\lambda_{ij}(t)$, **l**ateral);
c) the contribution due to the feedback excitatory projections from the multimodal neurons (say $\beta_{ij}(t)$, feed**b**ack);
d) the contribution due to the synapses from the inhibitory interneuron (say $\gamma_{ij}(t)$, **G**ABAergic interneurons).

In the following, each single contribution will be described.

The input $\varphi_{ij}^{s,L}$ that reaches the neuron ij in presence of an external stimulus is computed as the inner product of the stimulus and the receptive field, according to the following equation:

$$\varphi_{ij}^{s,L}(t) = \int_x \int_y \Phi_{ij}^{s,L}(x,y) \cdot I^{s,L}(x,y,t) dxdy \cong \sum_x \sum_y \Phi_{ij}^{s,L}(x,y) \cdot I^{s,L}(x,y,t) \Delta x \Delta y$$

s = t, v (5.2)

where $I^{s,L}(x,y,t)$ is the external stimulus (tactile or visual) applied on the right side of the body (hence, processed by the left hemisphere) at the coordinates x, y and at time t. The right hand member of Eq. (5.2) means that the integral is computed with the histogram rule (with $\Delta x = \Delta y = 0.2$ cm).

In the present work, the external stimulus is reproduced by a two-dimensional gaussian function:

$$I^{s,L}(x,y,t) = \begin{cases} 0, & t < t_0 \\ I_0^{s,L} \cdot exp\left(- \dfrac{\left(x_0^{s,L} - x\right)^2 + \left(y_0^{s,L} - y\right)^2}{2 \cdot \left(\sigma_I^{s,L}\right)^2} \right), & t \geq t_0 \end{cases} \quad \text{s=t,v} \qquad (5.3)$$

where t_0 is the instant of stimulus application, x_0, y_0 is the central point of the stimulus, and $I_0^{s,L}$ and $\sigma_I^{s,L}$ represent the amplitude and the standard deviation. We used a small standard deviation (see Table 5.1) to mimic quite a punctual external stimulus.

The input that a unisensory neuron receives from other neurons in the same area via the lateral synapses is defined as:

$$\lambda_{ij}^{s,L}(t) = \sum_{h=1}^{N^s} \sum_{k=1}^{M^s} \Lambda_{ij,hk}^{s,L} \cdot z_{hk}^{s,L}(t), \quad \text{s = t, v} \qquad (5.4)$$

$z_{hk}^{s,L}(t)$ represents the activity of the hk neuron in the area s (s = t, v) of the left hemisphere (computed below). $\Lambda_{ij,hk}^{s,L}$ indicates the strength of the synaptic connection from the pre-synaptic neuron at the position hk to the post-synaptic neuron at the position ij. These synapses are symmetrical and are arranged according to a “Mexican hat” function:

$$\Lambda_{ij,hk}^{s,L} = \begin{cases} \Lambda_{ex}^{s,L} \cdot exp\left(-\frac{(i-h)^2 + (j-k)^2}{2 \cdot \left(\sigma_{ex}^{s,L}\right)^2} \right) - \Lambda_{in}^{s,L} \cdot exp\left(-\frac{(i-h)^2 + (j-k)^2}{2 \cdot \left(\sigma_{in}^{s,L}\right)^2} \right), & ij \neq hk \\ 0, & ij = hk \end{cases}$$

s = t, v (5.5)

Parameters $\Lambda_{ex}^{s,L}$ and $\sigma_{ex}^{s,L}$ define the excitatory Gaussian function, parameters $\Lambda_{in}^{s,L}$ and $\sigma_{in}^{s,L}$ the inhibitory one: they establish the strength and extension of these synapses. To have a Mexican hat disposition, the following conditions must be satisfied: $\Lambda_{ex}^{s,L} > \Lambda_{in}^{s,L}$ and $\sigma_{ex}^{s,L} < \sigma_{in}^{s,L}$. The null term in Eq 5.5 avoids autoexcitation.

A further input to unisensory neurons is induced by the feedback synapses from the multimodal excitatory neurons:

$$\beta_{ij}^{s,L}(t) = \sum_{h=1}^{N^m} \sum_{k=1}^{M^m} B_{ij,hk}^{s,L} \cdot z_{hk}^{m,L}(t), \qquad \text{s = t, v} \tag{5.6}$$

$z_{hk}^{m,L}(t)$ represents the activity of the hk neuron in the multimodal area (computed below). $B_{ij,hk}^{s,L}$ indicates the strength of the synaptic connection from the pre-synaptic multimodal neuron at the position hk to the post-synaptic unimodal neuron at the position ij. We assume that the synaptic connections between unimodal and multimodal neurons have a Gaussian distribution; that is the synaptic strengths decrease with the distance between the centres of the receptive fields of the pre-synaptic and post-synaptic neurons. Accordingly, we have:

$$B_{ij,hk}^{s,L} = B_0^{s,L} \cdot exp\left(-\frac{\left(x_i^{s,L} - x_h^{m,L}\right)^2 + \left(y_j^{s,L} - y_k^{m,L}\right)^2}{2 \cdot \left(\sigma_B^{s,L}\right)^2} \right), \text{ s = t, v} \tag{5.7}$$

where $x_h^{m,L}$, $y_k^{m,L}$ represent the centre of the RF of the multimodal hk neuron, while $x_i^{s,L}$, $y_j^{s,L}$ the centre of the RF of the unimodal neuron ij in the unisensory area s. Parameters $B_0^{s,L}$ and $\sigma_B^{s,L}$ set the amplitude and extension of the synapses.

Finally, unimodal neurons receive input from the inhibitory interneuron:

$$\gamma_{ij}^{s,L}(t) = \Gamma_{ij}^{s,L} \cdot z^{g,L}(t), \text{ s = t,v} \tag{5.8}$$

where $z^{g,L}(t)$ represents the activity of the inhibitory interneuron. This activity depends on the visual-tactile information at the other hemisphere (see below). $\Gamma_{ij}^{s,L}$ is the strength of the synaptic connection from the interneuron to neuron ij in the unisensory area s (tactile or visual). We assume that this inhibition affects all neurons in the hand (both tactile and visual) and is independent on the position of neurons in the unisensory areas. Accordingly:

$$\Gamma_{ij}^{t,L} = \Gamma_0^{t,L}, \qquad \forall\, i = 1,2,...,N^T \qquad \forall\, j = 1,2,...,M^T \tag{5.9}$$

$$\Gamma_{ij}^{v,L} = \begin{cases} \Gamma_0^{v,L}, & \forall\, i = \left(1,2,...,N^T\right) + 5 \quad \forall\, j = 1,2...,M^T \\ 0, & otherwise \end{cases} \tag{5.10}$$

The total input (say $u_{ij}^{s}(t)$) received by a unisensory neuron is the sum of the four contributions:

$$u_{ij}^{s,L}(t) = \varphi_{ij}^{s,L}(t) + \lambda_{ij}^{s,L}(t) + \beta_{ij}^{s,L}(t) + \gamma_{ij}^{s,L}(t) \text{ = t, v} \tag{5.11}$$

Finally, neuron activity is computed from its input through a static sigmoidal relationship and a first order dynamics:

$$z_{ij}^{s,L}(t) = f^{s}\left(q_{ij}^{s,L}(t)\right) \qquad \text{s = t, v} \tag{5.12}$$

where

$$\tau \frac{dq_{ij}^{s,L}(t)}{dt} = -q_{ij}^{s,L}(t) + u_{ij}^{s,L}(t) \qquad \text{s = t, v} \tag{5.13}$$

$$f^{s}(q) = \frac{f_{\min}^{s} + f_{\max}^{s} \cdot e^{\left(q-\tilde{q}^{s}\right)\cdot r^{s}}}{1 + e^{\left(q-\tilde{q}^{s}\right)\cdot r^{s}}} \cdot H\left(\frac{f_{\min}^{s} + f_{\max}^{s} \cdot e^{\left(q-\tilde{q}^{s}\right)\cdot r^{s}}}{1 + e^{\left(q-\tilde{q}^{s}\right)\cdot r^{s}}}\right) \text{ s = t, v} \tag{5.14}$$

Parameters f_{min}^{s} and f_{max}^{s} set the lower and upper saturation of the sigmoid, $\tilde{q}^{s}$ is the value of the input at the central point, and r^{s} establishes

the slope at the central point. Since parameter f_{min}^{s} has a negative value (see Table 5.1), the Heaviside function H( ) has been introduced to avoid that neuron activity becomes negative. Hence, the activity of unimodal neurons is equal to zero until a given threshold of the sensory input is overcome. Parameter τ in Eq. 5.13 is the time constant of the differential equation.

iv) The activity of the multimodal excitatory neurons

These neurons receive inputs from neurons in the two unisensory areas via feedforward synapses with a Gaussian distribution. Hence, the overall input to a generic neuron ij in the multimodal area is computed as:

$$u_{ij}^{m,L}(t) = \sum_{h=1}^{N^t}\sum_{k=1}^{M^t} W_{ij,hk}^{t,L} \cdot z_{hk}^{t,L}(t) + \sum_{h=1}^{N^v}\sum_{k=1}^{M^v} W_{ij,hk}^{v,L} \cdot z_{hk}^{v,L}(t) \qquad (5.15)$$

$z_{hk}^{s,L}(t)$ (s = t, v) represents the activity of the neuron hk in the unimodal (tactile or visual) area, computed through Eq. 5.12. $W_{ij,hk}^{s,L}$ denotes the synapses (feedforward) from the unisensory neuron hk to the multimodal neuron in position ij. These synapses can be written as follows:

$$W_{ij,hk}^{s,L} = W_0^{s,L} \cdot exp\left(- \frac{\left(x_i^{m,L} - x_h^{s,L}\right)^2 + \left(y_j^{m,L} - y_k^{s,L}\right)^2}{2 \cdot \left(\sigma_W^{s,L}\right)^2} \right), \text{ s = t, v} \qquad (5.16)$$

$x_i^{m,L}$, $y_j^{m,L}$ represent the centre of the RF of the multimodal ij neuron, while $x_h^{s,L}$, $y_k^{s,L}$ the centre of the RF of the unimodal neuron hk in area s (tactile or visual). Parameters $W_0^{s,L}$ and $\sigma_W^{s,L}$ (s= t,v) set the amplitude and extension of the synapses.

The activity of a multisensory neuron is computed from its input by using equation similar to Eqs. 5.12, 5.13 and 5.14:

$$z_{ij}^{m,L}(t) = f^m\left(q_{ij}^{m,L}(t)\right) \qquad (5.17)$$

$$\tau \frac{dq_{ij}^{m,L}(t)}{dt} = -q_{ij}^{m,L}(t) + u_{ij}^{m,L}(t) \qquad (5.18)$$

$$f^m(q) = \frac{f^m_{\min} + f^m_{\max} \cdot e^{\left(q-\tilde{q}^m\right)\cdot r^m}}{1+e^{\left(q-\tilde{q}^m\right)\cdot r^m}} \tag{5.19}$$

The meaning of the symbols is the same as in Eq. 5.12, 5.13 and 5.14.

v) The activity of the inhibitory interneuron

The inhibitory interneuron in one hemisphere receives synapses from all the multimodal excitatory neurons in the other hemisphere. Hence, the input to the interneuron in the left hemisphere is:

$$u^{g,L}(t) = \sum_{h=1}^{N^m}\sum_{k=1}^{M^m} X^R_{hk} \cdot z^{m,R}_{hk}(t-D) \tag{5.20}$$

where $z^{m,R}_{hk}(t)$ is the activity of the multimodal hk neuron in the right hemisphere and D is a pure delay. The latter simulates the time necessary for competition mechanisms to become effective (i.e., we assumed that competition does not occur instantaneously, see section 5.4 for this aspect). X^R_{hk} represents the strength of the **cross**-connection linking the multimodal hk neuron in the right hemisphere to inhibitory interneuron in the left hemisphere. We assume that all these connections have the same value:

$$X^R_{hk} = X^R_0, \qquad \forall\, h = 1,...,N^m \quad \forall\, k = 1,...,M^m \tag{5.21}$$

Then, equations similar to Eq.12 and 13 are used to compute the activity of the interneuron:

$$z^{g,L}(t) = f^g\left(q^{g,L}(t)\right) \tag{5.22}$$

$$\tau \frac{dq^{g,L}(t)}{dt} = -q^{g,L}(t) + u^{g,L}(t) \tag{5.23}$$

$$f^g(q) = \frac{f^g_{\min} + f^g_{\max} \cdot e^{\left(q-\tilde{q}^g\right)\cdot r^g}}{1+e^{\left(q-\tilde{q}^g\right)\cdot r^g}} \tag{5.24}$$

The meaning of the symbols is the same as in Eqs. 5.12, 5.13 and 5.14.

5.2.2 Parameter assignement

The values of all model parameters are listed in Table 5.1. We assume that parameters of the left and right hemisphere have the same value in basal conditions. Criteria for parameter assignment are reported below.

Receptive fields of the unimodal neurons

Parameters Φ_0^t and Φ_0^v have been set to 1 to establish a scale for the inputs generated by the external stimuli. Standard deviations σ_0^t and σ_0^v have been assigned so that unimodal RFs are about 2-2.5 cm in diameter. This value is within the range of spatial resolution on the hand and arm (10 mm on the palm and 40 mm on the forearm) (Kandel et al. 2000).

Lateral synapses in unimodal areas

Parameters characterizing the Mexican hat arrangement of lateral synapses (Λ_{ex}, σ_{ex}, Λ_{in}, σ_{in}), in both tactile and visual area, have been given to reach a trade-off between excitation and inhibition, in order to satisfy the following criteria: i) an external stimulus produces an activation bubble of unimodal neurons with approximately the same dimension of the RF; ii) excitation must be maintained confined to avoid instability, that is uncontrolled excitation which propagates to the overall area.

Synaptic connections among the areas

The parameters of the feedforward connections from unimodal areas to the multimodal area (W_0^t, W_0^v, σ_W^t, σ_W^v) have been assigned to satisfy the following requirements: i) multimodal neurons have large RFs, with several centimetres in diameter, that may even encompass the entire surface of the hand (Rizzolatti et al. 1981;Graziano et al. 1997;Iriki et al. 2001;Maravita and Iriki 2004); ii) a single unimodal stimulus may significantly excites multimodal neurons (whose RFs cover that position). Indeed, data on monkeys indicate that even a light touch of the skin or a spot of light on/near the body produce a considerable response in these bimodal neurons (Rizzolatti et al. 1981;Graziano et al. 1997;Duhamel et al. 1998).

The extension of the feedback synapses from multimodal to unimodal neurons (parameters σ_B^t, σ_B^v) have been set equal to the extension of the feedforward synapses. In this way, cross-modal facilitation (i.e., the reinforcement that a unimodal stimulus exerts on a stimulus with different modality in the same hand, see sections 5.3 and 5.4) occurs only in case of a spatial coherence between the stimuli. The strength of the feedback synapses (B_0^t, B_0^v) has been maintained smaller than the feedforward synapses to avoid that activation of multimodal neurons consequent to a one-modality stimulus (e.g. tactile) produces a phantom activation bubble in the other modality area (e.g. visual).

The weight of the cross-connections between the two hemispheres (parameter X_0) has been chosen so that even the activation of a single multimodal neuron in one hemisphere (signalling the involvement of the contralateral perihand space) significantly excites the inhibitory interneuron in the other hemisphere; accordingly the model realizes a rivalry between the two hemispheres for peripersonal attention (Driver and Spence 1998;Graziano and Cooke 2006).

Finally, the strength of the inhibitory synapses (parameter Γ_0) has been set small enough to consent the perception of a right hand stimulus and a left hand stimulus, applied simultaneously, as it occurs in normal subjects (Hillis et al. 2006).

Parameters of the individual neurons

Parameters characterizing the static sigmoidal relationship of unimodal neurons have been assigned to have a high lower threshold (below which the neurons are completely silent) and a smooth transition from silence to saturation. These characteristics help to maintain stability of the unisensory areas.

The sigmoidal relationship of multimodal excitatory neurons has been set so that neuron response gradually decreases with a reduction in its input (for instance, when a visual stimulus is progressively moved away from one hand) (Colby et al. 1993;Graziano et al. 1997;Duhamel et al. 1998).

In the model, the inhibitory interneuron in one hemisphere signals the activation of the multimodal area in the other hemisphere; hence, the corresponding sigmoidal function has been set to mimic an on/off behaviour,

that is a negligible neuron activity at low input values and a rapid transition from silence to saturation.

For the sake of simplicity, we used the same time constant for the three types of neurons; its value (20 ms) is within the range of membrane time constants reported in the literature (Dayan and Abbott 2001). Finally, the pure delay in the connection between the two hemispheres reflects the time necessary for attention competitive mechanisms to become effective. Its value (80 ms) has been assigned according to ERP studies (Luck et al. 2000;Natale et al. 2006).

Table 5.1

Values of model parameters in basal conditions. Parameter values are the same for the right and left hemispheres.

Receptive fields of unimodal neurons			
$\Phi_0^t = 1$	$\sigma_\Phi^t = 0.5$ cm	$\Phi_0^v = 1$	$\sigma_\Phi^v = 0.5$ cm
Lateral synapses in unimodal areas			
$\Lambda_{ex}^t = 2.7$	$\Lambda_{in}^t = 2$	$\sigma_{ex}^t = 4$	$\sigma_{in}^t = 9$
$\Lambda_{ex}^v = 2.7$	$\Lambda_{in}^v = 2$	$\sigma_{ex}^v = 4$	$\sigma_{in}^v = 9$
Feedforward synapses			
$W_0^t = 2$	$\sigma_W^t = 3$ cm	$W_0^v = 1.8$	$\sigma_W^v = 3$ cm
Feedback synapses			
$B_0^t = 1$	$\sigma_B^t = 3$ cm	$B_0^v = 1$	$\sigma_B^v = 3$ cm
Cross-connections and inhibitory synapses			
$X_0 = 1$	$\Gamma_0^t = 1.8$	$\Gamma_0^v = 1.8$	
Sigmoidal characteristic of unimodal neurons			
$f_{min}^t = -0.6$	$f_{max}^t = 5$	$\tilde{q}^t = 19.43$	$r^t = 0.34$
$f_{min}^v = -0.6$	$f_{max}^v = 5$	$\tilde{q}^v = 19.43$	$r^v = 0.34$
Sigmoidal characteristic of multimodal neurons			
$f_{min}^m = 0$	$f_{max}^m = 5$	$\tilde{q}^m = 6$	$r^m = 0.8$
Sigmoidal characteristic of inhibitory interneurons			
$f_{min}^g = 0$	$f_{max}^g = 5$	$\tilde{q}^g = 2.95$	$r^g = 1.32$
Time constant and pure delay			
$\tau = 20$ ms	$D = 80$ ms		
External stimuli *(see also the legends to figures)*			
$I_0^t = 2.6$	$\sigma_I^t = 0.3$ cm	$I_0^v = 2.6$	$\sigma_I^v = 0.3$ cm

5.3 Results

In this section, we first present results of model simulations by using basal values for all parameters (Table 5.1), which mimic a normal healthy

subject. Then, responses of RBD patients suffering from extinction are reproduced by assuming plausible modifications of some model parameters in the right hemisphere. Finally, results of sensitivity analyses on some key network parameters are reported.

Visual-tactile coding of the perihand space

Figure 5.2 shows the neural activity in the unimodal areas and the response of the 8 multimodal neurons within the right hemisphere, in four different conditions of left hand stimulation: application of a tactile stimulus (panel A); application of a visual stimulus on the hand (panel B); application of a visual stimulus near the hand (panel C); application of a visual stimulus far from the hand (panel D). In all four cases, the stimulus produces activation of a bubble of neurons in the corresponding unimodal area. Multisensory neurons are activated in three out of the four examined conditions: they respond to the tactile stimulus and to the visual stimulus placed on the hand or in the space immediately surrounding it. On the contrary, a visual stimulus distal from the hand does not induce any significant response. Accordingly, multisensory neurons signal the involvement (either visual or tactile) of the perihand space, while a far visual stimulus is not perceived as belonging to the peripersonal space. It is worth-noting that activity of the eight multimodal neurons is not the same during activation of the peri-hand space, but it varies depending on whether the initial or terminal portion of the hand is involved.

Cross-modal influences on unisensory perception

Figure 5.3 shows an example of modulation of unisensory perception by crossmodal stimulation obtained with the model. In panel A, the network is stimulated by a tactile input of low intensity applied on the left hand (only the right hemisphere network is displayed). The stimulus produces a weak activation of a single neuron in the tactile area; this unimodal activity is not sufficient to evoke a response in the multimodal neurons, which remain silent. In panel B, the tactile stimulus is coupled with a weak visual stimulus deliverd at the same location on the hand. The concomitant presence of the two stimuli induces a strong activation in the multisensory neurons and a remarkable reinforcement of unimodal activity, which now shows a wide activation bubble. The crossmodal influence of vision on touch and vice-

versa occurs via the feedback projections from the multisensory neurons to the unisensory areas.

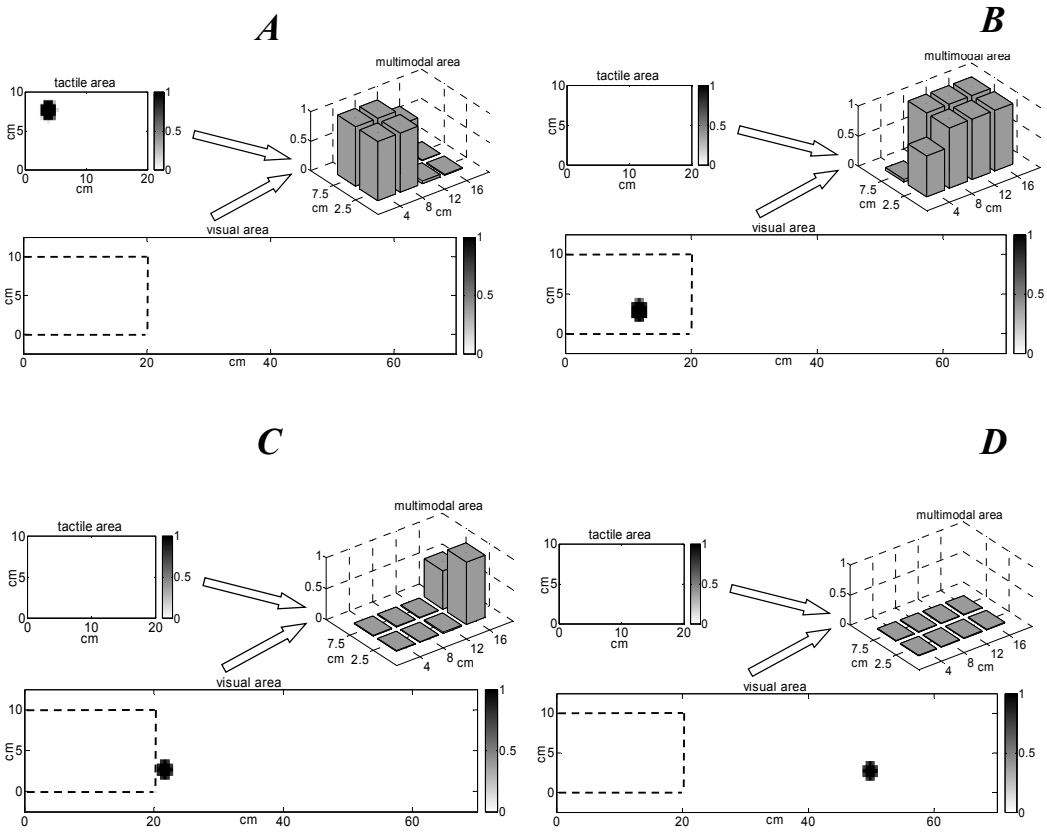

Figure 5.2 – Visual-tactile coding of perihand space. Network activity in response to tactile and visual stimuli of intensity $I_0^t = I_0^v$=2.6 on the left hand. Each panel shows the neuronal activity in unimodal areas and the response of the 8 multimodal neurons. The activity in unimodal area is represented by a gray scale, in multimodal area by a 3D visualization. Panel A: tactile stimulus located at x=7.5 cm and y=4 cm. Panel B: visual stimulus located at x=2.5 cm and y=12 cm. Panel C: visual stimulus near the hand located at x=2.5 cm and y=22 cm. Panel D: visual stimulus far from the hand located at x=2.5 cm and y=50 cm.

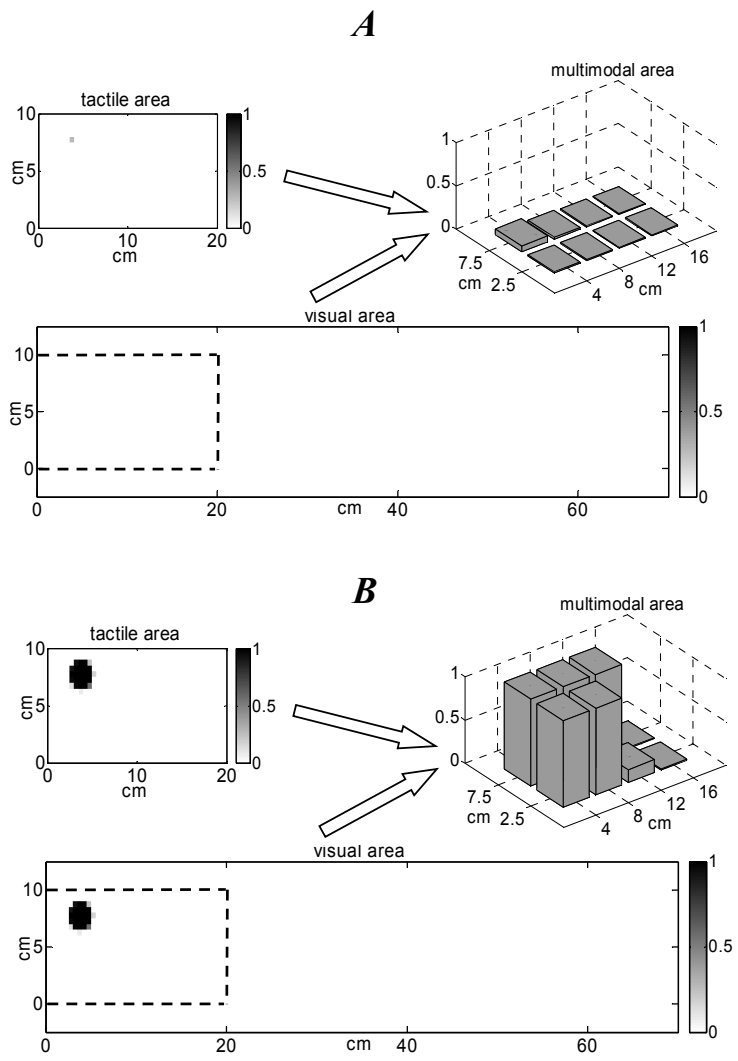

Figure 5.3 – Cross-modal influences on unisensory perception. Network activity in response to a tactile stimulus of low intensity I_0^t=1.68, located at x=7.5 cm and y=4 cm on the left hand (panel A) and to a tactile and a visual stimulus, both of low intensity $I_0^t = I_0^v$=1.68, located at the same position on the left hand, x=7.5 cm and y=4 cm (panel B). The panels show the same quantities of Fig. 5.2. The concomitant presence of the two weak stimuli induces a strong activation in the multisensory neurons and a remarkable reinforcement of unimodal activity.

Right and left hand interaction

The interaction between right and left hand representation is depicted in Fig. 5.4, in case of a healthy subject (i.e., by maintaining all parameters at their basal values). In panel A, a tactile stimulus is applied on the left hand (right hemisphere) and a simultaneous visual stimulus is presented on the right hand (left hemisphere). Each stimulus boosts the multisensory representation of the corresponding hand (via activation of the multimodal neurons), leading to a competition between the two representations (via activation of the inhibitory interneurons). In this normal subject, the competition is unbiased and the outcome is the coexistence of both right and left hand representations.

The panel B elucidates the effects of the competition. The two plots present a magnified image of the activation bubble in the right-hemisphere tactile area in the two different conditions: left-hand tactile stimulus presented alone (left plot, as in Fig. 5.2A); left-hand tactile stimulus coupled with a right-hand visual stimulus (right plot, as in Fig. 5.4A). In the latter condition, the activation bubble is reduced because of the inhibitory influence from the multisensory neurons in the left hemisphere.

RBD patients: unilateral stimulation

In order to simulate RBD patients suffering from left tactile extinction, we decreased the strength of all synapses originating from tactile unimodal neurons. Of course, this change may not really reflect synaptic depression, but rather a decrease in the number of effective neurons which contribute to the activity in right tactile area (see Discussion for more details). To this end, we reduced the strength of the lateral excitation in the tactile unimodal area ($\Lambda_{ex}^{t,R}$) and the weight of the feedforward synapses from the unimodal tactile area to the bimodal area ($W_0^{t,R}$). The modified values for these parameters are reported in Table 5.2. As a consequence of these parameter changes, a tactile stimulus on the left hand activates a weak neural representation of the hand. This result is presented in Figure 5.5, which simulates the application of an isolated left tactile stimulus in a RBD patient. The activation bubble in the tactile area is significantly reduced with respect to a normal subject (compare Fig. 5.2 panel A), involving only 9 neurons; this degraded tactile activity evokes the response of a few multimodal neurons (three versus five in a healthy subject).

Table 5.2

Modified parameters for simulation of Right Brain Damaged patients with left tactile extinction

$\Lambda_{ex}^{t,R} = 2.3$	$W_0^{t,R} = 0.8$

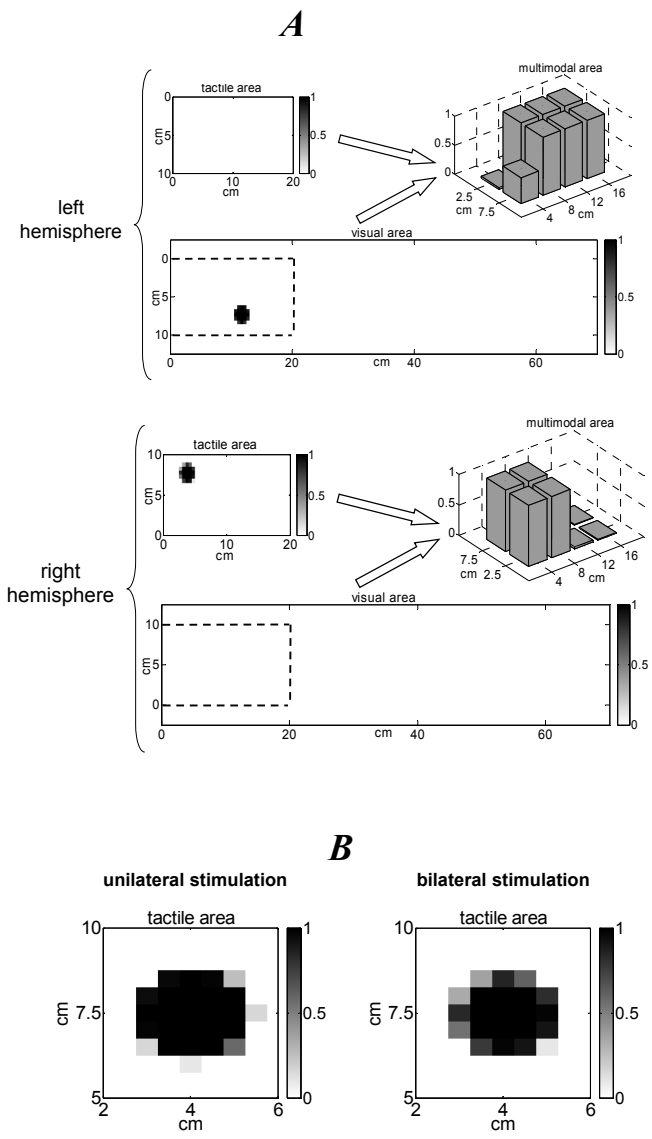

Figure 5.4 – Right and left hand interaction. Panel A: network activity in response to a tactile stimulus applied on the left hand at the position x=7.5 cm and y=4cm and of a simultaneous visual stimulus applied on the right hand at the position x=7.5 cm and y=12 cm. Both stimuli have the intensity $I_0^t = I_0^v$=2.6. The panel represents the same quantities of Fig. 5.2 for both hands (hemispheres). Panel B: representation of the activation bubble in the right-hemisphere tactile area in response to a tactile stimulus presented alone on the left hand (see plot of Fig. 5.2A) and in response to a left-hand tactile stimulus coupled with a right-hand visual stimulus (see Fig. 5.4A).

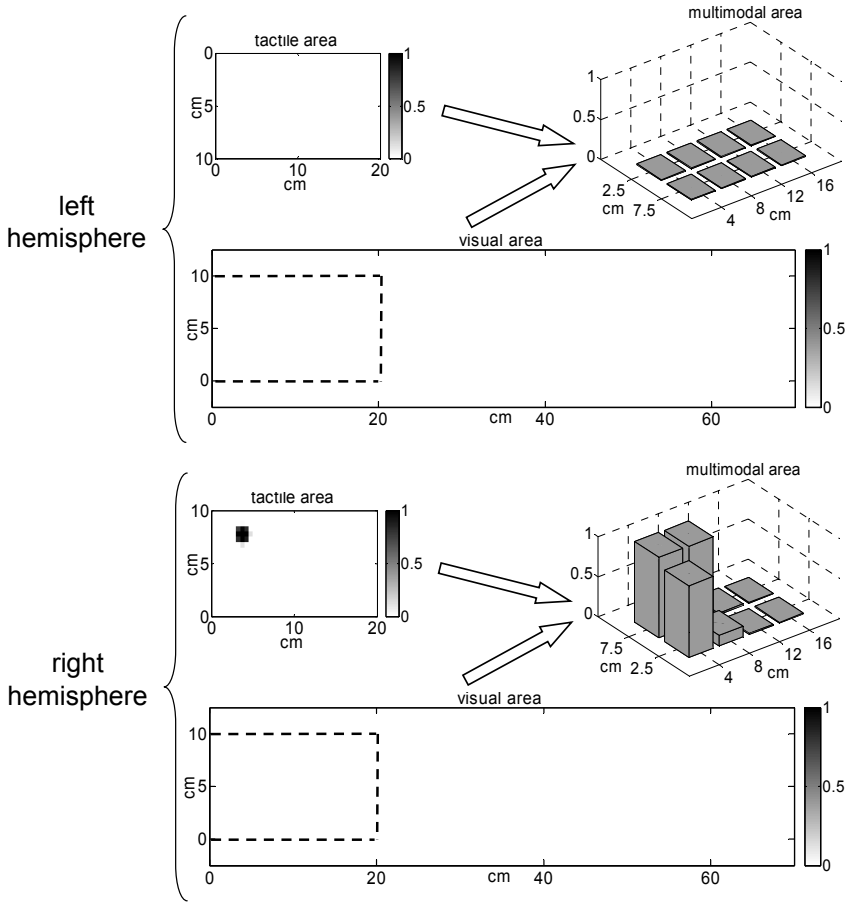

Figure 5.5 – RBD patients, unilateral stimulation. Network activity in response to a tactile stimulus of intensity I_0^t =2.6 applied on the left hand of a RBD subject, at the position x=7.5 cm and y=4cm. The plots represent the same quantities of Fig. 5.2 for both hemispheres.

RBD patients: bilateral stimulation (cross-modal extinction)

Figure 5.6A shows the same stimulation conditions as Fig. 5.4A (left hand tactile stimulus and right hand visual stimulus) applied to a RBD patient. The activation of the multimodal neurons in the left hemisphere (evoked by the visual stimulus) competes with that in the right hemishpere through the inhibitory interneurons. In this case the competition is uneven: because of the weaker right hemisphere activation, the ipsilesional stimulus has a higher competitive strength than the contralesional stimulus. The final outcome of the network is the extinction of the activity in the tactile area of the right hemisphere (only the central neuron remains slightly activated), and the consequent deactivation of multimodal neurons. Hence, only the right hand representation survives.

For the sake of clarity, panel B of Figure 5.6 compares the activity in the right hemisphere tactile area in case of unilateral stimulation (left plot, as in Fig. 5.5) and in case of bilateral stimulation (right plot, as in Fig. 5.6A).

RBD patients: bilateral stimulation (cross-modal facilitation)

Behavioural studies in RBD patients indicate that under conditions of bilateral stimulation, left tactile stimulus detection is improved by a simultaneous left visual stimulus. This situation is simulated in Fig. 5.7, where a visual stimulus is applied on the right hand and a double stimulation (tactile and visual) is delivered to the left hand. In these conditions, the left tactile stimulus is not extinguished thanks to the presence of the left visual stimulus which sustains the activation of the multisensory neurons; the latter, in turn, reinforce the tactile area activity via the feedback projections. Consequently, an activation bubble survives in the tactile area and right and left hand representations coexist.

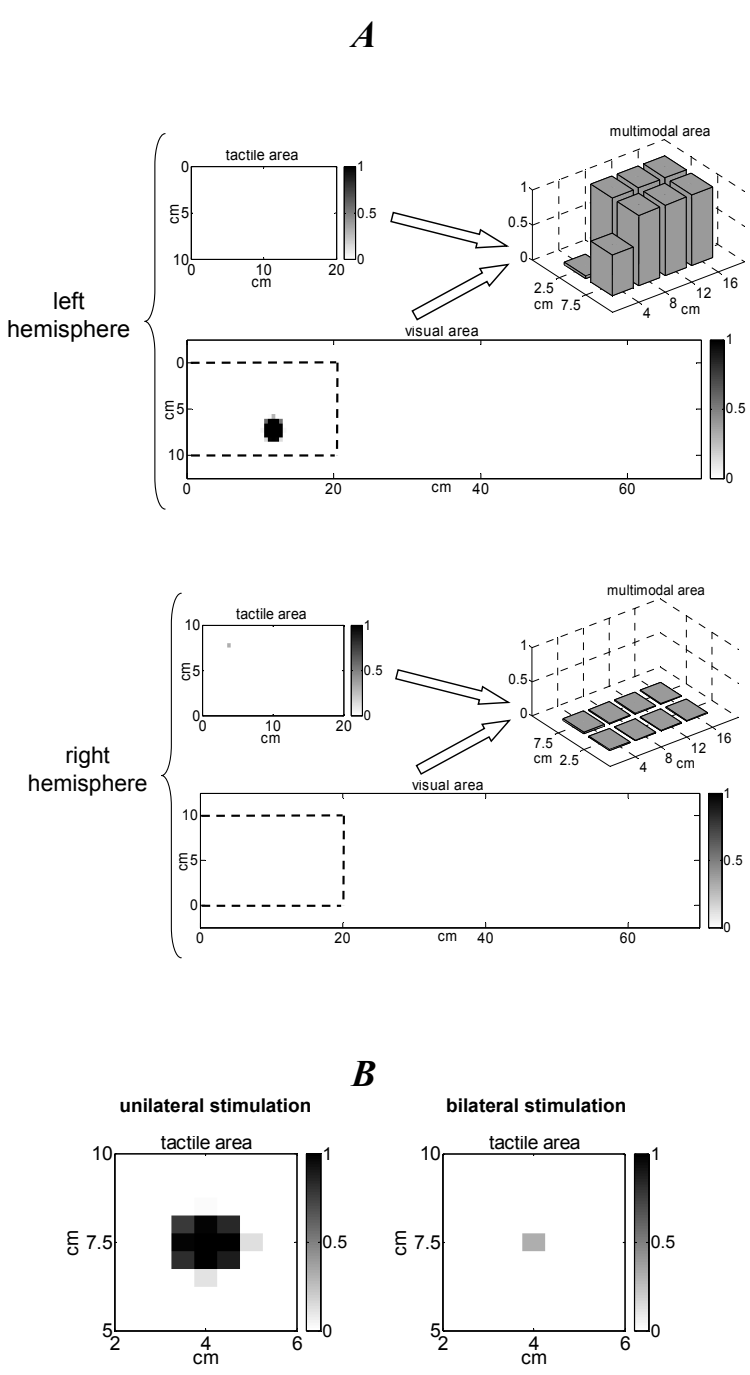

Figure 5.6 – RBD patients: bilateral stimulation (cross-modal extinction). The panels show the results of the same simulations of Fig. 5.4, applied to a RBD subject.

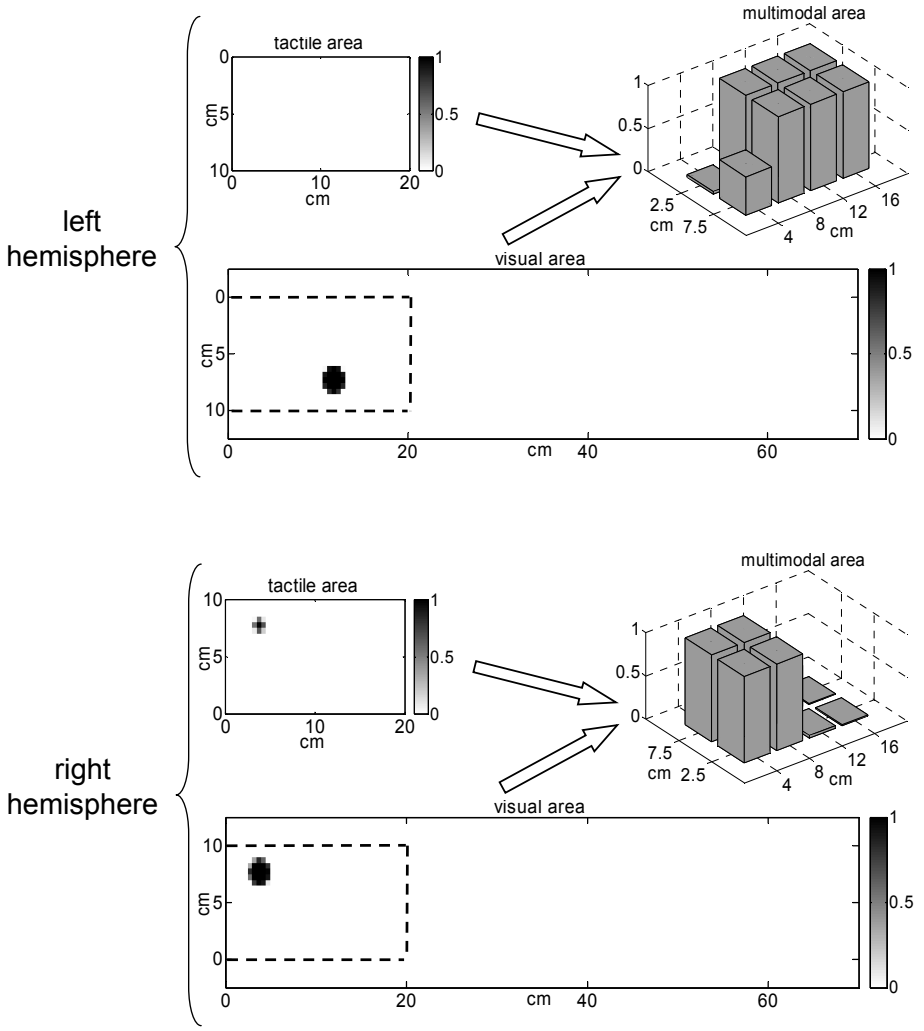

Figure 5.7 – RBD patients: bilateral stimulation (cross-modal facilitation). Network activity in response to a double stimulation on the left hand (tactile stimulus and visual stimulus located at the same position x=7.5 cm and y=4 cm) and to a visual stimulus on the right hand located at x=7.5 cm and y=12 cm. All the stimuli have the same intensity I_0^S=2.6. The panels show the same quantities of Fig. 5.2 for both hemispheres.

Sensitivity analyses

As described above, two parameters in the right hemisphere ($\Lambda_{ex}^{t,R}$, $W_0^{t,R}$, representing lateral and feedforward synaptic strength from tactile unimodal neurons), have been reduced to simulate RBD patients with left tactile

extinction. In order to elucidate the role of these two parameters, we performed a sensitivity analysis on each of them (Figure 5.8). In panel A, we simulated the condition of a left hand tactile stimulation with a simultaneous right hand visual stimulation by using different values of parameter $\Lambda_{ex}^{t,R}$, while maintaining parameter $W_0^{t,R}$ at its reduced pathological value. Parameter $\Lambda_{ex}^{t,R}$ has been progressively reduced from the basal value 2.7 to the value 2 (at which $\Lambda_{ex}^{t,R} = \Lambda_{in}^{t,R}$ and so the effect of lateral excitatory synapses is cancelled by lateral inhibition). The two plots display only the activities of the unimodal and multimodal neurons on which the two stimuli are centred. In order to obtain left tactile extinction, reduction in parameter $W_0^{t,R}$ has to be associated with a decrease of parameter $\Lambda_{ex}^{t,R}$ below 2.35. In these conditions, only the central tactile neuron is slightly activated in the right hemisphere, while multimodal neurons remain silent (see Fig. 5.5). On the contrary, for values above 2.5 a balanced coexistence of the two stimuli (with an unimodal activation bubble in both hemispheres) occurs.

In panel B, the same simulation has been repeated by progressively reducing parameter $W_0^{t,R}$ from its basal value 2 to the value 0.2, while maintaining parameter $\Lambda_{ex}^{t,R}$ at the pathological value (2.3). Reducing only parameter $\Lambda_{ex}^{t,R}$ is not sufficient to produce left tactile extinction: only for values of $W_0^{t,R}$ below 1.4, the left stimulus produces a response weaker than that of the right stimulus, showing extinction as $W_0^{t,R}$ is reduced under 1.

Finally, in order to gain a deeper understanding on how the competition occurs between the two peri-hand representations in the model, we performed a sensitivity analysis on the parameters representing the weight of inhibitory synapses (from the inhibitory interneuron to the tactile unimodal areas: $\Gamma_0^{t,R}$, $\Gamma_0^{t,L}$). In Fig. 5.9 panel A, we simulated a bilateral tactile stimulation in a healthy subject, with the left stimulus slightly weaker then the right stimulus, using different values of the inhibitory weights. With the basal value of these parameters (1.8) the two stimuli coexist even if they are of different intensity. Conversely, at higher values (above 2.7), extinction occurs even assuming normal values for all the excitatory synapses in the right hemisphere: the weaker stimulus is extinguished and only the stronger one (on the right hand) survives.

Panel B simulates a bilateral tactile stimulation of equal intensity delivered to a pathological subject ($\Lambda_{ex}^{t,R}$=2.3; $W_0^{t,R}$ = 0.8), by using different values of the inhibitory weights. Extinction does not occur for

values of inhibitory synapses below 1.5, despite the reduction in the other two parameters.

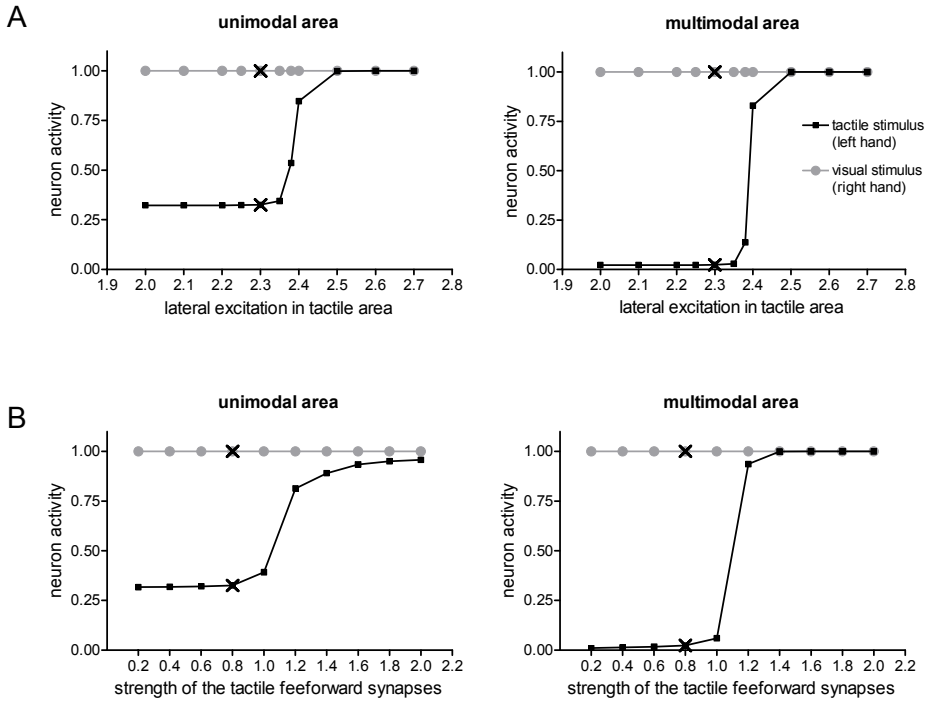

Figure 5.8 – Sensitivity analysis. Panel A: network activity in response to a tactile stimulus on the left hand, located at x=7.5 cm and y=4 cm and of a visual stimulus on the right hand, located at x=7.5 cm and y=12 cm. Both stimuli have the intensity $I_0^t = I_0^v$ =2.6. The plots show the neuronal activity of the unimodal (left plot) and multimodal (right plot) neurons on which the stimuli are centred. The simulations have been performed by progressively reducing the lateral excitation in tactile area ($\Lambda_{ex}^{t,R}$) from the basal value 2.7 to 2, while maintaining the strength of the tactile feedforward synapses at the pathological value $W_0^{t,R}$ =0.8. Panel B: the simulations are the same of Panel A, but they have been performed by progressively reducing the strength of the tactile feedforward synapses ($W_0^{t,R}$) from the basal value 2 to 0.2, while maintaining the lateral excitation in tactile area at the pathological value $\Lambda_{ex}^{t,R}$ =2.3. In both panels the marked points show the values used to simulate the RBD pathological conditions (see Table 5.2).

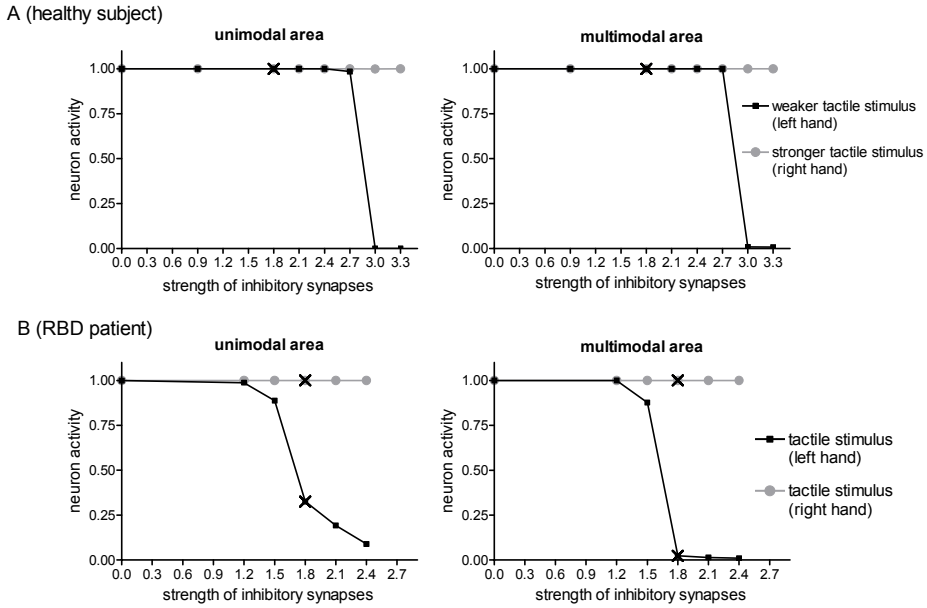

Figure 5.9 – Sensitivity analysis. Panel A: healthy subject. Network activity in response to a tactile stimulus of intensity I_0^t =2 on the left hand (x=7.5 cm and y=4 cm) and of a tactile stimulus of intensity I_0^t =2.6 on the right hand (x=2.5 cm and y=4 cm), in a healthy subject. The simulations have been performed by using different values (from 0 to 3) of the strength of inhibitory synapses (Γ_0^S). Panel B: RBD patient. Network activity in response the a tactile stimulus on the left hand (x=7.5 cm and y=4 cm) and of a tactile stimulus on the right hand (x=2.5 cm and y=4 cm), in a RBD patient. Both stimuli have the same intensity I_0^t =2.6. The simulations have been performed by using different values (from 0 to 2.4) of the strength of inhibitory synapses (Γ_0^S). Both panels show the neuronal activity of the unimodal (left plot) and multimodal (right plot) neurons on which the stimuli are centred; marked points show the values chosen as basal values (see Table 5.1).

5.4 Discussion

Investigation of the neural mechanisms underlying the representation of the external space has been assuming an increasing relevance in the last years. The brain appears to construct multiple and functionally segregated representations of space; these representations include personal, peripersonal

and extrapersonal space (Graziano and Gross 1995;Rizzolatti et al. 1997). Recent results from different approaches, involving electrophysiology, psychology and neurophsycology, converge in indicating that representation of peripersonal space is constructed in a multisensory fashion, plausibly related to multisensory neuronal populations which respond both to tactile stimuli on a particular body part and to visual stimuli in the surrounding external space (Rizzolatti et al. 1981;Graziano et al. 1997;Duhamel et al. 1998). Intrinsically linked with the mechanisms of internal representation of space, is the process of spatial attention (Driver and Spence 1998); it has been proven that attention to the space near the body operates crossmodally and not merely within single sensory modalities. The crossmodal links in spatial attention have been related to the activation of multimodal neural structures (Driver and Spence 1998;Bremmer et al. 2001;Macaluso and Driver 2005).

Despite the recent advances in the comprehension of peripersonal space representation, several questions still remain open, that may have important implications both for physiological and clinical knowledge. Among them: What is the organization of the neural circuitry underlying peripersonal space representation? How does it relate with the multimodal neurons identified electrophysiologically? How can information from unimodal areas convey toward multisensory neurons? May multimodal structures influence unimodal activity, e.g. via feedback projections? How can two simultaneous spatial representations interact? Which are the alterations in the neural circuitry that may explain extinction in brain damaged patients?

Neural network models and computer simulation techniques may provide important contributions to solve the previous questions and gain a deeper insight into the neural mechanisms at the basis of peripersonal space representation. This rationale has inspired the present work: by using the mathematical model, hypotheses on the involved neural networks have been formulated in rigorous quantitative terms, their reliability assessed vs. existing psycophysical data, the role of the included neural mechanisms elucidated by sensitivity analyses, and the multiple available knowledge summarized into a unique common framework. At present, we are not aware of any other neural network model focused on visual-tactile representation of peripersonal space, including competitive mechanisms among simultaneous representations.

The present model is concerned with the visual-tactile representation of the peripersonal space around both hands and their reciprocal influences, on which several electrophysiological and behavioural/neuropsychological data have been collected. It is worth noting that the proposed model does not aspire to reflect the neurophysiological and neuroanatomical knowledge in detail, but rather to identify a plausible structure of the network and the functional links between its different parts, to account for psychophysical and behavioural results. In the following, the organization of the network and the involved neural mechanisms are critically discussed on the basis of the obtained results and available in-vivo data.

The basic idea of the model is that the involvement of the perihand space by an event or object is signalled by the activation of multimodal visual-tactile neurons, that receive their inputs from two upstream unimodal areas: one is devoted to the somatotopic representation of the hand, the other is devoted to the coding of the visual space in hand-centred coordinates. Populations of neurons that respond to both visual and somatic stimuli in body-part centred coordinates have been found in several areas of macaque brain (especially in the frontal and parietal lobe, such as ventral intraparietal area, area 7b, area F4) and are believed to contribute to spatial representations (Hyvarinen 1981;Rizzolatti et al. 1981;Graziano and Gross 1995;Fogassi et al. 1996;Graziano et al. 1997;Duhamel et al. 1998). Anatomical data indicate that these multimodal neurons receive converging visual and somatosensory inputs from modality-specific areas, both primary and extraprimary (Rizzolatti et al. 1981;Graziano et al. 1997;Duhamel et al. 1998;Hihara et al. 2006). However, in the model, we did not establish any exact anatomical location for the multimodal and unimodal areas, that is the model does no reflect any definite anatomical structure.

Two sets of multimodal neurons (with the corresponding unimodal areas) have been considered in the model, in order to account for both hemispheres (i.e., both hands). Then, several different synaptic connections have been introduced within this structure, each with a distinct role and with specific implications on model outcomes.

Lateral synapses – Elements within the unimodal topological areas are linked via lateral synapses, modelled according to a "Mexican hat" disposition (a central excitatory area surrounded by an inhibitory annulus). This choice is justified by the fact that short-range excitation and long-range

inhibition among neurons - with a spatial function similar to that of a Mexican hat - is a pattern of connectivity that recurs frequently throughout the brain (Rolls and Deco 2002;Thivierge and Marcus 2007). Moreover, it is believed that this kind of connectivity plays a central role in the formation of topographically organized maps that can be found at different processing stages in the cortex (Thivierge and Marcus 2007). In the model, these connections are fundamental to sustain activation in the unisensory areas in response to a stimulus and to produce a sufficiently extended activation bubble.

Feedforward synapses – The feedforward synapses connecting unimodal to multimodal neurons affect the behaviour and properties of multimodal neurons. Thanks to the Gaussian arrangement of these synapses, multimodal neurons integrate information across homologous spatial locations in the two unisensory maps and create a multimodal map where visual and tactile receptive fields are aligned. By appropriately setting the standard deviation of the synapses, broad RFs - largely wider than unisensory neurons RFs - can be obtained for the multimodal neurons (see Fig.5.2 panels A and B). As a direct consequence of this disposition, multimodal area still responds to visual stimuli near the hand (provided they are applied approximately within three standard deviations from the hand) while remains silent in case of more distant stimuli (Fig. 5.2 panels C and D). All these characteristics (RFs alignment in different modalities, wide dimension of RFs, visually related activity degrading with the distance from the body) have been extensively documented by electrophysiological studies on multimodal neurons in the parietal and frontal lobes of the macaque brain (Rizzolatti et al. 1981;Colby et al. 1993;Graziano et al. 1997;Duhamel et al. 1998;Iriki et al. 2001).

Feedback synapses – Within the model, unimodal and multimodal areas interact not only via feedforward synapses, but also via feedback connections. Modulation of unisensory activity via back projections from multimodal areas is supported by a recent fMRI study by Macaluso et al. on healthy subjects (Macaluso and Driver 2005). They found that a visual stimulation near the right hand produced a cluster of activation in the left lingual gyrus (in the occipital lobe) that was significantly amplified by a concurrent tactile stimulation on the right hand. Amplification did not occur in case of a spatially incongruent bimodal stimulation (that is when the visual stimulus was applied far from the hand). Analysing changes in

effective connectivity, a circumscribed area in inferior parietal lobe (homolog to area 7b in the macaque brain) showed a higher coupling with the left lingual gyrus, during bimodal spatially congruent stimulation. The authors concluded that the tactile input to the somatosensory cortex may influence the visual cortex via back projections from multimodal populations in the parietal lobe, similar to that documented in area 7b of the macaque monkey. The model provides a theoretical sketch of this hypothesis: feedback synapses from multimodal to unimodal neurons produce an amplification of unimodal activity via crossmodal spatially-congruent stimulation (see Fig. 5.3). Thanks to the Gaussian distribution assigned to these synapses, the crossmodal amplification is spatially specific, occurring for visual and tactile stimuli applied approximately in the same position of the hand, and not in case of a visual stimulus delivered far from the hand.

Moreover, the presence of the feedback synapses is able to mimic behavioural results on pathological subjects. Halligan and colleagues (Halligan et al. 1997) reported that brain damaged patients with hemisensory loss of the upper limb felt a tactile sensation on the affected hand only when they were allowed to see the hand being touched. The authors proposed that this performance was determined by bimodal visual-somatosensory cells: "when limited tactile information is available, correlated visual input may boosts sub-threshold tactile stimulation into conscious awareness". Such situation corresponds to simulation results reported in Fig. 5.3: in that simulation a sub-threshold tactile stimulus, not perceived at the level of multisensory area, is impressively amplified by a concomitant visual stimulation in the homologous spatial location. Moreover, the model provides suggestions on neural correlates of perceptual awareness. According to the model, the absence of the tactile conscious percept in case of unimodal stimulation is due to the lack of activation of the multimodal neurons, despite the residual activity in the unisensory area. Conscious awareness of the tactile stimulus in case of bimodal stimulation is related to the activation of the multisensory neurons and to the consequent reinforcement of the unimodal tactile response thanks to the feedback synapses. That multimodal regions in the frontal-parietal area may be implicated in perceptual awareness has been suggested by recent studies on extinction patients (see discussion below).

Competitive inhibitory synapses – In the model, the two hemispheres are interconnected via inhibitory synapses realized through inhibitory interneurons. Accordingly, these connections realize a competitive mechanism between the two hemispheres when two events are simultaneously presented at the two sides of the peripersonal space. The existence of a competitive mechanism in attending two simultaneous bilateral events is strongly suggested by the observation that unilateral brain damaged patients show extinction only during bilateral stimulation. It has been recently proposed that extinction is a pathological, laterilazed exaggeration of an attentional limit that already exists for concurrent events in normals (Duncan 1996;Mattingley et al. 1997;Marzi et al. 2001). Furthermore, extinction has been found not only unimodally, but also crossmodally (e.g. visual-tactile extinction), suggesting that competition between two simultaneous events occurs also when they arise in separate modalities (as we assumed in the model). This is consistent with the "integrated competition" hypothesis of attention proposed by Duncan, according to which attention competition is played out across widespread neural networks, involving many sensory modalities (Duncan 1996).

The value assigned to the inhibitory interconnections play a critical role in the model. To allow the coexistence of two bilateral stimuli of similar intensity (as observed psychophysically in normals, (Hillis et al. 2006) (see Fig. 5.4), the strength of the competition has to be maintained limited. On the contrary, an excessively high competition produces a phenomenon analogous to extinction even by maintaining normal values of parameters in the right hemisphere: a subtle difference in stimulus intensity is sufficient to cause the extinction of the weaker stimulus (Fig. 5.9 panel A).

By assuming the previous structure, we used the model to shed light on the neural mechanisms underlying extinction in unilateral brain damaged patients. In particular, we focused on left tactile extinction. Nowadays, extinction is attributed to a pathological imbalance in attentional competition consequent to the lesion, which may lead the ipsilesional stimulus to extinguish the contralesional stimulus from awareness when both compete for attention. The fact that extinction patients are able to report isolated contralesional stimuli induced some authors to exclude any complete peripheral sensory loss (Mattingley et al. 1997). Despite this general

consensus, the neural correlates of extinction and perceptual awareness are still controversial.

Recent fMRI and ERP studies were designed to investigate the neural basis of extinction (Marzi et al. 2001;Eimer et al. 2002;Sarri et al. 2006). The main results are reported here. i) Sarri et colleagues (Sarri et al. 2006) performed an fMRI study on a right hemisphere stroke patient; they observed that unilateral tactile stimulation of the left hand produced a near-threshold activation in the right primary somatosensory cortex. However, the stimulus was consciously perceived. Eimer et al (Eimer et al. 2002), using ERP measures on a different patient, found that the P60 component (a sensory specific somatosensory component) was significantly reduced over the right hemisphere in response to unilateral left tactile stimulation, compared with the left hemisphere component in response to unilateral right tactile stimulation. Similar findings were observed in ERP studies on patients with left visual extinction (Marzi et al. 2001). The reduced activation in the sensory cortex suggests that an underlying deficit in extinction patients exists also for unilateral stimulation, but it is behaviourally unmasked only during bilateral stimulation. ii) Besides sensory cortex, also surviving right parietal and frontal cortices were activated by consciously perceived left touches (Sarri et al. 2006). iii) Extinguished left touch in the presence of a competing right event was still accompanied by some residual activation of the right somatosensory cortex (Sarri et al. 2006), and could still trigger some P60 and N110 components over right somatosensory cortex (Eimer et al. 2002). iv) However, no activation in the right parietal and frontal region was observed in case of left tactile extinction. The previous data suggest that activation of the sensory cortex alone is not sufficient to produce conscious percept; rather, higher-level multisensory regions in the frontal-parietal area could be implicated in perceptual awareness.

Consistent reproduction of these experimental findings has been obtained with the model by assuming only the reduction of two parameters in the right hemisphere, representing synapses from unimodal tactile neurons: the lateral excitation in the right tactile area, and the strength of the feedforward connections from the tactile neurons to the multimodal neurons. The first parameter influences the intensity and extension of the activation bubble in

the right tactile area in response to a left tactile stimulus; the second affects the responsiveness of multimodal neurons to a left tactile stimulus.

An important point is that, in the present model, a single neural unit should not be considered as an individual cell, but rather as a representation of a pool of cells, with the RF approximately located in the same position. Hence, the hypothesized reduction in synaptic strength should be interpreted not as a real synaptic depression, but rather as the effect of a reduction in the number of effective excitatory units which contribute to activity in that region. Of course, the smaller the number of effective excitatory cells, the smaller the overall excitatory input arriving to the other connected areas.

With these modifications the following results have been obtained. i) An unilateral left-hand tactile stimulus produces a significantly smaller cluster of activation in the tactile area compared with the normal subject (see Fig. 5.5). Hence, in the model a certain impairment exists also for unilateral stimulation (as observed in vivo). ii) However, the reduced unimodal activity is still able to evoke a response in the multimodal area (Fig. 5.5). This reflects the activation of right parietal and frontal region observed experimentally. iii) When the left tactile stimulus is coupled with a right hand stimulation, a large part of activation in the right tactile area is abolished but a weak activity still survives (fig. 5.6A). iv) The residual unimodal activity is not sufficient to excite multimodal neurons (fig. 5.6A). This corresponds to the lack of activation of right parietal-frontal cortex, despite activation of sensory cortex, reported by fMRI studies in extinguished left touches.

According to the previous description, the model identifies potential functional alterations in the neural circuitry able to explain extinction and relating cortical phenomena. It is worth noting that the achievement of the previous results crucially depends on two factors. First, both parameters have to be changed to reproduce left tactile extinction; reduction of only one parameter, while maintaining the other at its basal value, is not sufficient (Fig. 5.8). Furthermore, even the simultaneous reduction of the two parameters in the right hemisphere does not produce extinction of the left tactile stimulus in presence of a mild competition between the two hemispheres (Fig 5.9 panel B). Hence, several neural mechanisms are concurrently involved in extinction, and only certain combinations of parameters seem to be consistent with this perceptual impairment.

The scenario provided by the model is also able to reproduce the phenomenon of cross-modal visual-tactile facilitation (see Fig 5.7): model ascribes this phenomenon to activation of multisensory neurons by a simultaneous visual stimulus, with the consequent reinforcement of tactile activity in the same spatial position (and in the same hand) via feedback projections.

Finally, we wish to stress some possible limitations of the present model, that can be the subject of future extensions. First, in our model, the visual information reaching the multisensory layer is coded in a hand-centred frame of reference rather than in retinal (or eye-centred) coordinates. How the brain performs coordinate transformation and remapping of receptive fields in different frames of reference is an extremely complex problem for which different theories have recently been developed (Pouget et al. 2002). This problem is behind the aim of the present work; here, we just assumed that an upstream process converts the visual input from eye-centred to hand-centred coordinates.

Second, spatial attention mechanisms included in the model refer only to "exogenous" attention, that is captured reflexively and involuntarily. A different, more active form of attention, called "endogenous" attention, is directed in a voluntary manner on the basis of current spatial expectancies. Some studies indicate qualitative differences between the two forms of attention and distinct neural substrates (Driver and Spence 1998). The model simulates only exogenous spatial attention mechanisms, and does not account for possible top-down mechanisms of endogenous spatial attention.

Although the structure of the network and the set of parameter values provide a plausible scenario, other mechanisms not included in the network could play a role. For example, the two unimodal areas might be linked also via direct synapses (Schroeder and Foxe 2005); at present, neurons in the visual area and in the tactile area communicate only indirectly, via the feedback projections from the multimodal neurons. This choice has been adopted according to the criterion of parsimony, i.e. to reduce the number of mechanisms included in the model, and to find a good compromise between completeness and computational simplicity. However, a direct communication between unimodal neurons is possible and its role may be investigated in future studies.

Recent studies, performed both in animals and human subjects, have shown that peripersonal space representation is not fixed but exhibit plasticity properties (Iriki et al. 1996;Farne and Ladavas 2000;Ladavas 2002;Maravita and Iriki 2004). Data on peri-hand space show that the use of tools, the viewing of the hand in mirrors or in vide-screens may modulate the visuotactile representation of the peripersonal space. The issue of plastic modification of peripersonal space representation has not been faced in the present study. However, the model, with the addition of learning rules on synapses, may be used to simulate the dynamic properties of peripersonal space representation and to provide explanation for the neural basis of tool-use behaviours, testing the different and competing hypotheses suggested in literature (see Chapter 6).

CHAPTER 6

A NEURAL NETWORK MODEL OF MULTISENSORY REPRESENTATION OF PERIPERSONAL SPACE: EFFECT OF TOOL USE

6.1 Introduction

As discussed in Chapter 5, peripersonal space is defined as the space immediately surrounding the body (Rizzolatti et al. 1997). Representation of peripersonal space is crucial for a variety of actions, such as planning purposeful movements of reaching and grasping, avoiding obstacles during locomotion, protecting the body from attack and collision (Rizzolatti et al. 1997;Graziano and Cooke 2006). Neural maps receiving convergent inputs from different sensory modalities (such as somatosensory and visual information) are believed to be essential for the analysis of the spatial relations between body's parts and immediate surrounding and for the construction of a coherent and continuously updated representation of the peripersonal space. As described in Chapter 5, such neural maps have been documented in several areas of the macaque's brain. The existence of a similar multisensory representation of the peripersonal space in humans has been provided by neuropsychological studies on right-brain damaged patients affected by left tactile extinction.

Recent studies (Iriki et al. 1996;Farne and Ladavas 2000;Ishibashi et al. 2000;Berti and Frassinetti 2000;Maravita et al. 2002b) performed both on animals and human subjects have shown that the effective use of a tool to interact with distant objects may induce a plastic modification of the peripersonal space representation. In monkeys, visual RFs of bimodal neurons in intraparietal area were elongated to include the entire length of the tool after the animal was trained to use a handheld rake to reach distant food, whereas before training the visual RFs were limited near the hand (Iriki et al. 1996;Ishibashi et al. 2000). Expansion of visual RF followed only an active, intentional use of the tool, not its mere holding by the hand. A similar remapping of far space as near space emerge in behavioral studies on

human subjects (both patients and healthy subjects) (Farne and Ladavas 2000;Berti and Frassinetti 2000;Maravita et al. 2002b). For example, cross-modal extinction by presenting a visual stimulus far from the ipsilesional hand and near the tip of a handheld rake was more severe after the patient used the tool to reach distant objects with respect to conditions in which the rake was not used (Farne and Ladavas 2000).

Although plasticity of the peripersonal space induced by tool use has been extensively documented in the literature, the underlying neural mechanisms are still largely unknown. Few neurophysiological studies in recent years suggest that concrete morphological changes (including growth and sprouting of new synapses) could be induced by tool-use training (Ishibashi et al. 2002;Hihara et al. 2006)

Neural network models and computer simulation techniques represent a fundamental tool to gain a deeper insight into the mechanisms responsible for the plasticity of peripersonal space representation and to investigate the spatial properties of peripersonal space extension. Indeed, mathematical models allow the formulation of hypotheses in rigorous quantitative terms, the validation/rejection of these hypotheses on the basis of available data, and integration of the multiplicity of neurophysiological and neuro-psychological results into a coherent structure.

Aim of this work is to use the neural network model described in Chapter 5 to simulate peripersonal space representation after a tool-use training, both in healthy and RBD subjects. Plastic modification induced by tool-use training is reproduced by means of a Hebbian rule, according to which synaptic connections are reinforced in presence of simultaneous activation of the pre-synaptic and post-synaptic neurons.

6.2 Method

6.2.1 Mathematical description

The description of the model, as well as model equations, can be found in Chapter 5, section 5.2.1.; for this reason they are not reported here.

6.2.2 Model Plasticity

In this chapter, the model was used to simulate the results of learning experiments, in which the subject uses a long tool to connect his right hand with a visual stimulus located in distant space (Iriki et al. 1996;Ishibashi et al. 2000;Maravita et al. 2002b). To this end, we assumed that the synapses linking the unimodal to the multimodal areas in left hemisphere ($W_{ij,hk}^{s,L}$) are subject to Hebbian plasticity.

Figure 6.1 illustrates the inputs to the model used during the learning phase. We assumed that the subject uses an elongated tool extending from the centre of the hand to the horizontal direction. The upper panel shows the tactile input, corresponding to the portion of the hand stimulated when holding the tool. The lower panel shows the visual stimulus, which matches the overall tool, after the enhancement of the contrast performed by the retina cells. The portion of the visual response after the enhancement of the contrast is emphasized in red; the mechanism performed by retina cells acts along the length of the tool (along the y direction) selecting the handle and the tip (portions of the visual stimulus where the tool is functionally used). Figure 6.2 illustrates the network activity in response to the inputs described in Fig. 6.1; as we can see in the figure, all multimodal neurons are completely activated while, in the visual unimodal area, only the handle, the tip and the contour are emphasized.

After application of the previous inputs, synapses are modified with the following rule (for the meaning of symbols refers to Chapter 5):

$$W_{ij,hk}^{s,L}(t+T_s) = W_{ij,hk}^{s,L}(t) + \gamma \cdot z_{hk}^{s,L}(t) \cdot z_{ij}^{m,L}(t) \qquad (6.1)$$

where $W_{ij,hk}^{s,L}$ (s = t,v) represents the strength of the synaptic connection linking neuron hk in the tactile or visual area to neuron ij in the bimodal area, T_S is the sampling time, γ is the learning rate with assigned value 0.06.

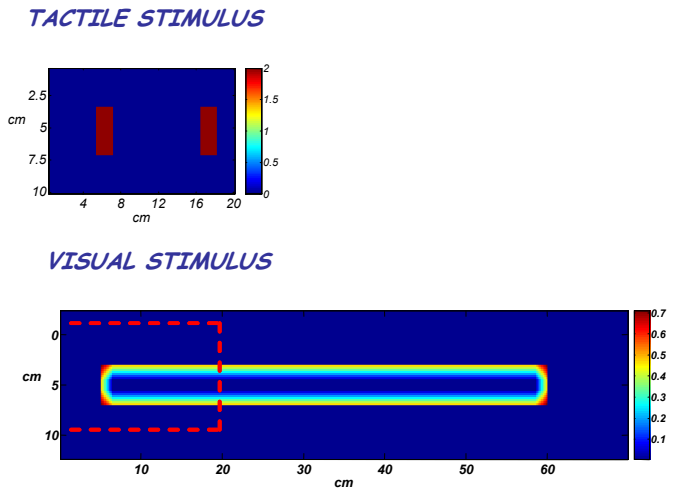

Figure 6.1 – Tactile and visual stimuli used during the learning phase. The upper panel shows the tactile input, corresponding to the portion of the right hand stimulated when holding the tool. The lower panel shows the visual stimulus, which matches the overall tool, after the enhancement of the contrast performed by the retina cells. The tool has dimensions 55 x 4 cm.

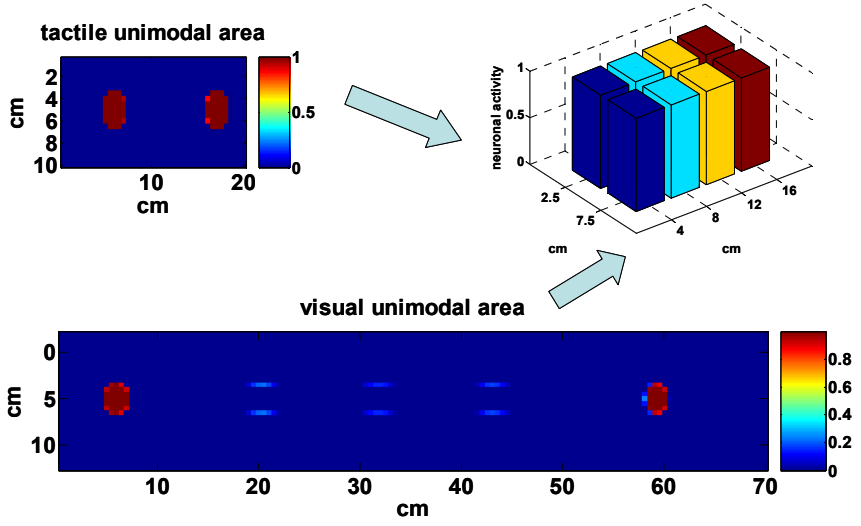

Figure 6.2 – Network activity in response to the tactile and visual stimuli used during the learning phase. The plot shows the neuronal activity in unimodal areas and the response of the 8 multimodal neurons. The activity in unimodal area is represented by a colormap scale, in multimodal area by a 3D visualization.

6.3 Results

In this work we first simulated the synapses plasticity. During the learning experiment the synapses linking unimodal to multimodal neurons are subject to plastic modifications (Hebbian learning rule). In Fig. 6.3 we represented, as an example of the plastic modification, one of the synapses linking unimodal areas to multimodal neurons; as we can see in the plots, after the training with the tool, the synapses expand to include the spatial regions where the tool was functionally used.

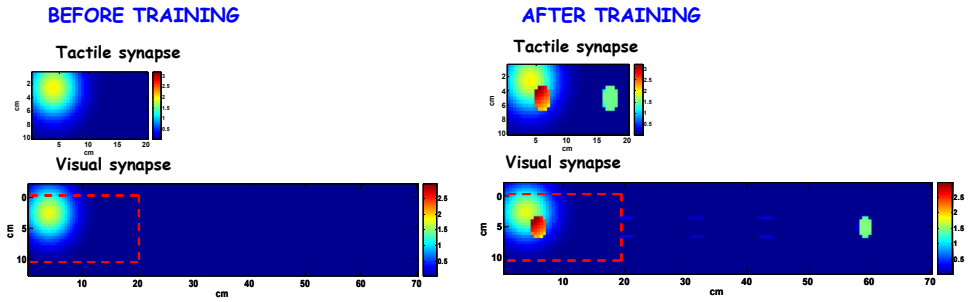

Figure 6.3 – Example of synapses plasticity. Representation of the synapses linking tactile and visual neurons to the multimodal neuron located in x=2.5 cm and y=4 cm. The plot shows by a colormap scale the synapses before and after training with the tool.

Subsequently we simulated the right and left hand interaction after a tool-use training in healthy and pathological subjects. As we described in Chapter 5, in basal conditions, a tactile or a visual stimulus placed on the hand is able to evoke a significant activation in multisensory neurons, while a visual stimulus distal from the hand does not induce any response (see Chapter 5, Fig. 5.2). In Fig. 6.4 we simulated the interaction between a tactile stimulus applied on the left hand and a visual stimulus applied far from the right hand in a healthy subject. As we can see, after the training, a visual stimulus located far from the right hand activates multimodal neurons provided it is applied in a position of space where the tool operated during training. After the synapses expansion in fact, the far visual stimuls is perceived as belonging to the right hand and it boosts the multisensory representation. Therefore, as we discussed in Chapter 5, the two stimuli lead

to the competition between the two multisensory representations of the corresponding hands. The competition is unbiased and the outcome is the coexistence of both right and left hand representations.

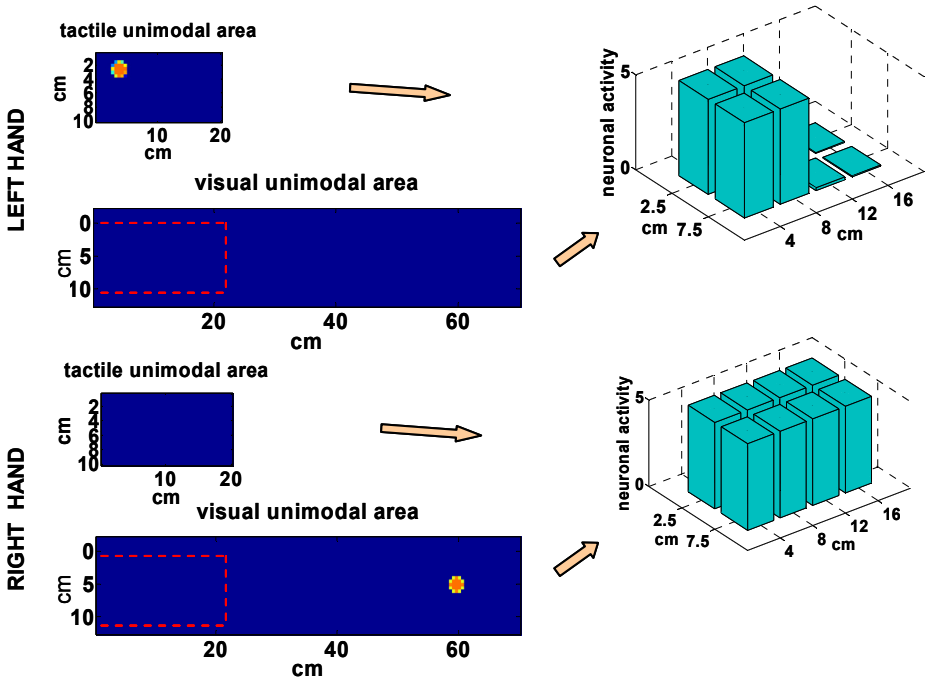

Figure 6.4 – Expansion of peripersonal space (Healthy subjects). Network activity in response to a tactile stimulus on the left hand (x=2.5 cm, y=4 cm) and a visual stimulus far from the right hand (x=5 cm, y=59.5 cm) after the training with the tool. The plots show the same quantities of Fig. 6.2 for both hemispheres.

Then, we simulated patients suffering from left tactile extiction. As we discussed in Chapter 5 (see Fig. 5.6) in these patients, a tactile stimulus applied on the left hand is extinguished by a visual stimulus applied near the right hand. In the simulation performed in this chapter, we demonstrated that, after the right hand has been trained to use a long tool, left tactile extinction occurs also when a visual stimulus is applied far from the right hand; in fact, as we explained for healthy subjects, a visual stimulus located far from the right hand, in a position of space where the tool operated during training, activates multimodal neurons and also the corresponding

representation of the hand. As we discussed in Chapter 5, in pathological subjects the competition between the representations of the two hands is uneven and the final outcome of the network is the extinction of the activity in the tactile area of the right hemisphere (only the central neuron remains slightly activated), and the consequent deactivation of multimodal neurons. Hence, only the right hand representation survives. This result is represented in Fig. 6.5.

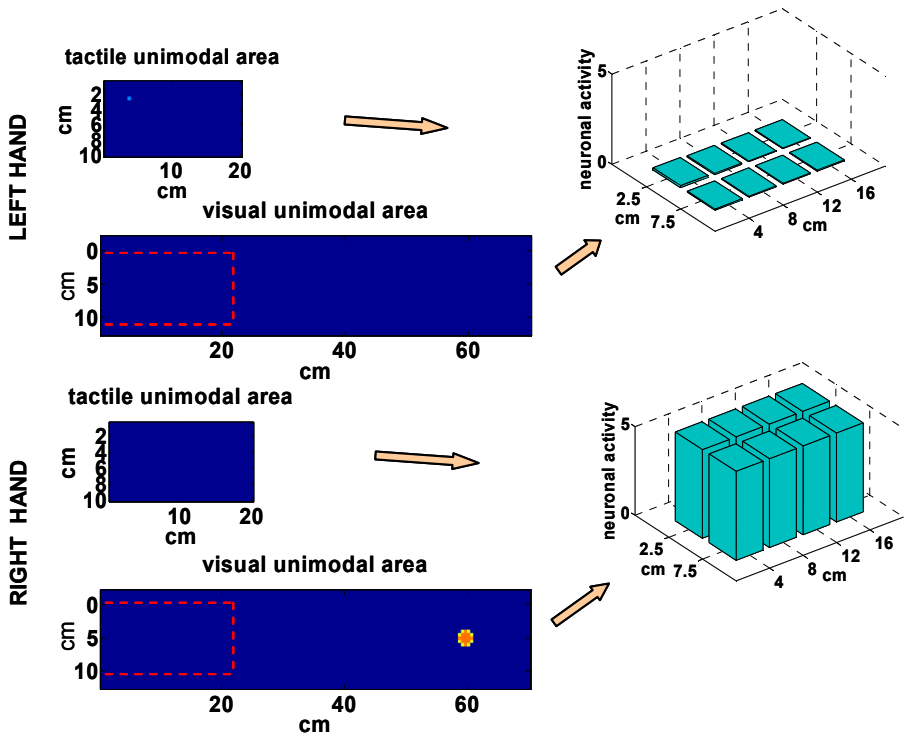

Figure 6.5 – Expansion of peripersonal space (RBD subjects). Network activity in response to a tactile stimulus on the left hand and (x=2.5 cm, y=4 cm) and a visual stimulus far from the right hand (x=5 cm, y=59.5 cm) after the training with the tool. The plots show the same quantities of Fig. 6.2 for both hemispheres.

6.4 Discussion

The main purpose of this chapter was to provide a preliminary instrument for analysis and planning of clinical studies. The perception of

the peripersonal space, and the link between visual and tactile body information, in fact, may be altered in pathological conditions (as in brain-damaged patients or in patients with arm-amputation). Furthermore, recent data demonstrate that our perception of the peripersonal space is not a static one, but can be modified by experience and training (Farne and Ladavas 2000;Berti and Frassinetti 2000;Maravita et al. 2002b). These modifications may reflect changes in the connections among the neurons (Ishibashi et al. 2002;Hihara et al. 2006), hence their full understanding requires a network able to summarize the main processing steps from the unimodal sensory areas to the bimodal specialized cortex, and their adapting changes.

In this work we used the model described in Chapter 5 to simulate the plastic expansion of peripersonal space by means of an Hebbian reinforcement of synapses converging into bimodal neurons. The exempla shown suggest that this model can explain the expansion of the peri-hand space occurring after the use of a tool, both in healthy and pathological subjects. The model ascribes such an expansion to the enlargement of the visual receptive field of bimodal neurons, induced by the reinforcement of synapses that were just latent before the experiment. Moreover, the model emphasizes the importance of retina cells, which permorm the enhancement of the contrast of the visual information, emphasizing only the portions of functional relevance to induce the reinforcement of synapses and produce the enlargement of bimodal neurons visual RF. Indeed, neurophysiological data on monkeys (Iriki et al. 1996;Ishibashi et al. 2000), show that the expansion of the peripersonal space occurs only if the tool is effectively used to reach objects, and not if the tool is simply hold in hand. This suggests that concurrent visuo-tactile information from the tool is not sufficient to elongate peri-hand space, without an attentive mechanism focused on the effective and functional use of the tool.

Finally, we wish to stress some possible limitations of the present model, that can be the subject of future extensions. In our model only the feedforward synapses linking the unimodal to multimodal neurons are subject to the Hebbian reinforcement; in future studies we could simulate the expansion also of the feedback synapses linking the multimodal to unimodal neurons. Furthermore, as we know from the experiments performed on monkeys and humans described in literature (Farne and Ladavas 2000;Ishibashi et al. 2002;Hihara et al. 2006), the effect of the expansion of

synapses due to the training with the tool is not permanent and it decreases with the time. In our model we didn't consider this behaviour but in future implementations we could include a mechanism which takes into account the decrease of the after training effect.

In addition to the potential benefits described in Chapter 5, we wish to discuss about another important potentiality of the model. The importance of the simulations performed in this Chapter and in Chapter 5 resides also in clinical application and rehabilitation of subjects with neurological deficits (for instance, brain-damaged subjects with a dense hemisensory loss of the upper limb). In these patients, cross-modal (visual-tactile) stimulation paradigms are frequently used during clinical tests, and interpretation of these trials with the model may be of potential interest. Therefore, the inclusion in our model of feedback projections from multimodal neurons to unisensory areas (see Chapter 5, Fig. 5.7), whose existence has been demonstrated by recent neurophysiological studies, may allow the simulation of experiments, in which activation of the bimodal visuo-tactile system improves sensory detection in the unimodal areas (Macaluso et al. 2000;Serino et al. 2007). In particular, with the model, we could also simulate the cross-modal facilitation effect in RBD subjects after the training with a tool used with the controlesional hand (Maravita et al. 2002a).

In general, the model may have potential benefits in suggesting a large number of clinical experiments for rehabilitation or treatment of neurological patients.

CONCLUSION

In this work we described mathematical models to simulate the integration among cortical regions in the brain. The problem has been deepened at two different levels: functional connectivity and multisensory integration.

Part 1. The first part of the thesis is focused on the use of neural mass models to infer information on integration among the activities of different cortical regions connected during a cognitive or a motor task, both using the model as a simulator to generate signals and gain a deeper insight into to possible effect of connectivity on measured data, and as a part of an algorithm, to derive connectivity from data. Modelling the relationship between connectivity and EEG power spectral density may be of the greatest value in neurophysiology. In Part 1 we described two different mathematical models. The main difference between the first model (Chapter 1-2) and the second model (Chapter 3-4) is that in the latter, multiple rhythms can be generated within a single population, which becomes representative of a ROI (Region Of Interest), while in the first model a ROI is built as the parallel arrangement of three populations. With both models we performed an analysis of coherence, and of the position of peaks in PSDs; this study revealed important information on the possible long-range connections among populations, especially useful to follow temporal changes in connectivity. But the most ambitious step of the research described in Part 1 was to check whether the models described in Chapters 1-4, trained with a minimization algorithm, could “discover” a simple pattern of connectivity, starting from real data, under a few basic hypotheses.

We focused attention on several related problems: which are possible mechanisms causing different rhythms in EEG spectra? Can these rhythms coexist within the same population of neurons? How are these rhythms modified by connectivity among populations? How these populations can integrate their activity during a task? Is it possible, using a model of interconnected ROIs, to infer a simple pattern of connectivity with an automatic algorithm, so that each ROI produces the same cortical EEG spectrum as data obtained from in vivo measurement?

Results obtained with the minimization algorithm are encouraging. Both with the model described in Chapters 1-2 and the model described in Chapter 3-4, the algorithm found simple patterns of connectivity, which explain EEG power spectral density carefully, and seemed quite repetitive in the subjects.

The results described in Part 1 show the potential benefits coming from the use of neural mass model in the study of functional connectivity. On the basis of the results, we claim that these models may have interesting potential applications:

i) to help validation or rejection of existing hypotheses. For instance, a model may be used to implement a hypothesized pattern of connectivity among neural populations (as suggested by neuphysiological theories, neuro-anatomical knowledge, or as obtained from empirical existing algorithms, such as the partial directed coherence). Model results can then be compared with existing data, to understand whether this scenario is compatible with data or not;

ii) the model may help to investigate the possible origin of temporal changes in data. As observed in Chapter 1, PSDs in brain regions change during the temporal evolution of a task, reflecting a change in connectivity and/or in the internal structure of a region. Starting from a given initial model, which simulates PSDs, cross-spectra and coherences in basal conditions, the model may reveal which possible changes in parameters are able to explain temporal variations in the data. This is for instance, the approach used by Wendling et al. to analyze epileptic phenomena;

iii) the model may suggest new experiments (for instance, concerning activation or de-activation of regions with Transcranial Magnetic Stimulation), able to discriminate among different possible hypotheses. The effect of alternative stimuli can be simulated with the model, using different sets of connectivity and/or different parameter values, and the stimuli which are more discriminative among the alternative scenarios suggested as physiological tests;

iv) the model can be used to link data obtained with different techniques. In Chapter 3 we focused attention or membrane potential of pyramidal neurons, as the best signal to mimic cortical EEG. Synaptic activity can be also included in the analysis to have a signal more closely related to fMRI or PET. Spike activity can be used to mimic measurement performed on individual neurons (as in animal experiments). All these signals can then be

simulated with the same model, to integrate results obtained with different measurement techniques into a coherent scenario;

v) the model can be used to test the reliability of methods (such as the partial directed coherence (PDC), the directed transfer function (DTF) and the direct DTF (dDTF) currently used to extract effective connectivity from data. To this end, simulated cortical EEGs can be produced by the model, using different patterns of connectivity and/or of different values of internal parameters. These data can then be propagated to the cortex with the addition of some noise, to simulated scalp EEGs. The results obtained on these scalp EEGs with current techniques for connectivity estimation can then be compared with the "true" connectivity values used in the model, to reveal in which cases the current methods can extract the original connectivity, and in which cases they fail. A similar approach has been proposed by David et al. .

Finally, the emphasis of this entire Part 1 is on the possibility to understand how the brain integrate the information coming from the activity of different cortical regions and to infer information on connectivity during cognitive or motor task. The results in fact may be of value for a deeper comprehension of mechanism causing EEG rhythms, for the study of brain connectivity, for the test of neurophysiological hypotheses, and for integration of results obtained with different neuroimaging techniques into a definite theoretical framework. Although this research is still at a preliminary stage, the present work represents a first promising attempt in that direction.

Part 2. The second part of the thesis is focused on the visual-tactile representation of the peripersonal space around both hands and their reciprocal influences, by means of an original mathematical model. Investigation of the neural mechanisms underlying the representation of the external space has been assuming an increasing relevance in the last years. Recent results from different approaches, involving electrophysiology, psychology and neuropsychology, converge in indicating that representation of peripersonal space is constructed in a multisensory fashion, plausibly related to multisensory neuronal populations which respond both to tactile stimuli on a particular body part and to visual stimuli in the surrounding external space, and integrate the information coming from different unimodal areas to create a multisensory representation of the peripersonal

space. In this context, neural network models and computer simulation techniques may represent a guide in solving the previous problems.

In Part 2 we described an original neural network model to simulate the organization of the neural circuitry underlying peripersonal space representation, and investigate the neural mechanisms involved in the integration among unimodal and multimodal information. With the model we summarized data coming from neuropsychological and clinical experiments and simulated different physiological conditions in healthy subjects: the visual-tactile coding of the perihand space, the cross-modal influences on unisensory perception, the right and left hand interaction. Furthermore we studied the alterations in the neural circuitry which explain extinction in right brain damaged (RBD) patients and we simulated some clinical experiments: unilateral stimulation, cross-modal extinction and cross-modal facilitation (see Chapter 5). We used the model also to reproduce the plastic modification of the peripersonal space after the training with a tool, both in healthy and RBD subjects (see Chapter 6).

At present, we are not aware of any other neural network model focused on visual-tactile representation of peripersonal space, including competitive mechanisms among simultaneous representations. However, it is worth noting that the proposed model does not aspire to reflect the neurophysiological and neuroanatomical knowledge in detail, but identify a possible structure of the network to take into account for psychophysical and behavioural results.

It is also important to discuss some possible limitations of the present model. In our model, the visual information reaching the multisensory layer is coded in a hand-centred frame of reference rather than in retinal (or eye-centred) coordinates. The problem of how the brain performs coordinate transformation and remapping of receptive fields in different frames of reference is extremely complex; in this work we didn't examine this problem, we just assumed that an upstream process converts the visual input from eye-centred to hand-centred coordinates. Furthermore, although with the model we reproduced a plausible scenario, we didn't include some mechanisms which could play an important role. At present, neurons in the visual area and in the tactile area communicate only indirectly, via the feedback projections from the multimodal neurons; this choice has been adopted according to reduce the number of mechanisms included in the

model, and to find a good compromise between completeness and computational simplicity. However, a direct communication between unimodal neurons is possible and its role may be investigated in future studies.

On the basis of the results obtained in Chapters 5 and 6, we state the importance of modelling in electrophysiology, psychology and neuropsychology fields. With the model we have the possibility to simulate different psychological and neurophysiological experiments, and to test different pathological conditions. Potential benefits of the studies described in Part 2 reside in clinical application and rehabilitation of subjects with neurological deficits (for instance, brain-damaged subjects with a dense hemisensory loss of the upper limb). In these patients, cross-modal (visual-tactile) stimulation paradigms are frequently used during clinical tests, and interpretation of these trials with the model may be of potential interest. In this context, the feedback projections from multimodal neurons to unisensory areas described in our model, may allow the simulation of experiments, in which activation of the bimodal visuo-tactile system improves sensory detection in the unimodal areas.

Finally, models may be used to test the reliability of alternative hypotheses on the neural networks involved in the perihand representation and gain a deeper insight into the neural mechanisms implicated in the process of integration in the brain.

REFERENCES

1. Almeida R, Stetter M (2002) Modeling the link between functional imaging and neuronal activity: synaptic metabolic demand and spike rates. Neuroimage. 17: 1065-79.

2. Astolfi L, Cincotti F, Mattia D, Babiloni C, Carducci F, Basilisco A, Rossini PM, Salinari S, Ding L, Ni Y, He B, Babiloni F (2005) Assessing cortical functional connectivity by linear inverse estimation and directed transfer function: simulations and application to real data. Clin. Neurophysiol. 116: 920-32.

3. Astolfi L, Cincotti F, Mattia D, Fallani F, V, Salinari S, Ursino M, Zavaglia M, Marciani MG, Babiloni F (2006) Estimation of the cortical connectivity patterns during the intention of limb movements. IEEE Eng Med. Biol. Mag. 25: 32-8.

4. Astolfi L, Cincotti F, Mattia D, Marciani MG, Baccala LA, de Vico FF, Salinari S, Ursino M, Zavaglia M, Ding L, Edgar JC, Miller GA, He B, Babiloni F (2007) Comparison of different cortical connectivity estimators for high-resolution EEG recordings. Hum. Brain Mapp. 28: 143-57.

5. Astolfi L, Cincotti F, Mattia D, Salinari S, Babiloni C, Basilisco A, Rossini PM, Ding L, Ni Y, He B, Marciani MG, Babiloni F (2004) Estimation of the effective and functional human cortical connectivity with structural equation modeling and directed transfer function applied to high-resolution EEG. Magn Reson. Imaging ; 22: 1457-70.

6. Avillac M, Ben HS, Duhamel JR (2007) Multisensory integration in the ventral intraparietal area of the macaque monkey. J. Neurosci. 27: 1922-32.

7. Babiloni F, Cincotti F, Babiloni C, Carducci F, Mattia D, Astolfi L, Basilisco A, Rossini PM, Ding L, Ni Y, Cheng J, Christine K, Sweeney J, He B (2005) Estimation of the cortical functional connectivity with the multimodal integration of high-resolution EEG and fMRI data by directed transfer function. Neuroimage. 24: 118-31.

8. Baccala LA, Sameshima K (2001) Partial directed coherence: a new concept in neural structure determination. Biol. Cybern. 84: 463-74.

9. Baccalà L, Sameshima K (1998) Direct Coherence: a tool for exploring functional interactions among brain structures. In: Nicolelis M (ed) Methods for neural ensemble recordings. CRC Boca Raton, Fla., pp 179-92

10. Bartos M, Vida I, Frotscher M, Geiger JR, Jonas P (2001) Rapid signaling at inhibitory synapses in a dentate gyrus interneuron network. J. Neurosci. 21: 2687-98.

11. Bartos M, Vida I, Frotscher M, Meyer A, Monyer H, Geiger JR, Jonas P (2002) Fast synaptic inhibition promotes synchronized gamma oscillations in hippocampal interneuron networks. Proc. Natl. Acad. Sci. U. S. A ; 99: 13222-7.

12. Berti A, Frassinetti F (2000) When far becomes near: remapping of space by tool use. J. Cogn Neurosci. 12: 415-20.

13. Bremmer F, Schlack A, Shah NJ, Zafiris O, Kubischik M, Hoffmann K, Zilles K, Fink GR (2001) Polymodal motion processing in posterior parietal and premotor cortex: a human fMRI study strongly implies equivalencies between humans and monkeys. Neuron ; 29: 287-96.

14. Colby CL, Duhamel JR, Goldberg ME (1993) Ventral intraparietal area of the macaque: anatomic location and visual response properties. J. Neurophysiol. 69: 902-14.

15. Dale AM, Liu AK, Fischl BR, Buckner RL, Belliveau JW, Lewine JD, Halgren E (2000) Dynamic statistical parametric mapping: combining fMRI and MEG for high-resolution imaging of cortical activity. Neuron ; 26: 55-67.

16. David O, Cosmelli D, Friston KJ (2004) Evaluation of different measures of functional connectivity using a neural mass model. Neuroimage. 21: 659-73.

17. David O, Friston KJ (2003) A neural mass model for MEG/EEG: coupling and neuronal dynamics. Neuroimage. 20: 1743-55.

18. David O, Harrison L, Friston KJ (2005) Modelling event-related responses in the brain. Neuroimage. 25: 756-70.

19. Dayan P, Abbott LF (2001) Model Neurons I: Neuroelectronics. In: Theoretical Neuroscience. MIT Press, Cambridge, MA, pp 153-94

20. Di Pellegrino G, Ladavas E, Farne A (1997) Seeing where your hands are. Nature ; 388: 730.

21. Driver J, Spence C (1998) Attention and the crossmodal construction of space. TRENDS in Cognitive Sciences ; 2: 254-62.

22. Duhamel JR, Colby CL, Goldberg ME (1998) Ventral intraparietal area of the macaque: congruent visual and somatic response properties. J. Neurophysiol. 79: 126-36.

23. Duncan J (1996) Coordinated brain systems in selective perception and action. In: Innui T, McClelland JL (eds) Attention and Performance. MIT Press, Cambridge, MA, pp 549-78

24. Ebersole JS, Milton J (2002) The electroencephalogram (EEG): a measure of neural synchrony. In: Milton J, Yung P (eds) Epilepsy as a dynamical disease. Springer Verlag, Berlin, pp 51-68

25. Eimer M, Maravita A, van VJ, Husain M, Driver J (2002) The electrophysiology of tactile extinction: ERP correlates of unconscious somatosensory processing. Neuropsychologia ; 40: 2438-47.

26. Erickson KI, Ringo Ho MH, Colcombe SJ, Kramer AF (2005) A structural equation modeling analysis of attentional control: an event-related fMRI study. Brain Res. Cogn Brain Res. 22: 349-57.

27. Farne A, Ladavas E (2000) Dynamic size-change of hand peripersonal space following tool use. Neuroreport ; 11: 1645-9.

28. Fogassi L, Gallese V, Fadiga L, Luppino G, Matelli M, Rizzolatti G (1996) Coding of peripersonal space in inferior premotor cortex (area F4). J. Neurophysiol. 76: 141-57.

29. Freeman WJ (1978) Models of the dynamics of neural populations. Electroencephalogr. Clin. Neurophysiol. 34: 9-18.

30. Freeman WJ (1987) Simulation of chaotic EEG patterns with a dynamic model of the olfactory system. Biol. Cybern. 56: 139-50.

31. Friston KJ, Frith CD, Liddle PF, Frackowiak RS (1993) Functional connectivity: the principal-component analysis of large (PET) data sets. J. Cereb. Blood Flow Metab ; 13: 5-14.

32. Goldberg D. Genetic Algorithms in Search, Optimization, and Machine Learning. Addison-Wesley: Reading, MA, 1989.

33. Grave de Peralta R, Gonzalez Andino SL (1999) Distributed source models: standard solutions and new developments. In: Uhl C (ed) Analysis of neurophysiological brain functioning. Springer Verlag, Berlin, pp 176-201

34. Graziano MS, Cooke DF (2006) Parieto-frontal interactions, personal space, and defensive behavior. Neuropsychologia ; 44: 2621-35.

35. Graziano MS, Gross CG (1995) The representation of extrapersoanl space: a possible role for bimodal, visual-tactile neurons. In: Gazzaniga MS (ed) The cognitive neurosciences. MIT Press, Cambridge, MA, pp 1021-34

36. Graziano MS, Hu XT, Gross CG (1997) Visuospatial properties of ventral premotor cortex. J. Neurophysiol. 77: 2268-92.

37. Halligan PW, Hunt M, Marshall JC, Wade DT (1996) When seeing is feeling: acquired synaesthesia or phantom touch? Neurocase ; 2: 21-9.

38. Halligan PW, Marshall JC, Hunt M, Wade DT (1997) Somatosensory assessment: can seeing produce feeling? J. Neurol. 244: 199-203.

39. Hasselmo ME, Bodelon C, Wyble BP (2002) A proposed function for hippocampal theta rhythm: separate phases of encoding and retrieval enhance reversal of prior learning. Neural Comput. 14: 793-817.

40. Hasselmo ME, Wyble BP, Wallenstein GV (1996) Encoding and retrieval of episodic memories: role of cholinergic and GABAergic modulation in the hippocampus. Hippocampus ; 6: 693-708.

41. Hihara S, Notoya T, Tanaka M, Ichinose S, Ojima H, Obayashi S, Fujii N, Iriki A (2006) Extension of corticocortical afferents into the anterior bank of the intraparietal sulcus by tool-use training in adult monkeys. Neuropsychologia ; 44: 2636-46.

42. Hillis AE, Chang S, Heidler-Gary J, Newhart M, Kleinman JT, Davis C, Barker PB, Aldrich E, Ken L (2006) Neural correlates of modality-specific spatial extinction. J. Cogn Neurosci. 18: 1889-98.

43. Holmes NP, Spence C (2004) The body schema and the multisensory representation(s) of peripersonal space. Cogn Process ; 5: 94-105.

44. Horwitz B (2003) The elusive concept of brain connectivity. Neuroimage. 19: 466-70.

45. Horwitz B, Friston KJ, Taylor JG (2000) Neural modeling and functional brain imaging: an overview. Neural Netw. 13: 829-46.

46. Horwitz B, Tagamets MA, McIntosh AR (1999) Neural modeling, functional brain imaging, and cognition. Trends Cogn Sci. 3: 91-8.

47. Hyvarinen J (1981) Regional distribution of functions in parietal association area 7 of the monkey. Brain Res. 206: 287-303.

48. Iriki A, Tanaka M, Iwamura Y (1996) Coding of modified body schema during tool use by macaque postcentral neurones. Neuroreport ; 7: 2325-30.

49. Iriki A, Tanaka M, Obayashi S, Iwamura Y (2001) Self-images in the video monitor coded by monkey intraparietal neurons. Neurosci. Res. 40: 163-73.

50. Ishibashi H, Hihara S, Iriki A (2000) Acquisition and development of monkey tool-use: behavioral and kinematic analyses. Can. J. Physiol Pharmacol. 78: 958-66.

51. Ishibashi H, Hihara S, Takahashi M, Heike T, Yokota T, Iriki A (2002) Tool-use learning selectively induces expression of brain-derived neurotrophic factor, its receptor trkB, and neurotrophin 3 in the intraparietal multisensorycortex of monkeys. Brain Res. Cogn Brain Res. 14: 3-9.

52. Jansen BH, Rit VG (1995) Electroencephalogram and visual evoked potential generation in a mathematical model of coupled cortical columns. Biol. Cybern. 73: 357-66.

53. Jiang ZY (2005) Study on EEG power and coherence in patients with mild cognitive impairment during working memory task. J. Zhejiang. Univ Sci. B ; 6: 1213-9.

54. Jueptner M, Weiller C (1995) Review: does measurement of regional cerebral blood flow reflect synaptic activity? Implications for PET and fMRI. Neuroimage. 2: 148-56.

55. Kadekaro M, Crane AM, Sokoloff L (1985) Differential effects of electrical stimulation of sciatic nerve on metabolic activity in spinal cord and dorsal root ganglion in the rat. Proc. Natl. Acad. Sci. U. S. A ; 82: 6010-3.

56. Kaminski M, Blinowska K, Szclenberger W (1997) Topographic analysis of coherence and propagation of EEG activity during sleep and wakefulness. Electroencephalogr. Clin. Neurophysiol. 102: 216-27.

57. Kaminski M, Blinowska K, Szelenberger W (1995) Investigation of coherence structure and EEG activity propagation during sleep. Acta Neurobiol. Exp. (Wars.) ; 55: 213-9.

58. Kaminski M, Ding M, Truccolo WA, Bressler SL (2001) Evaluating causal relations in neural systems: granger causality, directed transfer function and statistical assessment of significance. Biol. Cybern. 85: 145-57.

59. Kaminski MJ, Blinowska KJ (1991) A new method of the description of the information flow in the brain structures. Biol. Cybern. 65: 203-10.

60. Kandel ER, Schwartz JH, Jessell TM (2000) The bodily senses. In: Principles of neural science. McGraw-Hill, New York, pp 430-50

61. Kennett S, Taylor-Clarke M, Haggard P (2001) Noninformative vision improves the spatial resolution of touch in humans. Curr. Biol. 11: 1188-91.

62. Korzeniewska A, Manczak M, Kaminski M, Blinowska KJ, Kasicki S (2003) Determination of information flow direction among brain structures by a modified directed transfer function (dDTF) method. J. Neurosci. Methods ; 125: 195-207.

63. Kubota Y, Sato W, Toichi M, Murai T, Okada T, Hayashi A, Sengoku A (2001) Frontal midline theta rhythm is correlated with cardiac autonomic activities during the performance of an attention demanding meditation procedure. Brain Res. Cogn Brain Res. 11: 281-7.

64. Ladavas E (2002) Functional and dynamic properties of visual peripersonal space. TRENDS in Cognitive Neuroscience ; 6: 17-22.

65. Ladavas E, Di Pellegrino G, Farne A, Zeloni G (1998) Neuropsychological evidence of an integrated visuotactile representation of peripersonal space in humans. J. Cogn Neurosci. 10: 581-9.

66. Ladavas E, Farne A, Zeloni G, Di Pellegrino G (2000) Seeing or not seeing where your hands are. Exp. Brain Res. 131: 458-67.

67. Lee L, Harrison LM, Mechelli A (2003b) A report of the functional connectivity workshop, Dusseldorf 2002. Neuroimage. 19: 457-65.

68. Lee L, Harrison LM, Mechelli A (2003a) The Functional Brain Connectivity Workshop: report and commentary. Network. 14: R1-15.

69. Lopes da Silva FH, van RA, Barts P, van HE, Burr W (1976) Models of neuronal populations: the basic mechanisms of rhythmicity. Prog. Brain Res. 45: 281-308.

70. Luck SJ, Woodman GF, Vogel EK (2000) Event-related potential studies of attention. Trends Cogn Sci. 4: 432-40.

71. Macaluso E, Driver J (2005) Multisensory spatial interactions: a window onto functional integration in the human brain. TRENDS in Neurosciences ; 28: 264-71.

72. Macaluso E, Frith CD, Driver J (2000) Modulation of human visual cortex by crossmodal spatial attention. Science ; 289: 1206-8.

73. Magosso E, Ursino M, Zavaglia M, Serino A, di Pellegrino G (2008) Visuotactile representation of peripersonal space: a neural network study. Submitted to Neural Computation .

74. Makarov VA, Panetsos F, de FO (2005) A method for determining neural connectivity and inferring the underlying network dynamics using extracellular spike recordings. J. Neurosci. Methods ; 144: 265-79.

75. Maravita A, Clarke K, Husain M, Driver J (2002a) Active tool use with the contralesional hand can reduce cross-modal extinction of touch on that hand. Neurocase ; 8: 411-6.

76. Maravita A, Iriki A (2004) Tools for the body (schema). Trends Cogn Sci. 8: 79-86.

77. Maravita A, Spence C, Kennett S, Driver J (2002b) Tool-use changes multimodal spatial interactions between vision and touch in normal humans. Cognition ; 83: B25-B34.

78. Marzi CA, Girelli M, Natale E, Miniussi C (2001) What exactly is extinguished in unilateral visual extinction? Neurophysiological evidence. Neuropsychologia ; 39: 1354-66.

79. Mattingley JB, Driver J, Beschin N, Robertson IH (1997) Attentional competition between modalities: extinction between touch and vision after right hemisphere damage. Neuropsychologia ; 35: 867-80.

80. McIntosh AR, Gonzalez-Lima F (1994) Network interactions among limbic cortices, basal forebrain, and cerebellum differentiate a tone conditioned as a Pavlovian excitor or inhibitor: fluorodeoxyglucose mapping and covariance structural modeling. J. Neurophysiol. 72: 1717-33.

81. Molyneaux BJ, Hasselmo ME (2002) GABA(B) presynaptic inhibition has an in vivo time constant sufficiently rapid to allow modulation at theta frequency. J. Neurophysiol. 87: 1196-205.

82. Natale E, Marzi CA, Girelli M, Pavone EF, Pollmann S (2006) ERP and fMRI correlates of endogenous and exogenous focusing of visual-spatial attention. Eur. J. Neurosci. 23: 2511-21.

83. Nudo RJ, Masterton RB (1986) Stimulation-induced [14C]2-deoxyglucose labeling of synaptic activity in the central auditory system. J. Comp Neurol. 245: 553-65.

84. Nunez P. Neocortical dynamics and human EEG rhythms. Oxford University Press: New York, 1995.

85. Pfurtscheller G, Graimann B, Huggins JE, Levine SP (2004) Brain-computer communication based on the dynamics of brain oscillations. Suppl Clin. Neurophysiol. 57: 583-91.

86. Pfurtscheller G, Lopes da Silva FH (1999) Event-related EEG/MEG synchronization and desynchronization: basic principles. Clin. Neurophysiol. 110: 1842-57.

87. Pouget A, Deneve S, Duhamel JR (2002) A computational perspective on the neural basis of multisensory spatial representations. Nat. Rev. Neurosci. 3: 741-7.

88. Rizzolatti G, Fadiga L, Fogassi L, Gallese V (1997) The space around us. Science ; 277: 190-1.

89. Rizzolatti G, Scandolara C, Matelli M, Gentilucci M (1981) Afferent properties of periarcuate neurons in macaque monkeys. II. Visual responses. Behav. Brain Res. 2: 147-63.

90. Robinson PA, Rennie CJ, Rowe DL, O'Connor SC, Wright JJ, Gordon E, Whitehouse RW (2003) Neurophysical modeling of brain dynamics. Neuropsychopharmacology ; 28 Suppl 1: S74-S79.

91. Rodriguez E, George N, Lachaux JP, Martinerie J, Renault B, Varela FJ (1999) Perception's shadow: long-distance synchronization of human brain activity. Nature ; 397: 430-3.

92. Rolls ET, Deco G. Computational neuroscience of vision. Oxford University Press: New york, 2002.

93. Rowe DL, Robinson PA, Rennie CJ (2004) Estimation of neurophysiological parameters from the waking EEG using a biophysical model of brain dynamics. J. Theor. Biol. 231: 413-33.

94. Rowe JB, Stephan KE, Friston K, Frackowiak RS, Passingham RE (2005) The prefrontal cortex shows context-specific changes in effective connectivity to motor or visual cortex during the selection of action or colour. Cereb. Cortex ; 15: 85-95.

95. Saito Y, Harashima H (1981) Tracking of information within multichannel EEG record. In: Yamaguchi N, Fujisawa K (eds) Recent advances in EEG and EMG Data Processing. Elsevier, Amsterdam, pp 133-46

96. Sarri M, Blankenburg F, Driver J (2006) Neural correlates of crossmodal visual-tactile extinction and of tactile awareness revealed by fMRI in a right-hemisphere stroke patient. Neuropsychologia ; 44: 2398-410.

97. Schillen TB, Konig P (1994) Binding by temporal structure in multiple feature domains of an oscillatory neuronal network. Biol. Cybern. 70: 397-405.

98. Schroeder CE, Foxe J (2005) Multisensory contributions to low-level, 'unisensory' processing. Curr. Opin. Neurobiol. 15: 454-8.

99. Serino A, Farne A, Rinaldesi ML, Haggard P, Ladavas E (2007) Can vision of the body ameliorate impaired somatosensory function? Neuropsychologia ; 45: 1101-7.

100. Singer W (1999) Neuronal synchrony: a versatile code for the definition of relations? Neuron ; 24: 49-25.

101. Strelets VB, Garakh Z, Novototskii-Vlasov VY, Magomedov RA (2006) Relationship between EEG power and rhythm synchronization in health and cognitive pathology. Neurosci. Behav. Physiol ; 36: 655-62.

102. Tagamets MA, Horwitz B (2001) Interpreting PET and fMRI measures of functional neural activity: the effects of synaptic inhibition on cortical activation in human imaging studies. Brain Res. Bull. 54: 267-73.

103. Tagamets MA, Horwitz B (1998) Integrating electrophysiological and anatomical experimental data to create a large-scale model that simulates a delayed match-to-sample human brain imaging study. Cereb. Cortex ; 8: 310-20.

104. Tagamets MA, Horwitz B (2000) A model of working memory: bridging the gap between electrophysiology and human brain imaging. Neural Netw. 13: 941-52.

105. Taylor-Clarke M, Kennett S, Haggard P (2002) Vision modulates somatosensory cortical processing. Curr. Biol. 12: 233-6.

106. Thivierge JP, Marcus GF (2007) The topographic brain: from neural connectivity to cognition. Trends Neurosci. 30: 251-9.

107. Tipper SP, Lloyd D, Shorland B, Dancer C, Howard LA, McGlone F (1998) Vision influences tactile perception without proprioceptive orienting. Neuroreport ; 9: 1741-4.

108. Trappenberg TP (2002) Neurons in a Network. In: Fundamentals of Computational Neuroscience. Oxford University Press, New York, pp 56-88

109. Traub RD, Contreras D, Cunningham MO, Murray H, Lebeau FE, Roopun A, Bibbig A, Wilent WB, Higley MJ, Whittington MA (2005) Single-column thalamocortical network model exhibiting gamma oscillations, sleep spindles, and epileptogenic bursts. J. Neurophysiol. 93: 2194-232.

110. Traub RD, Jefferys JGR, Whittington MA. Fast Oscillations in Cortical Circuits (Computational Neuroscience). The MIT Press: Boston, MA, USA, 1999.

111. Treves A (1993) Mean-field analysis of neuronal spike dynamics. Network ; 4: 259-84.

112. Ursino M, La Cara GE, Sarti A (2003) Binding and segmentation of multiple objects through neural oscillators inhibited by contour information. Biol. Cybern. 89: 56-70.

113. Ursino M, Zavaglia M (2007) Modeling analysis of the relationship between EEG rhythms and connectivity among different neural populations. J. Integr. Neurosci. 6: 597-623.

114. Ursino M, Zavaglia M, Astolfi L, Babiloni F (2007) Use of a neural mass model for the analysis of effective connectivity among cortical regions based on high resolution EEG recordings. Biol. Cybern. 96: 351-65.

115. Uutela K, Hamalainen M, Somersalo E (1999) Visualization of magnetoencephalographic data using minimum current estimates. Neuroimage. 10: 173-80.

116. Wallenstein GV, Hasselmo ME (1997a) Functional transitions between epileptiform-like activity and associative memory in hippocampal region CA3. Brain Res. Bull. 43: 485-93.

117. Wallenstein GV, Hasselmo ME (1997b) GABAergic modulation of hippocampal population activity: sequence learning, place field development, and the phase precession effect. J. Neurophysiol. 78: 393-408.

118. Wang D, Terman D (1997) Image segmentation based on oscillatory correlation. Neural Comput. 9: 805-36.

119. Welch PD (1967) The Use of Fast Fourier Transform for the Estimation of Power Spectra: A Method Based on Time Averaging Over Short, Modified Periodograms. IEEE Trans. Audio Electroacoustics ; AU-15: 70-3.

120. Wendling F, Bartolomei F, Bellanger JJ, Chauvel P (2002) Epileptic fast activity can be explained by a model of impaired GABAergic dendritic inhibition. Eur. J. Neurosci. 15: 1499-508.

121. Wendling F, Bellanger JJ, Bartolomei F, Chauvel P (2000) Relevance of nonlinear lumped-parameter models in the analysis of depth-EEG epileptic signals. Biol. Cybern. 83: 367-78.

122. Wilson HR, Cowan JD (1972) Excitatory and inhibitory interactions in localized populations of model neurons. Biophys. J. 12: 1-24.

123. Wolpaw JR, Birbaumer N, McFarland DJ, Pfurtscheller G, Vaughan TM (2002) Brain-computer interfaces for communication and control. Clin. Neurophysiol. 113: 767-91.

124. Zavaglia M, Astolfi L, Babiloni F, Ursino M (2008a) A model of rhythm generation and functional connectivity during a simple motor task: preliminary validation with real scalp EEG data. International Journal of Bioelectromagnetism, IJBEM ; 10: 68-75.

125. Zavaglia M, Astolfi L, Babiloni F, Ursino M (2008b) The effect of connectivity on EEG rhythms, power spectral density and coherence among coupled neural populations: analysis with a neural mass model. IEEE Transactions on Biomedical Engineering ; 55: 69-77.

126. Zavaglia M, Astolfi L, Babiloni F, Ursino M (2006) A neural mass model for the simulation of cortical activity estimated from high resolution EEG during cognitive or motor tasks. J. Neurosci. Methods ; 157: 317-29.

PUBLICATIONS

Publications on international journals

1. L. Astolfi, F. Cincotti, D.Mattia, M.Lai, F. de Vico Fallani, S. Salinari, L.A. Baccalà, M. Ursino, M. Zavaglia and F. Babiloni, "Causality estimates among brain cortical areas by Partial Directed Coherence: simulations and application to real data", **International Journal of Bioelectromagnetism, IJBEM**, Vol. 7, No. 1, pp. 62-65, 2005.

2. L. Astolfi, F. Cincotti, D.Mattia, F. deVico-Fallani, S. Salinari, M. Ursino, M. Zavaglia, M.G. Marciani and F. Babiloni, "Estimation of the cortical connectivity patterns during the intention of limb movements", **IEEE Engineering in Medicine and Biology Magazine**, 2006 Jul-Aug;25(4):32-8.

3. L. Astolfi, F. Cincotti, D.Mattia, M.G. Marciani, L. Baccalà, F. de Vico Fallani, S. Salinari, M. Ursino, M. Zavaglia, and F. Babiloni, "Assessing cortical functional connectivity by partial directed coherence: simulations and application to real data", **IEEE Transactions on Biomedical Engineering**, 2006 Sep;53(9):1802-12.

4. M. Zavaglia, L. Astolfi, F. Babiloni, M. Ursino, "A neural mass model for the simulation of cortical activity estimated from high resolution EEG during cognitive or motor tasks", **Journal of Neuroscience Methods**, vol. 157, no. 2, pp. 317-329, Oct.2006.

5. L. Astolfi, F. Cincotti, D.Mattia, M.G. Marciani, L. Baccala, F. de Vico Fallani, S. Salinari, M. Ursino, M. Zavaglia, L. Ding, J.C. Edgar, G.A. Miller, B. He and F. Babiloni, "A Comparison of Different Cortical Connectivity Estimators for High Resolution EEG Recordings", **Human Brain Mapping,** 2007 Feb;28(2):143-57.

6. M. Ursino, M. Zavaglia, L. Astolfi, F. Babiloni, "Use of a neural mass model for the analysis of effective connectivity among cortical regions based on high resolution EEG recordings", **Biological Cybernetics,** 2007 Mar;96(3):351-65.

7. M. Ursino and M. Zavaglia, "Modeling analysis of the relationship between rhythms and connectivity among different neural populations", **Journal of Integrative Neuroscience**, 2007 Dec;6(4):597-623.

8. M. Zavaglia, L. Astolfi, F. Babiloni and M. Ursino, "The effect of connectivity on EEG rhythms, power spectral density and coherence among coupled neural populations: analysis with a neural mass model", **IEEE Transactions on Biomedical Engineering**, 2008 Jan;55(1):69-77.

9. L. Astolfi, F. Cincotti, D. Mattia, F. De Vico Fallani, A. Colosimo, S. Salinari, M. G. Marciani, W. Hesse, H. Witte, M.Ursino, M. Zavaglia, and F. Babiloni, "Tracking the time-varying cortical connectivity patterns by adaptive multivariate estimators", **IEEE Transactions on Biomedical Engineering**, in press.

10. M. Zavaglia, L. Astolfi, F. Babiloni, M. Ursino, "A model of rhythm generation and functional connectivity during a simple motor task: preliminary validation with real scalp EEG data", **International Journal of Bioelectromagnetism, IJBEM**, 2008, 10(1):68-75.

11. E. Magosso, M. Ursino, M. Zavaglia, A. Serino, G. di Pellegrino, "Visuotactile representation of peripersonal space: a neural network study", submitted to **Neural Computation.**

Publications on international books

1. M. Zavaglia, E. Magosso, L. Astolfi, F. Babiloni, M. Ursino. "A model of power spectral density in cortical EEG, for the study of cortical connectivity", in **Modelling in Medicine and Biology VI** (Vol. 8 of WIT Transactions on Biomedicine and Health), ed. by M. Ursino, C.A. Brebbia, G. Pontrelli, E. Magosso, pp. 203-212, WIT press, Southampton, 2005.

Peer Reviewed Proceeding Articles

1. L. Astolfi, F. Cincotti, D. Mattia, M. Lai, F. de Vico Fallani, S. Salinari, L.A. Baccalà, M. Ursino, M. Zavaglia and F. Babiloni, "Causality estimates among brain cortical areas by Partial Directed Coherence: simulations and application to real data", **Proceedings of BEM & NFSI 2005**, 12-15 May 2005, Minneapolis, USA.

2. L. Astolfi, F. Cincotti, D.Mattia, M.Lai, L. Baccala, F. de Vico Fallani, S. Salinari, M. Ursino, M. Zavaglia and F. Babiloni, "Comparison of different multivariate methods for the estimation of cortical connectivity: simulations and applications to EEG data", **Proceedings of the 27th Annual International Conference of the IEEE Engineering in Medicine and Biology Society (EMBS)**, 1-4 September 2005, Shangai, China, pp. 4484 - 4487.

3. L. Astolfi, F. Cincotti, D.Mattia, F. deVico-Fallani, S. Salinari, L.A. Baccalà, M. Ursino, F. Nocchi, M. Zavaglia and F. Babiloni, "Using multivariate estimates to assess directed causality between cortical areas of the brain. Simulations and application during the imagination of a limb movement in Spinal Cord Injured patients", **Proceedings of the 16th Meeting of the International Society for Brain Electromagnetic Topography**, 5-9 October, Bern, Switzerland, 2005.

4. M. Zavaglia, E. Magosso, L. Astolfi, F. Babiloni, M. Ursino. "Simulation of functional connectivity among brain cortical areas using a neural mass model". **Proceedings of the 3rd European Medical and Biological Engineering Conference EMBEC'05** (Praga, Repubblica Ceca, 20-25 November 2005), CD-ROM (ISSN: 1727-1983).

5. M. Zavaglia, L.Astolfi. F. Babiloni, M. Ursino. "Assessment of effective connectivity among cortical regions based on a neural mass model", **Proceedings of the 28th Annual International Conference of the IEEE Engineering in Medicine and Biology Society 2006 (IEEE EMBS 2006)**, August 30-September 3, 2006, New York City (USA), pp. 590-594, The Printing House, Inc. (CD-ROM, ISBN 14244-0033-03).

6. L. Astolfi, F. Cincotti, D. Mattia, M. Mattiocco, F. De Vico Fallani, M.G. Marciani, M. Ursino, M. Zavaglia, S. Gao, W. Wu, F. Babiloni. "Cortical connectivity patterns during imagination of limb movements in normal subjects and in a spinal cord injured patient", **Proceedings of the 28th Annual International Conference of the IEEE Engineering in Medicine and Biology Society 2006 (IEEE EMBS 2006)**, August 30-September 3, 2006, New York City (USA), pp.996-999, The Printing House, Inc. (CD-ROM, ISBN 14244-0033-03).

7. L. Astolfi, F. Babiloni, F. Cincotti, D. Mattia, F. De Vico Fallani, H. Witte, W. Hesse, S. Salinari, A. Colosimo, M. Ursino, M. Zavaglia, MG. Marciani, "Time-varying cortical connectivity by adaptive multivariate estimators applied to a combined foot-lips movement", **Proceedings of the 29th Annual International Conference of the IEEE Engineering in Medicine and Biology Society 2007 (EMBC 2007)**, 23-26 August 2007, Lyon (France), pp. 4402-4405, The Printing House, Inc. (CD-ROM, ISBN 1-4244-0788-05).

8. M. Ursino, M. Zavaglia, E. Magosso, A. Serino, G. di Pellegrino, "A neural network model of multisensory representation of peripersonal space: effect of tool use", **Proceedings of the 29th Annual International Conference of the IEEE Engineering in Medicine and Biology Society 2007 (EMBC 2007)**, 23-26 August 2007, Lyon (France), pp. 2735-2739, The Printing House, Inc. (CD-ROM, ISBN 1-4244-0788-05).

9. M. Zavaglia, L. Astolfi, F. Babiloni, M. Ursino, "A model of rhythm generation and functional connectivity during a simple motor task: preliminary validation with real scalp EEG data", **Proceedings of the Neuromath Workshop 2007,** 4-5 December 2007, Rome, Italy, pp. 125-132.

Peer Reviewed Proceeding Abstracts

1. M. Zavaglia, M. Ursino, L. Astolfi, F.Babiloni. "The use of neural mass models for the analysis of brain connectivity from high resolution scalp EEG", **Proceeding of the 12th Annual Meeting Human Brain Mapping**, Florence, Italy, June 11-15, 2006 (CD-ROM, n. 471 M-AM).

2. M. Ursino, E. Magosso, M. Zavaglia, C. Cuppini " Mathematical models of integration among different brain areas during simple cognitive tasks" , **Proceedings of the 1 st Workgroups Meeting**, 2-3 December 2007, Rome, Italy, pp. 70.